QUANTIFICATION OF LOADING FOR BEHIND SHIELD BLUNT IMPACTS

DEVELOPMENT OF A MODIFIED ANTHROPOMORPHIC TEST DEVICE FOR THE QUANTIFICATION OF BEHIND SHIELD BLUNT IMPACTS

By NOAH STEINMANN, B. ENG.

A Thesis Submitted to the School of Graduate Studies in Partial Fulfilment of the

Requirement for the Degree Master of Applied Science

A Thesis Submitted to the School of Graduate Studies in Partial Fulfilment of the Requirements for the Degree Master of Applied Science

McMaster University MASTER OF APPLIED SCIENCE (2020) Hamilton, Ontario

(Mechanical Engineering)

TITLE:	Development of a modified anthropomorphic test device for the quantification of behind shield blunt impacts
AUTHOR:	Noah Steinmann, B.Eng. (McMaster University)
SUPERVISOR:	Cheryl E. Quenneville, B.Sc., M.E.Sc., Ph.D.
NUMBER OF PAGES:	xv, 149

Lay Abstract

When a ballistic shield is impacted by a bullet it deforms to absorb the incoming energy. The high-speed deformation of the shield material can impact the arm leading to fracture and possible life-threatening risks if the shield is dropped due to this injury. At the time of this work, there were no standards that limited the amount of allowable back-face deflection or tools available that could measure the force transferred to the arm in this scenario.

The purpose of this work was to develop a measurement device that could measure the force transferred to the arm from the behind shield impact. An existing crash test dummy arm was modified to provide measurement capabilities for this loading scenario. Ballistic shield testing was conducted where two different ballistic shield models were impacted to observe how the impact force changed with shield design, as well as the distance the device was placed behind the shield. A pneumatic impacting apparatus was then re-designed in the McMaster Injury Biomechanics lab that will allow the ballistic impact conditions to be re-created for evaluating the injury tolerance of the arm. The results of this work will be used to inform the future development of a ballistic shield evaluation standard.

Abstract

Ballistic shields are used by defense teams in dangerous situations as protection against threats such as gunfire. When a ballistic shield is struck, the shield material will deform to absorb the kinetic energy of the incoming projectile. The rapid back-face deformation of the shield can contact the arm, which can impart a large force over an extremely short duration. This work modified an Anthropomorphic Test Device (ATD) to be used for the characterization of behind ballistic shield blunt impact loading profiles.

The modified ATD was instrumented to measure impacts at the hand, wrist, forearm, and elbow to compare the force transfer at different locations of impact. A custom jig was designed to support the ATD behind a ballistic shield, provide a high degree of adjustability, and be subjected to impact testing. Two ballistic shield models, both with the same protection rating, were tested and showed to have statistically different responses to the same impact conditions, indicating further need for shield safety evaluation.

To apply these loading profiles to future injury criteria development tests, a pneumatic impacting apparatus was re-designed that will allow the high energy impact profiles to be re-created in the McMaster Injury Biomechanics lab. Understanding the ballistic impact conditions, as well as the response of different ballistic shield models provided insight into the possible methods available to reduce upper extremity injury risk. This work has provided essential data for informing a future standard for shield safety evaluation.

Acknowledgements

I would firstly like to thank my supervisor, Dr. Cheryl Quenneville. Your guidance and support over the last two years have helped me grow so much in my ability to face challenging problems head-on. Even when things didn't go as planned, you were patient and helped put problems into perspective. For the countless hours you spent in project meetings or helping to edit this thesis, I appreciate them all.

I would like to thank all who made this project possible, the DRDC research team who facilitated the ballistic testing: Jean-Sébastien, Daniel, Benoit, and Steven. To all the guys in the mechanical engineering machine shop: Mark, Justin, Rob, Michael, and John. Thank you to the Injury Biomechanics Lab group: Fatemeh, Marisa, Cooper, Ariana, and Julian. I have enjoyed our laughs in the office and am thankful that you were all there to keep me distracted. A special thanks Julia for all the help you gave on this project and support through the challenges I faced. Your company and lighthearted attitude made the long days easier. I'd also like to thank McMaster University, DRDC, NSERC, and OGS for providing me with funding to conduct this work.

I would like to thank my family. For always inviting me over for games, a home-cooked meal, or just some company when I needed a break. And finally, my wife, Sonya. You have encouraged me and supported me like no one else could. I certainly could not have done it without you.

Table of Contents

List of Figures

List of Tables

List of Abbreviations and Symbols

%	Percent
±	Plus/minus
α	Significance level
AE	Armor express
ANOVA	Analysis of variance
ATD	Anthropomorphic test device
BABT	Behind armor blunt trauma
CAD	Computer aided design
cm	Centimeter
DAQ	Data acquisition system
DRDC	Defense research and development Canada
F	Force
fps	Frames per second
g	Grams
Hz	Hertz
IEPE	Integrated electronics piezo-electric
in	Inches
kg	Kilograms
kHz	Kilohertz
kN	Kilonewtons
M	Moment
m	Meters
MCP	Metacarpophalangeal joint
MHz	Megahertz
mm	Millimetres
m/s	Meters per second

N	Newtons
Ns	Newton-second
NIJ	National institute of justice
p	P-value
PIP	Proximal interphalangeal joint
PMHS	Post-mortem human specimen
psi	Pounds per square inch
PVC	Polyvinyl chloride
R^2	Coefficient of determination
s	Second
SID-II	Small side impact dummy
TAB	Trauma attenuating backing
THOR	Test device for human occupant restraint
TYRT	TYR tactical
WorldSID	Worldwide harmonized side impact dummy

Declaration of Academic Achievement

The following is a declaration that I, Noah Steinmann, completed the research outlined in this thesis and recognize the contributions of Dr. Cheryl Quenneville, Julia de Lange, Jean-Sébastien Binette, Daniel Bourget, Benoit Gauthier, and Steven Kelly. I performed all mechanical design and manufacturing, experimental testing, data analysis, and writing of this thesis. Dr. Cheryl Quenneville developed the project plan and contributed to the review of mechanical designs, experimental testing plans, and this thesis. Julia de Lange contributed to the experimental testing and review of mechanical designs. Jean-Sébastien Binette, Daniel Bourget, Benoit Gauthier, and Steven Kelly contributed to the ballistic experimental testing at Defense Research and Development Canada.

Chapter 1 – Introduction

1.1 Motivation

Ballistic shields are used by defense teams for diffusing dangerous situations that could include terrorism, hostages, and riots. Shields are strapped to a user's arm and provide the first line of defense against projectiles, gunfire, and explosions. While these devices are rated to prevent ballistic penetration, the force of these impacts can cause the back of the shield to deform due to the high energy being transferred from the projectile. The back-face deformation can impact the user's upper extremity putting them at risk for injury, which could lead to dropping the shield. This becomes especially dangerous because it not only exposes the shield holder, but also any people behind them, to danger.

This impact energy is transferred to the upper limb in two ways: through the straps and handle contacting the arm/hand and through the back-face of the shield due to its deflection. This research has focused on the localized force application that comes from the contact between the back-face of the shield and the upper extremity. Currently, there are no standards in place for limiting the force transfer from back-face deformations, only standards pertaining to projectile penetration through ballistic materials [1]. Therefore, it is important to develop a standardized measurement tool, as well as associated injury criteria, that specify allowable forces that can be applied to the upper extremity in this scenario.

Publishing on the frequency of this injury mechanism is limited due to restrictions surrounding defense privacy; however, Defense Research and Development Canada (DRDC) has identified the importance of characterizing this risk. The first step in

understanding the injury risk is quantifying the loading that is transferred to the upper extremity through back-face shield deformation. There has only been one known previous study, conducted by Bolduc et al. [2], that carried out ballistic shield impact testing for the evaluation of behind shield force transfer. During these tests, a single rigidly mounted force sensor was placed behind the ballistic shield to capture the transferred force during impact. The distance between the arm and the shield, termed "stand-off distance", was moved from 20 mm to 40 mm and resulted in a reduction of peak force from 16 kN to 4 kN [2]. Given the limited number of tests and overly rigid boundary conditions, more work was needed to characterize the back-face shield response.

This thesis highlights the development of a tool that could be used to set a standard for evaluating future shield design. This device was designed to evaluate loading at four specific locations that are particularly vulnerable to injury: the hand, wrist, forearm, and elbow. This project further evaluated the loading curves behind the ballistic shield by using the custom measurement tool, which provided more realistic boundary conditions when compared to the work by Bolduc et. al [2]. Additionally, this work compared different ballistic shield designs to evaluate their relationship to the transferred force.

There have been numerous previous studies regarding the injury limit of the upper extremity, relevant ones being explored in Section 1.4. Injury criteria have been developed for a wide range of scenarios, with critical forces that cause injury ranging from 1700 N to 6500 N [3], [4]. This force range has substantial overlap with the forces recordzd in previous ballistic shield testing [2], indicating that shield designers have a good chance of modifying shield design to ensure the transferred forces are within a safe range. Developing

a measurement tool that can be used to evaluate the loading profiles during ballistic shield impacts is the first step in providing shield designers with appropriate metrics for informing their designs.

The overall purpose of this thesis was to evaluate the loading event behind a ballistic shield due to high energy, short-duration impact. These were characterized through the measurement of peak impact forces, durations of impact, and force impulses. These data will be used in the future to define the injury criteria for the upper extremity during the same impact conditions. The following topics will be presented in the first chapter: behind armor blunt trauma, shield design, existing upper extremity injury criteria, and Anthropomorphic Test Devices (ATDs).

1.2 Anatomy of the Arm[1]

The upper extremity is comprised of three long bones: the humerus, the ulna, and the radius. There are an additional 27 bones that make up the wrist and hand. The anatomical features of the upper extremity long bones as well as the hand are depicted in Figure 1.1. The humerus is the largest bone in the upper extremity and runs between the shoulder and the elbow. The forearm consists of two long bones with the ulna, the longer of the two, located on the medial aspect of the forearm and the radius being located on the lateral aspect [5].

[1] Anatomical terms used throughout document are listed in Appendix A – Anatomical Glossary

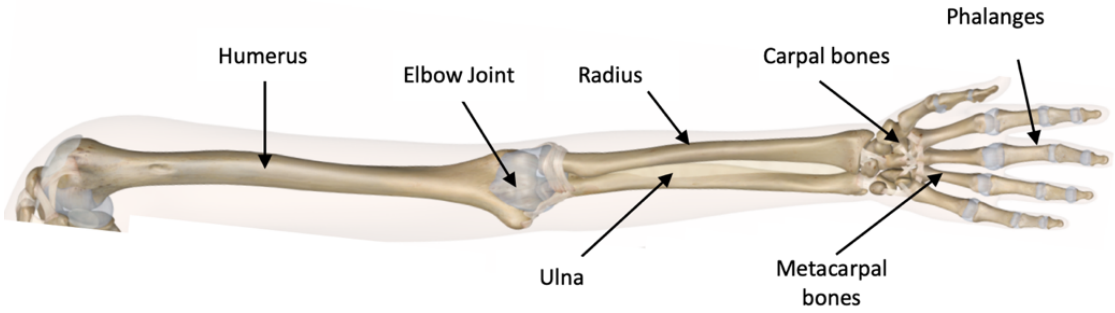

Figure 1.1: Bones of the upper extremity

Three bones make up the arm are shown, with the humerus forming the structure of the upper arm and the lower arm being comprised of the radius and ulna. The hand consists of the carpal bones, metacarpal bones, and phalanges. Image modified from [5].

The 27 hand and wrist bones can be separated into three groups: the carpals, metacarpals, and phalanges. The carpal bones, which make up the wrist and base of the hand, consist of eight irregularly formed bones organized in two rows of four (one proximal and one distal). The proximal row consists of the scaphoid, lunate, triquetrum, and pisiform, which articulate with the radius to form the wrist joint. The distal row of carpal bones, which articulate with the metacarpal bones, consists of the trapezium, trapezoid, capitate, and hamate. There are five metacarpal bones, all of which articulate with the carpal bones on the proximal end and the phalanges on the distal end. These are the bones that make up the internal structure of the hand. Finally, the remaining 14 bones are the phalanges, which make up the digits [5].

1.3 Ballistic Impacts

1.3.1 Behind Armor Blunt Trauma

The primary goal of personal armor is to stop ammunition from penetrating the body. However, as armor and material designs have advanced to address this issue, Behind Armor Blunt Trauma (BABT) has become more relevant. This is the non-penetrating injury that results from the contact between the rapid back-face deformation of the impacted armor and the body. Even when projectiles do not penetrate through the armor, there is still a risk of injury through BABT mechanisms [6]. Armor is designed to be light-weight to allow mobility of its users, which can lead to the selection of less energy absorbent materials, increasing the risk of BABT related injuries [7].

During a ballistic impact to worn body armor, the initial contact between the projectile and outer face of the armor causes a shock wave to travel through the material and directly into the body. During this stage of the impact, very little back-face deformation of the armor occurs [8], [9]. After the initial shockwave, the back-face deforms to dissipate the projectile's kinetic energy, leading to force transfer to the body and risk of injury. As the back-face deformation is generally unavoidable, the National Institute of Justice created a standard to specify the allowable back-face deformation during a ballistic impact to worn personal body armor, NIJ 0101.04 [10]. This standard is evaluated as a 'pass/fail' criterion, where a clay plate is placed behind the back-face of the armor and any deformation of the armor will leave an indentation in the clay plate. The armor is considered 'safe' if the indentation is less than 44 mm deep [10].

Similar to body armor, ballistic shields provide a valuable first line of defense against high-velocity projectiles, aiming to absorb a projectile's kinetic energy through rapid material deformation. Since they are secured against the user's forearm (Figure 1.2), back-face deformation can result in contact between the shield and the arm, resulting in the hand, wrist, forearm, and elbow being particularly vulnerable to injury.

Figure 1.2: Ballistic shield held with left arm
Illustration of a ballistic shield's position related to the forearm while being held in front of the user [11].

The previously mentioned standard cannot be directly applied to ballistic shields as it was developed based on the compliance of the soft tissues in the torso, whereas impacts to the bones of the upper extremity would respond differently as there is relatively little soft tissue coverage. Therefore, a different standard is required to evaluate the injury risk for the upper extremity due to ballistic shield BABT.

This injury risk has not been well investigated. Only one known previous study was completed in 2018 by Bolduc et al. [2], who developed a testing protocol for tactical

ballistic shields, wherein they evaluated forces that were present due to transient back-face shield deformation. They adjusted the spacing between a force sensor and the back-face of a shield from 20 mm to 40 mm and found the maximum forces were 16 kN and 4 kN, respectively [2]. While this study only briefly covered shield back-face deformation, it highlights the high forces that can be present due to the BABT that comes from ballistic shield impacts. It does not, however, investigate any relationship between the impact force and associated injury risk, or use realistic boundary conditions during the back-face shield measurements. Therefore, further investigation was needed.

1.3.2 Shield Design

Shields can be manufactured of either solid metals or composite materials, where this thesis will be focusing on composite shield designs, as they were identified by DRDC to exhibit greater back-face deformation during impact. Current composite shields are comprised of layers of fabric such as aramids or Kevlar® to stop projectiles during impacts. These fabric layers can be separated by brittle polymer films such as polyimide, metallic films, or ceramic films; however, not all shield designs incorporate brittle layers. The brittle layers shatter the projectile to spread out its impact energy, then the fabric deforms to dissipate the kinetic energy and stop the projectile [12].

A feature of some shield designs is a Trauma Attenuating Backing (TAB) (Figure 1.3). While there were no studies identified that evaluate TABs in the context of ballistic shields, they have been evaluated with worn body armor. These are placed between the body and armor (whether shield or worn armor) and are made from stiff-foamed polymer materials to dissipate, re-distribute, and absorb the impact energy [13]. They have been

shown to increase the protection as they reduce the pressure, impulse, accelerations, and the dynamic indent [14], [15].

Figure 1.3: Trauma Attenuating Backing on the ballistic shield

An Armor Express ballistic shield with an attenuating backing located behind the handle and forearm strap. The forearm would rest against this material when the shield is being used to reduce force transfer between the shield and upper extremity.

A 2009 study by Sondén et al. evaluated the effect of TABs on the back-face deformation of armor [16]. They found that without a TAB present the mean back-face deformation was 28 mm (24-31 mm), while with a TAB the mean back-face deformation was 19 mm (17-21 mm). Furthermore, the addition of TAB's reduced under armor lacerations, even when no penetration was present [16]. Ballistic shields require the ability to dissipate large amounts of energy very rapidly while ensuring projectile penetration does not occur. For this reason, composite materials are commonly used, and TABs are often added to reduce the transferred force from the back-face deformation.

Unfortunately, there are very few standards in place that guide shield design. The only known standard, NIJ 0108.01, categorizes ballistic materials into discrete levels specifying the type of threat a material must be able to defeat. Ballistic materials can be classified into four categories ranging from Type 1, which is capable of stopping standard test rounds and lesser threats (12-gauge No. 4 lead shot), to Type IV, which must be able to stop armor-piercing rounds (Table 1.1) [1]. Based on the armor classification, a material for the shield and appropriate TAB can be selected.

Table 1.1: Summary of NIJ 0108.01 ballistic material ratings

Ballistic Rating	Threat
Level I	22 LR, 38 Special
Level II-A	Lower Velocity 357 Magnum, 9 mm
Level II	Higher Velocity 357 Magnum, 9 mm
Level III-A	44 Magnum, Submachine Gun 9 mm
Level III	High-Powered Rifle
Level IV	Armor-Piercing Rifle

1.4 Injury Criteria

In the scope of shield BABT the elbow, forearm, wrist, and hand have been highlighted as the most vulnerable locations for injury. Injury criteria have previously been developed at these locations for a variety of reasons, including fall and sports injury prevention, and automotive safety. These injury criteria are statistical probabilities that are used to predict the likelihood of injury occurring based on an applied load (force, moment, acceleration, etc.). Once developed, an acceptable level of injury risk can be selected, and a corresponding load limit can be specified.

Some additional factors that must be considered when applying previously developed injury criteria to BABT scenarios are the dynamic loading rate, magnitude, posture, anthropomorphic size, and sex. The anthropomorphic size represents the size and mass relative to the population average and is often given as a percentile (average is the 50th percentile). This work focused on 50th percentile male as this represents the typical soldier and is the usual starting point for injury criteria development. Existing injury criteria, unless developed for an exact application, must be applied with caution. For example, injury criteria developed for automotive research cannot necessarily be directly applied to ballistics as their impact conditions are inherently different in durations and magnitudes [17]–[19].

However, these prior studies can still provide a starting point for an investigation into injury during ballistic impact. Previously developed injury criteria provide an indication of the range of forces that can pose a risk for injury to the upper extremity and provide a target range of forces that must be measured during safety evaluation with a new shield standard. Each of the four vulnerable locations will be discussed herein to provide both a basis for understanding the limits of force that may cause injury at each region and the ranges of load that must be captured in a safety evaluating device.

1.4.1 Elbow

Elbow injuries have been investigated in the automotive industry from airbag deployment, with all studies conducted on 5th percentile females, due to their vulnerability. Two prior studies quantified the loading limits that the elbow can withstand, both in the context of airbag type injuries. A study by Duma et al. [20] determined that there was a

50% risk of injury when a force of 1680 N was applied to the elbow. Additionally, another study by Duma et al. [21] compared moments in the elbow due to hyperextension to both fracture and dislocation potential. They found that there was a 50% chance of elbow fracture with a bending moment of 56 Nm, where a 100% risk of fracture occurred at 186 Nm. They also found a 50% risk of dislocation at 93 Nm and a 100% risk of elbow dislocation at 194 Nm [21]. These injury limits were developed using a small female specimen, as such, it is likely that a soldier (50^{th} percentile male) would have an injury tolerance higher than those identified in these studies. Further, shield scenarios will not experience hyperextension at the elbow due to the different orientation of the loading vector.

1.4.2 Forearm

Studies have been conducted to evaluate the injury risk of the forearm when impacted in the transverse direction, for the evaluation of the safety of side airbag deployment in automotive scenarios. The dynamic injury tolerance of both female and male forearms has been investigated when the arm was in the supinated vs. pronated position [18], [19]. They noted that when the arm was in the supinated position it was able to carry approximately 17-21% (female versus male) more load than when in the pronated position. In these tests, the injury tolerance was defined as the mean moment that resulted in a fracture in the pronated position, as this orientation provided more conservative injury criteria. For a fifth percentile female, the dynamic injury tolerance for the forearm was 58 Nm [18]. For the 50^{th} percentile adult male, the dynamic injury tolerance for the forearm was 108 Nm [19]. Alternatively, Pintar et al. [22] impacted forearms at two velocities in

the supinated position, where they found that the mean fracture forces for males and females were 2368 N and 1377 N, respectively [22].

The research into the dynamic injury limit of the forearm has been focused on airbag deployment, as such these injury criteria cannot be directly applied to BABT since the loading rates associated with the BABT mechanism will be much more rapid. Higher velocity impacts associated with BABT are expected to result in higher mean fracture forces [22], and therefore higher injury criteria. This highlights a gap in the literature where no dynamic forearm injury criteria for ballistic impacts exist, which must be identified if a standard is to be developed for shield design. Additionally, the higher injury criteria that is expected during ballistic impacts require the shield evaluation tool to measure forces that are greater than those indicated in previous literature.

1.4.3 Wrist

The development of injury criteria for the wrist has primarily focused on injuries from forward falls. In 1998, Chiu and Robinovitch [23] used human participants to develop a preliminary set of injury criteria for forward fall conditions. They found that the average force from forward falls that could cause a fracture to the distal radius was 1780 ± 650 N where fall arrest strategies could reduce applied forces by up to 40% by decreasing the angle of elbow extension and reducing the impact velocity. Nine additional studies have been identified that tested Postmortem Human Specimens (PMHS) in both quasi-static and dynamic loading conditions to evaluate mean fracture forces (Table 1.2). These studies provide a preliminary indication of the ranges at which the wrist may be susceptible to injury; however, they cannot be directly applied to BABT for shields as the orientation that

these were evaluated in is different than what is experienced during behind shield impacts. This highlights that wrist injury criteria must be properly developed in the transverse loading direction if a shield evaluation standard is to be created.

Table 1.2: Summary of wrist fracture testing

Nine wrist fracture studies were compared, where the type of study and the mean failure load that was observed during testing were noted. Duma et al. [3] is the exception where a 50% injury risk was reported.

Study	Year	Type	Mean Fracture Forces (N)
Muller et al. [24]	2003	Quasi-Static	3231 ± 825
Myers et al. [25]	1991	Quasi-Static	3390 ± 877
Augat et al. [26]	1996	Quasi-static	females: 2008 ± 913 males 3773 ±1573
Augat et al. [27]	1998	Quasi-Static	2648 ± 1489
Myers et al. [28]	1993	Quasi-Static	1780 ± 650
Spadaro et al. [29]	1994	Quasi-Static	Distal radius: 1640 ± 980 Scaphoid: 2410 ± 913
Greenwald et al. [30]	1998	Dynamic	2821 ± 763
Reeves et al. [4]	2014	Dynamic	6565 ± 866
Duma et al. [3]	2003	Dynamic	1700 (50% injury risk)

These studies identify a large range of mean fracture forces from 1700 N to 6565 N [3], [4]. The large variation in fracture force comes from three PMHS-dependent variables (sex, age, anthropomorphic size) that affect the physical properties of the tested specimen and one situation-dependent factor (loading rate) that influences the response of the specimen. These studies provide a preliminary indication of the ranges at which the wrist may be susceptible to injury; however, they cannot be directly applied to BABT for shields as the orientation in which these were evaluated is different than what is experienced during

behind shield impacts. This highlights that wrist injury criteria must be properly developed in the transverse loading direction if a shield evaluation standard is to be created.

1.4.4 Hand

Most research regarding hand injury has come from the development of safety standards in ergonomics. Four studies were found to evaluate injury at the hand; three quantifying pain tolerance and one evaluated injury thresholds for the metacarpophalangeal (MCP) and the proximal interphalangeal (PIP) joints. Development of pain tolerance does not involve actual fracture or physical injury but instead looked at the amount of force that can be applied before pain was experienced.

One of the studies that evaluated pain threshold was completed by Fransson-Hall and Asa in 1993 [31] where they identified locations on the hand that were most susceptible to pain. It was also observed that the pressure pain threshold for females was 130 ± 34 kPa, while it was 258 ± 119 kPa for males. Another study, by Mewes et al. [32], was conducted to create better safety measures for automatic closing doors, where they applied force to the backs of the participant's hands until pain was deemed unbearable. They recommended a force limit of 400 N because at this value almost all participants found this force to be bearable and those who felt pain only experienced pain while the force was being applied [32]. Finally, a study by Hohendorff et al. [33] aimed to evaluate the safety of automotive windows by applying force to the fingers. They found tolerable entrapment forces for the proximal interphalangeal joints, index proximal interphalangeal joint, and index distal interphalangeal joint to be 97.2 ± 51.8 N, 43.4 ± 19.9 N, and 36.9 ± 17.8 N, respectively [33].

The only study that developed injury criteria for the hand was completed by Carpanen et al. [34] whereby injury criteria for blunt impacts to the MCP and PIP joints were developed. Drop testing was conducted on PMHS where the impact velocity was between 2 m/s and 4 m/s. The 50% injury risks for the MCP and PIP joints were evaluated to be 3.0 kN and 4.2 kN, respectively.

During BABT of ballistic shields, the MCP joints (knuckles) will be more susceptible to injury than the PIP, as they will be in closest proximity to the back of the shield and directly between the handle and the shield back-face. For this reason, the MCP injury criterion is more relevant to this work than the PIP injury criterion. Secondly, this study evaluated injury risk using drop testing, which would result in lower injury tolerances when compared to ballistic testing as the impact velocity was much lower. For this reason, it is likely that during ballistic shield impacts the injury criterion for the hand will be higher than what is presented here due to the viscoelastic response of bone.

1.5 Anthropomorphic Test Device Design, Application, and Selection

1.5.1 Anthropomorphic Test Devices

Anthropomorphic Test Devices (ATDs), also known as crash test dummies, are instrumented surrogates that are used for safety evaluations. They were first introduced into the automotive industry in 1949 to assess restraints and have become standardized and widely accepted in industry [35]. As such, ATDs are a valuable tool when establishing new safety standards. They are typically built from metallic components, covered in a PVC flesh surrogate, and contain instrumentation to collect load and acceleration data for common

injuries. Different ATDs have been designed with physical properties to represent different demographics, with the most common anthropomorphic size being 50th percentile male, which is intended to represent an average males' size and mass distribution.

These devices are typically used alongside injury criteria to determine injury risk. Loads (forces, accelerations, moments, etc.) are measured using an ATD and compared to the injury criteria (established through research on PMHS) to provide an estimation of the risk associated with the load. While these devices are designed to be biofidelic by "represent[ing] the geometry, mass, mass distribution, kinematics, and kinetics of the human body" [36], they still do not truly represent human body response. Issues have been noted including anatomically incorrect components, limitations of mimicking biological material properties using engineering materials, and lack of muscles and other soft tissues [36].

1.5.2 Design Considerations

There are three primary considerations when selecting and using an ATD: the measurements that the device is capable of taking, the degree of correlation between the measurements and the associated injury criteria, and the biofidelity of the ATD [35]. Typically, ATDs are designed using a collection of force, moment, linear and angular acceleration, pressure, and displacement sensors to quantify the total loading in a situation. These sensors can either be piezoresistive (PR) or piezoelectric (PE), where PR sensors are typically smaller and easier to incorporate into ATDs. Piezoresistive sensors are also capable of quick calibration immediately before testing, making them a more common choice of instrumentation in ATDs [37].

1.5.3 Existing ATDs

Approximately 60% of injuries in automotive collisions occur to the head, face, and neck, while only 3.5% occur in the upper extremity [37]. This has pushed the design of ATDs to focus more heavily on the measurement of loading in the more severe injury locations such as the torso, head, neck, and even lower extremities. There are currently only three ATD options that contain upper extremity instrumentation: the Small Side Impact Dummy (SID-II), the Test Device for Human Occupant Restraint (THOR), and the Worldwide harmonized Side Impact Dummy (WorldSID).

The SID-II was designed and made by First Technology Safety Systems, and Occupant Safety Research Partnership of the United States Council for Automotive Research program in 1994. It is a full-body ATD with instrumentation in the head/neck, upper/lower torso, spine, pelvis, lower extremity, and upper extremity. In the upper extremity, it contains six uniaxial accelerometers (x, y, and z measurement in upper and lower arm), but contains no instrumentation to measure force or moments. This ATD was designed to evaluate side impacts, as such the focus during the design of the upper limb was how it would transfer force to the torso. Two previous studies compared the mechanical response of PMHS arms to that of the SID-II arm and found that the ATD did not account for a toe-in loading region when compared to the PMHS, which limited the response corridor of this surrogate [38], [39]. This evaluation focused on impacts to the humerus and had no investigation into the response of the elbow to hand portion.

Another ATD that was identified to contain an instrumented upper extremity was the THOR 50th percentile male, designed by General Engineering and Systems Analysis in

1995. The THOR ATD has been adopted into the 2020 roadmap for the European New Car Assessment Program and is primarily used as a frontal impact ATD [40]. The primary focus of the upper extremity component was again in transferring energy through the arm, primarily focusing on the shoulder joint.

Progress has been made with the THOR to increase the biofidelity of this shoulder by improving the range of motion, repeatability, and dynamic responses [41]. But with the focus being primarily on the shoulder, the THOR ATD instrumentation is limited to a load cell in the clavicle and a load cell in the upper arm. This instrumentation allows the measurement of the forces transmitted through the arm but gives no indication of how loading in the distal portion of the arm occurs.

The most highly instrumented upper extremity ATD that was identified is the WorldSID (50^{th} percentile male) which was designed by the International Standards Organization (ISO) WorldSID Task Group in 1997 and is manufactured by Humanetics Innovative Solutions, Inc. (Humanetics Innovative Solutions, Farmington Hills, MI, USA). There are two options available for the arm: half arm or full arm. The half arm (upper arm) is a plastic bone with a PVC skin. It provides a greater range of motion for the shoulder joint but does not contain any instrumentation.

The full arm (Figure 1.4) can be instrumented to measure upper arm and forearm forces and moments (6-axis load cell in each location), elbow moments (2-axis), elbow angular rotation, and 3-axis acceleration at the elbow and wrist. To date, injury criteria and injury risk functions have not been fully defined, and only preliminary WorldSID injury criteria have been used to make comparisons to other ATDs [41].

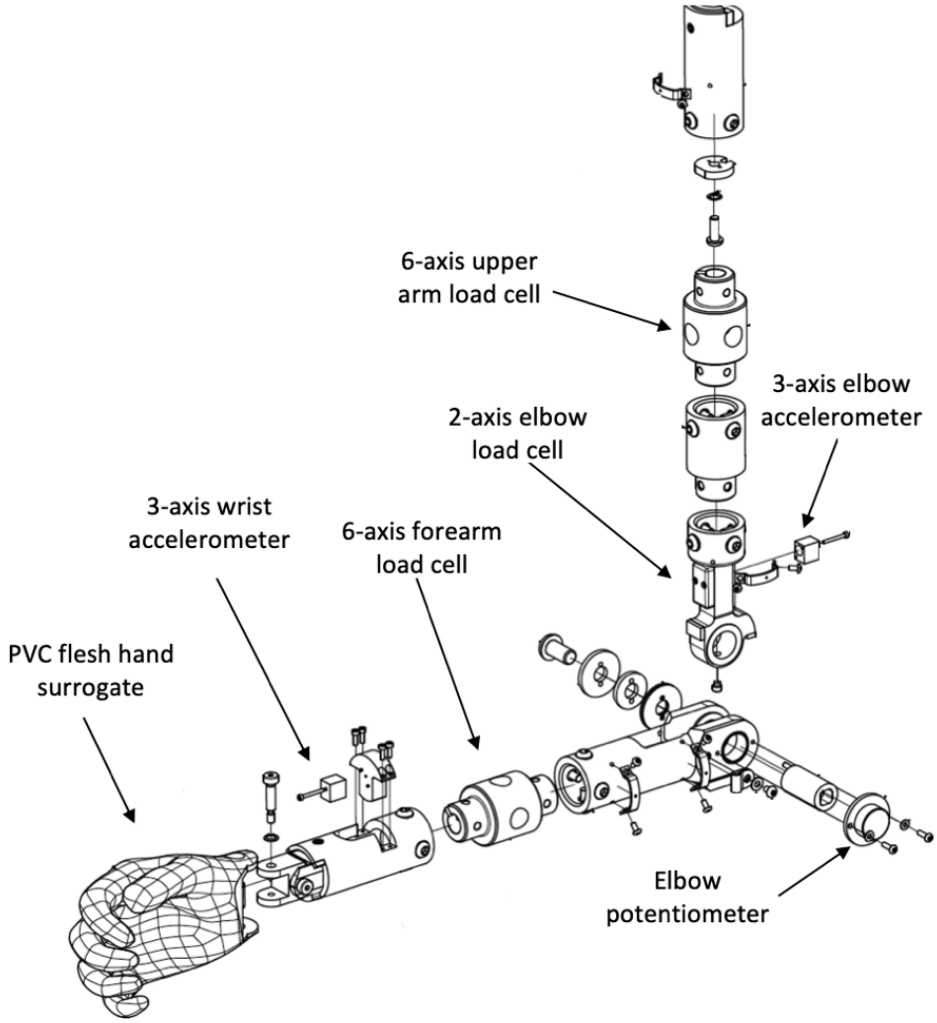

Figure 1.4: WorldSID 50th percentile male arm assembly

The exploded assembly drawing of the WorldSID full arm was modified from Humanetics Innovative Solutions Inc. technical drawings [42] with the available instrumentation labeled. PVC flesh surrogate is not shown.

1.6 Study Rationale and Overview

During a ballistic shield impact, due to the close proximity of the upper limb to the back-face of the shield, there is a risk of injury due to the energy transfer through BABT mechanisms. To the author's knowledge, there has only been one study [2] that evaluated

force transfer due to shield BABT but was conducted with a limited number of tests and unrealistic boundary conditions. Further, to date, there have been no standards in place that limit transferred forces during ballistic shield impacts that can be used to evaluate the safety of shield designs. This is the gap in knowledge that this research aimed to fill.

This thesis was the first stage in a two-phase research project that aims to develop upper extremity injury criteria for this ballistic shield impact scenario. This thesis focused on characterizing the loading experienced behind ballistic shields due to the contact between the back-face of the shield and the upper extremity. The second (future) stage of this research will conduct PMHS testing to develop these injury criteria.

Considering this work would be, one day, incorporated into industry standards, the focus was to build off an existing ATD, to increase industry acceptance. Therefore, the WorldSID 50th percentile full upper arm ATD was modified whereby additional instrumentation, as well as new structural components, were added (Chapter 2). This device was then used during ballistic impact trials to characterize the loading profiles experienced during behind shield impacts (Chapter 3). To facilitate future injury criteria testing on PMHS, a pneumatic impacting apparatus at McMaster University [43] was redesigned to accommodate both the modified ATD and PMHS. Additionally, improvements were made that aimed to reduce losses, produce more repeatable impacts, and make it possible to re-create the impact profiles measured during ballistic shield testing (Chapter 4).

1.7 Objectives and Hypotheses

The objectives of this thesis were:

1. To develop an ATD capable of measuring ballistic impact data at the elbow, forearm, wrist, and hand including peak impact force, duration of impacts, and impulse.
2. To construct jigs so the ATD could be tested both in the custom pneumatic impacting apparatus and behind the DRDC ballistic shield mounting system while maintaining consistent boundary conditions between the two locations.
3. To carry out ballistic testing and quantify the relationship of the impact parameters with the stand-off distance and impact location, as well as compare two different ballistic shields to observe how shield selection affects the impact profile.
4. To modify a custom pneumatic impacting apparatus [43] so higher velocity impacts can be conducted to create impact profiles that are more representative of those found during the ballistic testing in the McMaster Injury Biomechanics laboratory.

The corresponding hypotheses were:

1. Increasing stand-off distance would reduce the peak impact force, duration, and impulse.

2. The impact profile will be dependent on the shield type that is used. There will be a significant difference in the peak forces, durations, and impulses between the different shields with the same standoff distance.

Chapter 2 – Design of a Modified Anthropomorphic Test Device and Testing Jigs

2.1 Introduction

Ballistic shields are strapped directly to the forearm where the back-face may be in contact with, or close to, the arm. Even when a projectile does not pass through the shield (penetration), local deformations can cause the back-face of the shield to impact the arm with high energy, posing a risk of upper extremity fracture. This injury risk has serious implications, as an upper extremity fracture could result in the user dropping the shield, having potentially life-threatening consequences.

Currently, National Institute of Justice standard 0108.01 is the only standard used to assess the safety of shields, which is based on whether or not projectile penetration occurs [1]. This standard does not provide any limitations to allowable back-face deformations or force transfer between the shield and the upper extremity. As reducing the risk of upper extremity injury comes from understanding the transferred forces during this contact, evaluation of the forces transferred is essential for developing a standard or safety metric. Using Anthropomorphic Test Devices (ATDs) to evaluate force application is a common practice when evaluating loading in the context of human injury. For upper extremity injuries, the WorldSID 50th percentile (Humanetics Innovative Solutions, Farmington Hills, MI, USA) was (at the time of writing) the most advanced upper limb ATD on the market. It was designed for the evaluation of side impact automotive collisions and contained some integrated instrumentation. This instrumentation was still not adequate to characterize the force loading in a behind ballistic shield impact scenario. Therefore, the purpose of the

work performed for this chapter was to develop a measurement device that was capable of characterizing the loading profiles experienced during ballistic shield Behind Armor Blunt Trauma (BABT) impacts, which can be used for the evaluation of future shield designs.

2.2 Design Requirements

2.2.1 Modified ATD

The measurement device needed to be capable of evaluating the force application at four critical locations: the hand, wrist, forearm, and elbow. Modifying an existing ATD was advantageous as it provided both a device that had industry history (increasing acceptance) and already had some built-in instrumentation. As such, the basis of the measurement device was the WorldSID 50th percentile upper limb (Humanetics Innovative Solutions, Farmington Hills, MI, USA). The structure of the ATD upper limb (Figure 2.1) consisted of a distal humerus, elbow joint, forearm, wrist joint, molded PVC hand, and was encased in a removable Polyvinyl Chloride (PVC) flesh analog. It was instrumented with a 6-axis forearm load cell (three forces, three moments) and a 2-axis elbow load cell (two moments).

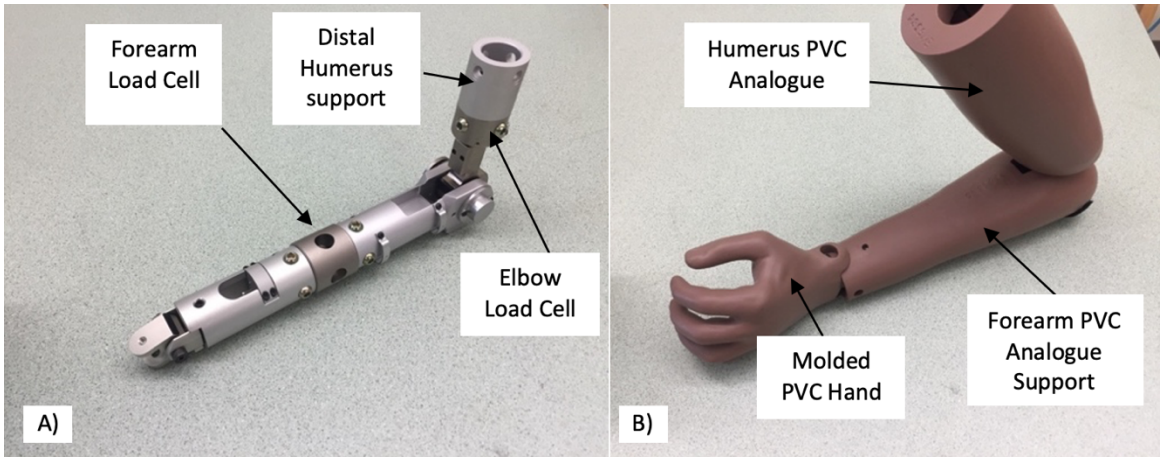

Figure 2.1 WorldSID 50th percentile upper limb

The WorldSID left arm is shown A) as just the base structure and B) with the PVC flesh. The ATD consisted of a load cell at the forearm and elbow as well as structural components to represent the forearm, hand, and the distal humerus. The PVC flesh was separated into three sections; the upper arm, the forearm, and the hand (with the flesh molded onto the structural hand component).

Based upon the anticipated direction of loading for the behind shield configuration and the four important locations, the required measurement capabilities were established (Figure 2.2). The base model WorldSID arm provided the two bending moments about the elbow and the six axes of measurement at the forearm. Therefore, uniaxial force sensors were incorporated into the ATD at the elbow, wrist, and hand to satisfy the remaining required directions of measurement. It is important to note that not all channels shown were critical for measurement, as loading in some axes (*i.e.* elbow My; forearm Fx, Mz, My) were not expected in this loading scenario. However, these are indicated as the instrumentation included with the WorldSID already had these channels. All instrumentation needed to be mounted on the side of the arm that contacted the shield to ensure direct impact forces were measured.

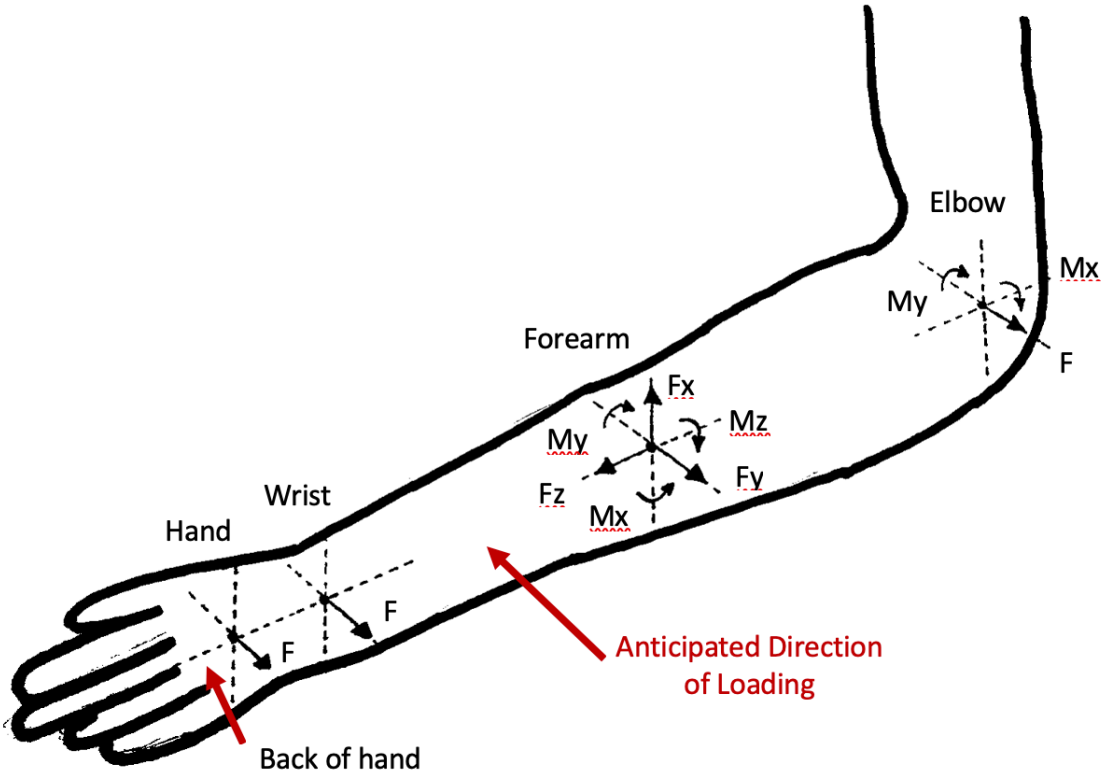

Figure 2.2: ATD required measurement directions

This image illustrates the required measurement capabilities of the modified WorldSID ATD based on the anticipated direction of loading (force applied to the posterior aspect of the left arm). The elbow moments and all forearm measurements were captured using instrumentation included with the WorldSID. Force was measured at the elbow, wrist, and hand with additional instrumentation.

The requirements of the modified upper limb ATD were heavily influenced by the work of Bolduc et al. in providing the limits of force that the ATD must be able to withstand, where the maximum force identified behind shield impacts was 16 kN, with impact durations of approximately 2 ms [2]. The only other comparable scenario was behind body armor impacts, where the peak force for Behind Armor Blunt Trauma (BABT) type injuries was 10.6 kN with an impact duration of 2 ms [44]. The DRDC technical team

recommended that due to the short duration limited global motion of the arm would occur during the impact event. Therefore, kinetic measurements such as accelerometers were not necessary.

The hand needed to be capable of supporting instrumentation to evaluate the impact force (at the knuckles/metacarpophalangeal joint), maintain consistent orientation relative to impact and wrap tightly around the handle so that compressive/crushing loads would occur between the hand and handle. The hand included with the WorldSID (Figure 2.3) could not satisfy any of the requirements. There was no solid material at the location of impact upon which to mount instrumentation and the orientation of this hand would be unreliable during ballistic impacts due to its irregular shape. Finally, replicating the compressive forces between the hand and handle would prove difficult due to the inability to position and maintain this hand's orientation during impact as there was no gripping capability. Therefore, the final requirement for the ATD was the design of a novel hand structure that provided both the ability to grip a handle and have a rigid structure onto which instrumentation could be mounted.

The final consideration was that during a ballistic impact there is no guarantee that the impact will be applied directly over the expected location of impact, and a slight offset can be present. This can result in a risk of eccentric sensor loading or cable damage if the load is not well aligned. Therefore, all instrumentation had to be implemented so that they would not be damaged by misaligned impacts.

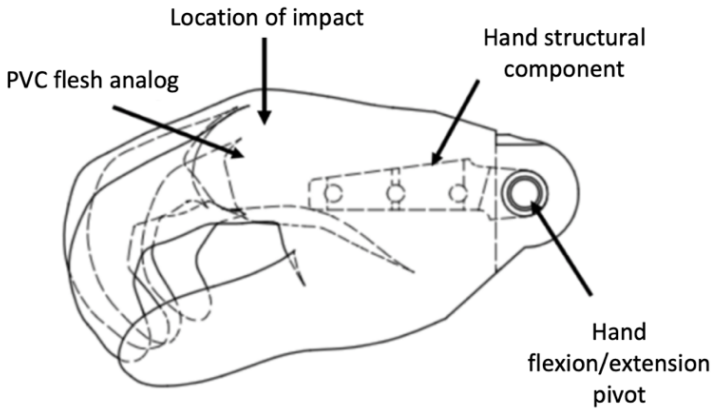

Figure 2.3: Schematic drawing of hand included with WorldSID 50th percentile ATD arm

The hand that was delivered with the ATD was made from two components, a solid metal structure (in the palm) and a PVC molded flesh [45]. The solid structural component included a hole for pivot motion at the wrist, as well as five holes through the structural component that filled with PVC when molded.

2.2.2 Data Acquisition

When collecting data, it is important to select an appropriate sampling rate for the Data Acquisition System (DAQ). Selecting an appropriate sampling rate will allow data to be collected that accurately represent the events being measured. Selecting an appropriate sampling frequency requires knowledge of the signal that is being collected. The minimum required sampling frequency was based on two metrics: video analysis of previous back-face shield impacts and literature values from BABT to the thorax.

Video footage of behind shield impacts provided by DRDC was analyzed in Tracker 5.1.5 (open source software), where the approximate duration of loading was found to be on the order of 2 ms. For BABT impacts to the thorax, the duration of impact was reported

to be approximately 2 ms, where data was collected at 20 kHz [44]. Since the anticipated impact profile for behind shield impacts had a similar duration to the thorax impacts, a minimum required sampling frequency of 20 kHz was selected to match previous literature.

2.2.3 Support Jigs

The four primary requirements for the supporting jigs were that they had appropriate boundary conditions to represent real behind shield impacts, be strong enough to withstand applied loading, be able to be used in both ATD and Post-Mortem Human Specimen (PMHS) testing, and interface with the apparatus in both the McMaster Injury Biomechanics lab and the DRDC ballistic test range. The boundary conditions for the arm were critical to ensure that the loading applied to the limb was realistic and consistent. These needed to be defined in two directions – the direction of gravity and the direction of impact. The forces acting in the direction of gravity were the weight of the shield and the limb, where the weight of the limb was already accounted for by the ATD. Simulating the weight of the shield was considered unnecessary since its estimated weight was 10 kg leading to a force of approximately 100 N in the direction of gravity. Impact forces were expected to be in the range of 4 kN to 16 kN [2], meaning the weight of the shield would be at most 3% of the force applied from the back-face deflections. Furthermore, it would be applied in the perpendicular direction to the impact loading; therefore, this gravitational force would not greatly contribute to a person's fracture risk from behind shield impacts.

During testing, impact energy is transferred to testing jigs and if not controlled could damage the jig structure. The jig required translation in the direction of impact as a means of absorbing impact energy, reducing the risk of structural damage, as well as mimicking

how an arm may move back towards the user. Furthermore, a method for controlling the translation would provide consistent ATD positioning between trials, as such linear translation was selected as the boundary condition in the direction of impact. In addition, the jigs had to be compatible with both testing facilities (DRDC and McMaster University) so that consistent boundary conditions were used during all tests. Finally, the jigs had to be designed to accommodate both the ATD and PMHS, ensuring that the same boundary conditions would be used when the PMHS were tested for the development of injury criteria.

2.3 Design

2.3.1 Modified Upper Limb ATD

All technical drawings for the ATD design can be found in Appendix B and the final assembled ATD can be seen in Figure 2.4. A PCB piezoelectric uniaxial washer style force sensor (model 201B05, PCB Piezotronics, MTS Systems Corporation, Depew, NY, USA) with a capacity of 22.25 kN was selected to collect direct impact forces at the elbow, wrist, and hand (Figure 2.5a). The addition of this single sensor model at three locations met all the requirements for directions of measurement outlined in Section 2.2.1. This sensor was advantageous as it could be easily mounted, had a high capacity, had small dimensions to allow its integration into the ATD, and had a very rapid response, making it suitable for measuring loading events with microsecond durations [46].

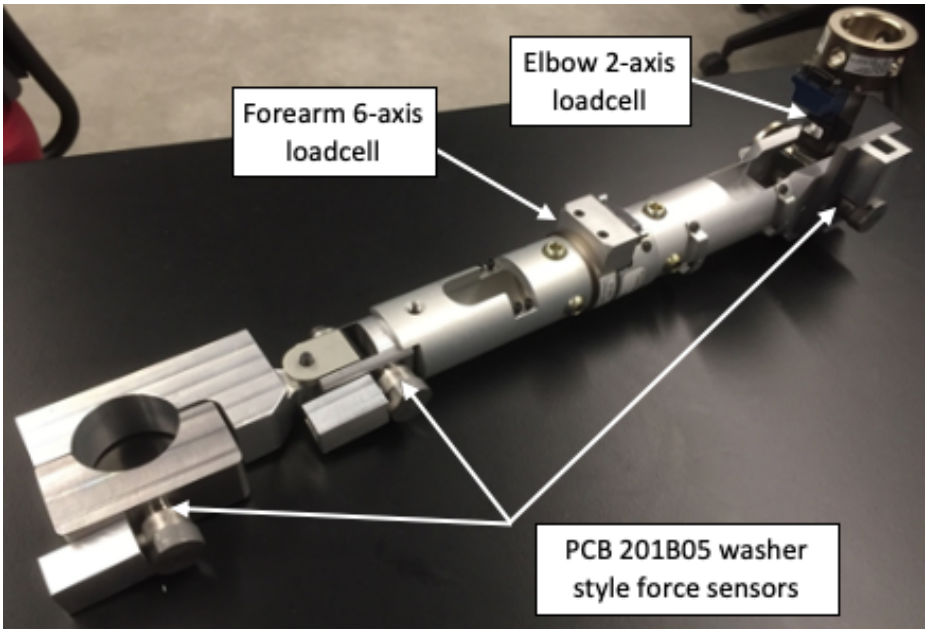

Figure 2.4: Final ATD design

The new hand, wrist, and elbow structures are shown fully assembled with the impact caps, force sensors, and cable protection channels installed.

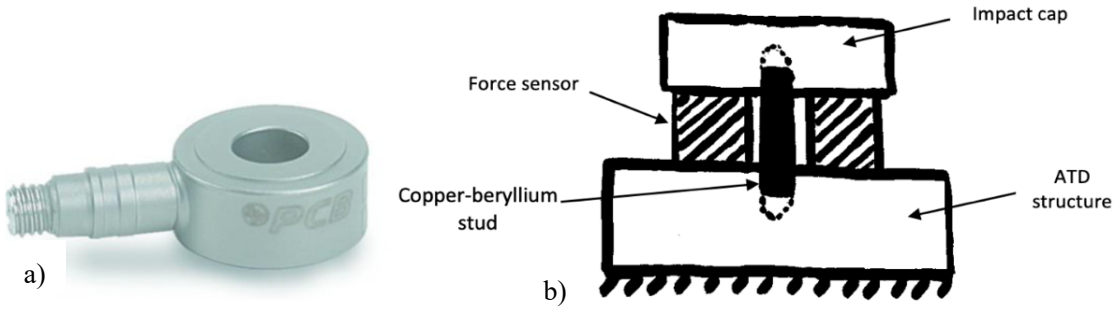

Figure 2.5: Impact force sensor that was integrating into the ATD

This image shows both a) the washer style force sensor with a measurement capacity of 22.25 kN shown without additional cabling or bolted connections [47] and b) the mounting of the force sensor between the ATD structure and an impact cap using a copper-beryllium stud to pre-load the force sensor.

To appropriately mount these sensors (per manufacturer instructions), each force sensor was clamped between a structural base and an impact cap, where a copper-beryllium mounting stud (supplied by PCB Piezotronics) was threaded into both the base and the impact cap (Figure 2.5b). The impact cap was then tightened to apply the required pre-load on the force sensor. In all locations where this sensor was added the ATD structure acted as the structural base.

Three impact caps were manufactured from steel and had threaded holes into which the beryllium-copper mounting studs fastened. Steel was selected as it would provide stronger threads for mounting and better resistance to damage from the impact forces. The impact caps were designed with a diameter slightly greater than that of the PCB force sensor (1.75 cm vs. 1.65 cm). This diameter was selected because the force sensors were susceptible to damage if load was applied eccentrically. Manufacturing the impact cap with a diameter just larger than the force sensor itself ensured that the load would be fully applied to the sensor but could not be applied eccentrically to the force sensor, thus avoiding damage. The impact cap was manufactured to have two flat faces on the sides spaced at 5/8-inch that would allow a wrench to tighten the impact caps, providing the pre-load.

When applying the pre-load to the force sensors the BNC connection between the DAQ and the PCB was split and a multimeter was put in series with the PCB to measure its voltage output. Each sensor had a specific sensitivity that related the voltage to an output force, so the impact caps were slowly tightened until the voltage reached that which was associated with the required 1000 lb pre-load, as per manufacturer specifications. This technique allowed each force sensor to be properly calibrated.

The BNC cable connections on the force sensors were very close to the location of impact, and as such were susceptible to damage during testing. During ballistic shield impacts, the shield can exhibit 'wrap-around', where the back-face of the shield travels past the edges of the impact cap. This could lead to the shield's back-face contacting the BNC connection, possibly causing damage. Furthermore, if impacts were ever offset from the force sensor (as is possible during ballistic testing) this risk would be further exaggerated. For this reason, steel channels were manufactured that would be taped over the BNC cable and connection point, providing protection. This channeling was designed with clearance between the inside of the channel and the cable. It sat below the impact cap to ensure that the force would be transferred through the force sensor before there was a chance of the shield back-face contacting the channel. Three of these channels were manufactured, one for each location.

The elbow, wrist, and hand all had components re-designed to accommodate the new PCB force sensors, as well as to provide locations onto which the protection channels could sit. All new components were manufactured of steel to provide greater strength.

2.3.1.1 Elbow

To allow the PCB force sensor to mount at the elbow location, a steel mounting plate was manufactured, onto which the elbow load cell could be fastened using the copper-beryllium stud (Figure 2.6). Two existing threaded holes on the ATD (originally used to mount an elbow potentiometer) were used to secure this plate at the elbow location. The force sensor was positioned over the center of the elbow joint. It also provided a structure against which to securely tape the protection channel.

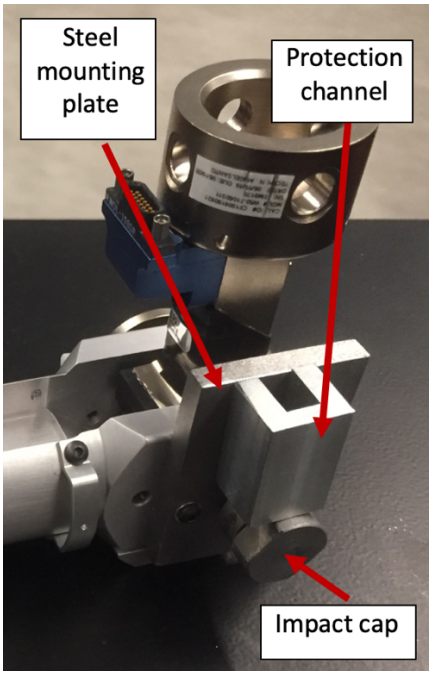

Figure 2.6: Modified elbow structure to allow mounting of PCB force sensor

The new elbow structure is shown, which included a rectangular plate onto which the force sensor was threaded is and against which a protection channel was secured.

2.3.1.2 Wrist

The original structure at the end of the forearm did not provide sufficient material upon which to mount the new load cell assembly or have a surface available to support the protection channel. A new wrist component was designed that maintained a very similar structure to the one included in the ATD; however, this new wrist component was made approximately 0.65 cm longer and had a flat face milled to allow the load cell assembly to be mounted flush with the wrist. The additional 0.65 cm of material provided sufficient support for the load cell mounting stud to be threaded into the wrist and the milled face provided a mating surface for the channel guard to be put in place (Figure 2.7).

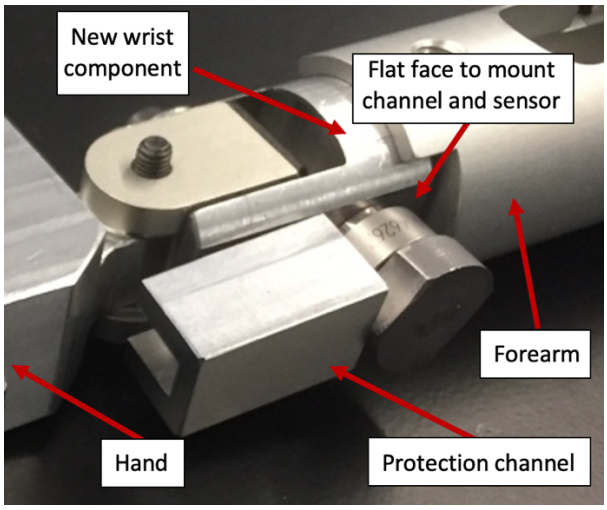

Figure 2.7: Re-designed wrist component to mount the PCB force sensor

The fully assembled wrist component included both the protection channel and force sensor. The flat face on the new wrist component provided a mating surface for both the protection channel and impact cap.

2.3.1.3 Hand

The ATD was modified to entirely remove the original hand component, as discussed in the ATD requirements. The new hand surrogate (Figure 2.8) addressed the aforementioned issues with the original hand (the lack of structure to mount a force sensor and no ability to consistently grip a handle). Two dimensions were critical in the design of the hand: the wrist to the center of the grip and the offset of the force sensor surface from the center of the grip (representing the distance from the inside palm to the back of the knuckles). These dimensions were specified to ensure the hand dimensions matched those associated with 50th percentile male anthropometrics. Two metal blocks were manufactured, each with a 3.8 cm cylindrical cut out [48] between which the handle was

placed and clamped, ensuring the hand and force sensor were always centered on the handle. The center of these cutouts was 7 cm from the wrist joint, representing the center of grip dimension for a 50th percentile male [49]. The impact cap surface was positioned 5 cm from the center of grip to be in the same position as the dorsal surface of the metacarpophalangeal joint, based on 50th percentile male anthropometric data [50].

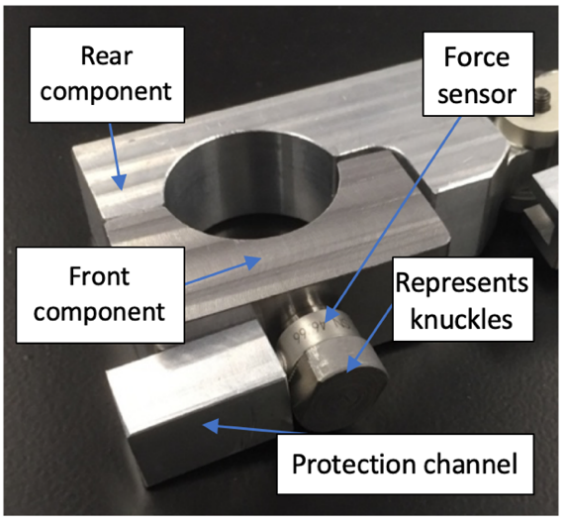

Figure 2.8: New hand design
The new hand design provided the ability to clamp onto a 3.8 cm diameter handle and mounting for both the force sensor and the cable protection channel.

The metal component that was positioned behind the handle represented the back of the hand ("rear component") and was manufactured from aluminum. Alternatively, the component positioned on the front side of the handle (closest to the shield) represented the fingers ("front component") and was manufactured of steel. This was because the rear component had clearance holes allowing the lighter material to be selected, whereas the

front component had tapped holes with specific strength requirements leading to the selection of the stronger material.

2.3.1.4 Assembled Design

The final ATD design that was used during the ballistic trials is shown in Figure 2.4. The three PCB 201B05 washer style force sensors were mounted on the side of the arm closest to the shield at the hand, wrist, and elbow. The six-axis load cell was located in the middle of the forearm and the two-axis elbow moment load cell was positioned in the elbow. The steel impact caps were threaded onto the copper-beryllium mounting studs at each location and the steel cable protection channels were aligned and taped in place over top of the PCB cabling.

The final modification to the ATD was the removal of the PVC flesh. This was removed because during initial impact trials at DRDC (Chapter 3) the PVC flesh that was included with the ATD caused two problems: it interfered with properly aligning the ballistic impacts at the forearm and did not provide consistent attenuation between impact locations. It was very difficult to align the impacts at the forearm as it was unclear of the exact location of the load cell beneath the PVC flesh. The flesh could move relative to the ATD, so consistent alignment was challenging. The included PVC flesh also only covered the forearm load cell and did not cover the hand, wrist, or elbow, making the comparison between the locations problematic as they had different force attenuation. Finally, to the author's knowledge, there was no scientific basis for the shape or properties of the PVC flesh, so no justification for requiring this material in the design.

In its place, two 2 cm x 2 cm x 0.16 cm sections of Infinisil silicon rubber with a durometer of 50 shore A (Warco Biltrite, Orange, CA, USA) were taped at the location of impact (overtop of the impact caps and forearm load cell) to attenuate the high-frequency vibrations associated with impact, while providing a small degree of protection to the sensors. This rubber allowed consistent attenuation in comparison to the PVC flesh included with the ATD as the same material was placed at all locations of impact. After each trial, the rubber material was replaced with new pieces to provide consistent damping and ensure any damage from previous trials would not affect future tests.

2.3.2 Data Acquisition

The different instrumentation required specific input types, where the PCB force sensors required an Integrated Electronic Piezo-Electric (IEPE) current and the forearm and elbow load cells only needed an excitation voltage. Additionally, the forearm and elbow load cells were wired in a full bridge orientation. As mentioned previously, the forearm and elbow load cells had to be sampled at a frequency of at least 20 kHz. However, in the interest of collecting as much data as possible for the short duration impacts, a sampling frequency of 100 kHz was selected for the forearm and elbow load cell sampling (the maximum frequency of the DAQ card).

The PCB force sensors had a bandwidth of 90 kHz that required data to be acquired at a rate of at least five times this value, preferably ten [51]. After discussion with the DRDC technical team, a sampling frequency of 1 MHz was selected for the PCB force sensors. A second DAQ was used to sample at this higher rate, as discussed in Section 3.2.

2.3.3 Jigs

All technical drawings for the jigs can be found in Appendix C. The first requirement of the designed jigs was to represent the boundary conditions of real-world impact scenarios. This was accomplished by securing the test jig to a mounting plate (Figure 2.9), where four linear bearings were fastened. Upon impact, the linear bearings allowed the mounting plate and jigs to translate along two parallel linear rails (double bearings used to resist bending moments generated by eccentric impacts). The shock absorbers, attached to the moving structure, compressed against the impact plate behind the jig to dissipate the kinetic energy.

A vertical support structure was manufactured from aluminum extrusion, which supported the limb at the mid-humerus (above the elbow load cell). The connection between the ATD and the jig can be replaced in the future by a component that will support a PMHS. The handle was manufactured of aluminum and fastened onto aluminum extrusion. The use of aluminum extrusion provided a great deal of adjustability in the positioning of the ATD behind the ballistic shield. It also was designed to accommodate PMHS ranging from 5^{th} to 95^{th} percentile sizes when used for future injury criteria tests [50]. As previously mentioned, it was important that for consistency this testing jig had to be compatible with both the DRDC testing apparatus and a custom pneumatic impacting apparatus in the McMaster Injury Biomechanics lab (Chapter 4). The base testing jig was unchanged but had to be integrated into the two test facilities in different ways due to the constraints of each setup.

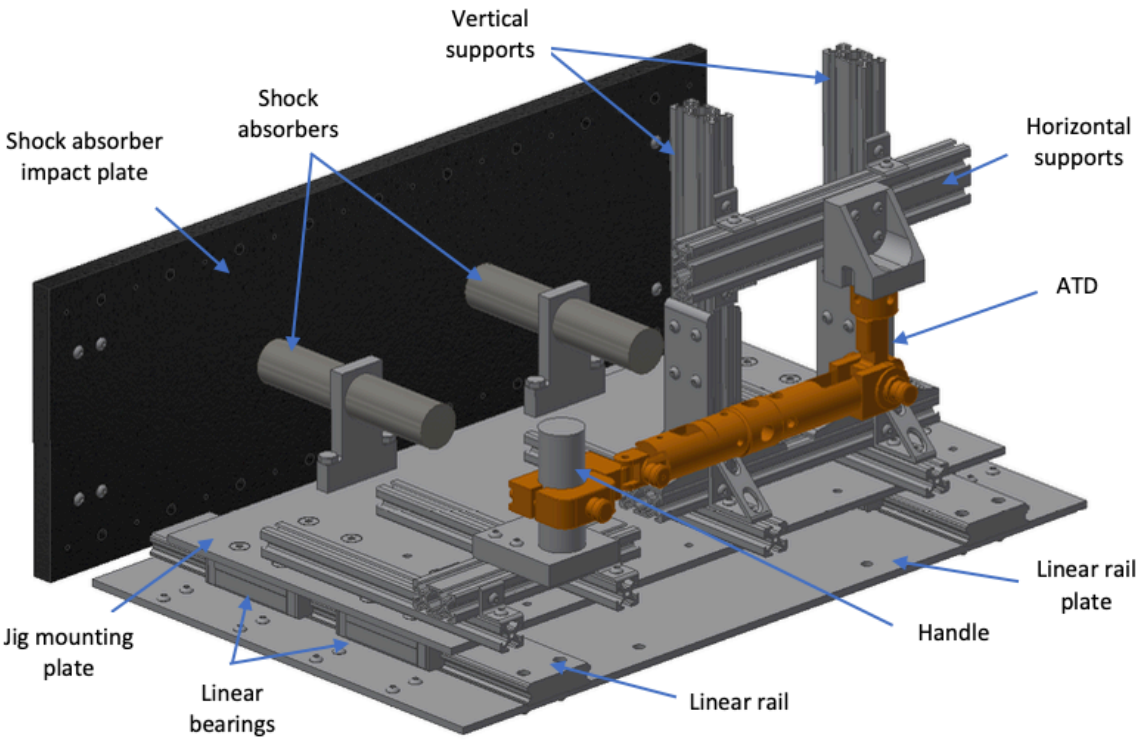

Figure 2.9: The base test jig used at both McMaster University and DRDC

The jig contained two vertical supports to adjust the height of the ATD, and one horizontal support to adjust the horizontal placement. Two shock absorbers were mounted behind the ATD and the entire system was mounted on four linear bearings for energy dissipation.

2.3.3.1 DRDC Facility

The DRDC team already had a ballistic shield support frame set up in their test range with which the ATD interfaced (Figure 2.10). The existing frame provided support for the ballistic shield and a base plate behind the shield to which the ATD support structure was mounted.

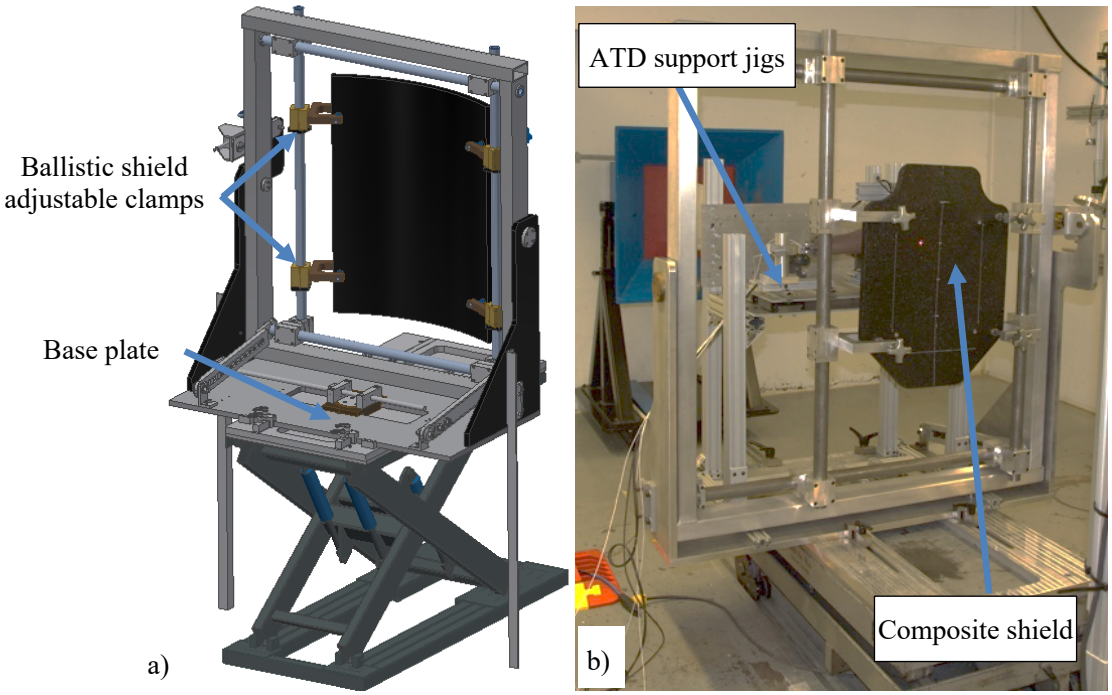

Figure 2.10: Jigs assembly in DRDC shield support structure

These images show a) the rear-view CAD model of behind the DRDC ballistic shield support structure and b) the front view of the ballistic shield support structure with both jigs and a composite shield installed.

As the location of the universal receiver (the device used to fire test rounds) was fixed, the ATD had to be elevated to be aligned with the test barrel. An aluminum extrusion frame, supporting the linear rail plate, was rigidly bolted to the base of the DRDC shield mount using L-brackets at the each of the four corners of the structure (Figure 2.11a). The linear rails were then fastened to the linear rail plate allowing the jigs to be installed behind the ballistic shield (Figure 2.11b). The assembly was positioned so the arm would be normal to the direction of impact.

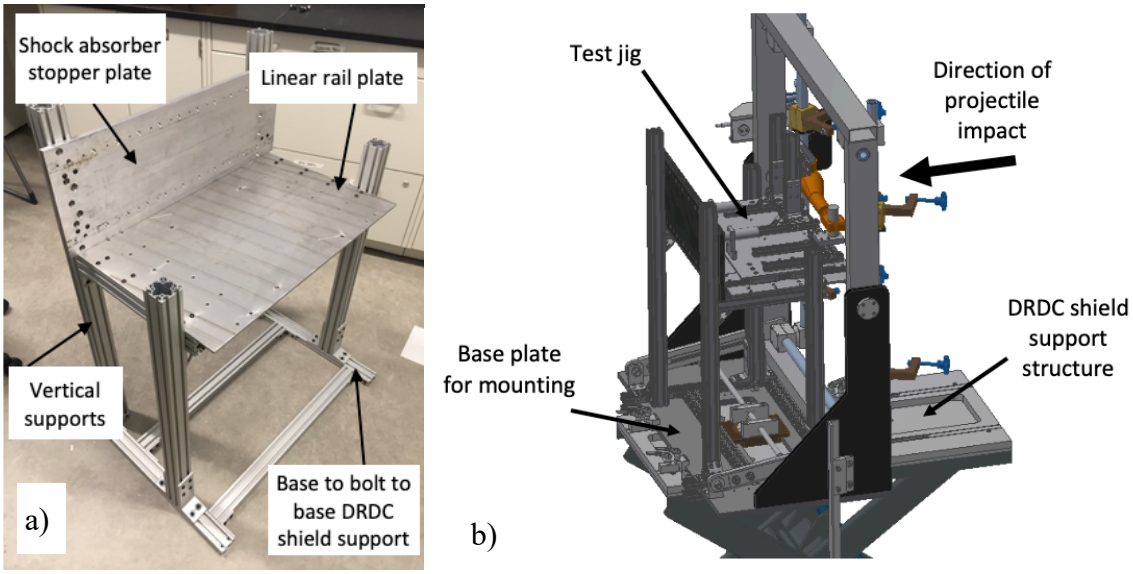

Figure 2.11: Support structure to mount ATD jigs in the DRDC shield support structure

This image shows the a) jig support frame and b) the fully assembled jigs in the DRDC shield mount, shown without a shield. The jig support frame was made of an aluminum extrusion support that interfaced with the base plate on the DRDC shield support structure as well as vertical supports used to elevate jigs to be in line with the universal receiver.

2.3.3.2 McMaster University Facility

The test jigs were designed to also be installed in a custom pneumatic impactor at McMaster (Figure 2.12a). At the front of the pneumatic impactor, there was a steel mounting plate that allowed a single linear bearing to be fastened (used for previous work). This was permanently welded to the impactor frame, which meant the linear rail plate could not be fastened flush against the impactor frame. To resolve this, four 1.25 cm aluminum spacers were positioned between the linear rail plate and the impactor frame to provide clearance for the existing steel mounting plate (Figure 2.12b). Once this structure was secured, the rest of the jig was assembled, and the shock absorber stopper plate was

installed. The addition of the spacers allowed the linear rails to be secured to the welded frame of the pneumatic impactor and the arm to be positioned in front of the projectile acceleration tube.

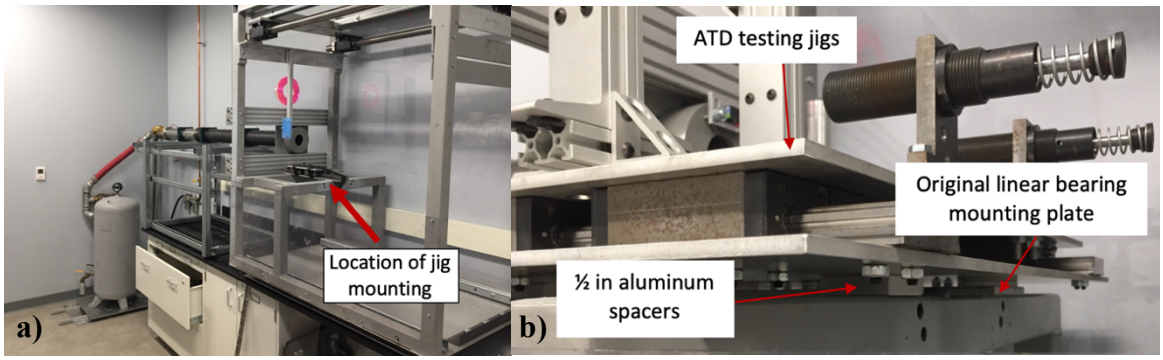

Figure 2.12: The custom pneumatic impacting apparatus with the ATD test jigs
This image shows a) the custom pneumatic impacting apparatus in the McMaster Injury Biomechanics laboratory and b) the aluminum spacers that were placed between the pneumatic impactor frame and the jig's aluminum plate for mounting the linear rails.

2.4 ATD Repeatability Evaluation

Upon completion of the custom ATD, its repeatability was characterized. Since the WorldSID ATD had a high degree of repeatability inherent in it and was designed to measure loading in the same orientation, evaluating the repeatability of the forearm and elbow load cells was considered unnecessary. However, the PCB force sensor's repeatability had not been determined in this specific set-up, and as such was characterized. Additionally, the elbow, wrist, and hand locations were tested to observe how the boundary conditions at each location affected the loading curves.

Ten impacts were conducted at each of the hand, wrist, and elbow locations, with the first five at a low impact velocity of 2.49 ± 0.07 m/s and the next five at a higher impact

velocity of 6.09 ± 0.23 m/s. All shots were conducted using the modified pneumatic impacting apparatus (Chapter 4) and used a projectile mass of 2.88 kg. The impact locations were compared using a one-way ANOVA analysis (α=0.05).

For the lower impact velocity, the mean peak force and standard deviation for the hand, wrist, and elbow were 2700 ± 140 N, 1620 ± 50 N, and 2050 ± 80 N, respectively (Figure 2.13). The forces at the three locations were all found to be statistically different from one another ($p<0.005$). At the higher impact velocity, the mean peak force and standard deviation for the hand, wrist, and elbow were 17710 ± 1610 N, 4790 ± 230 N, and 7400 ± 290 N, respectively. Similarly, at the higher velocity condition, all impact locations were found to be statistically different from one another ($p<0.005$). All impacts tended to have very low coefficients of variation ranging from 2.8% to 5.4%, except for the high-velocity hand impact, which had a higher coefficient of variation of 9.1%.

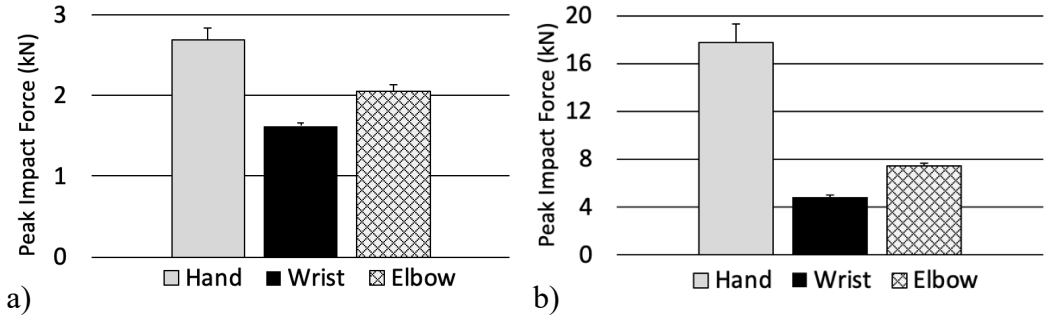

Figure 2.13: ATD mean peak impact forces for the hand, wrist, and elbow

Repeatability evaluation for the PCB force sensors at the hand, wrist, and elbow locations impacted at a) 2.49 m/s and b) 6.09 m/s velocity. The highest forces were measured in the hand, followed by the elbow, then the wrist.

2.5 Discussion

Since the primary objective of this work was to evaluate the forces experienced behind ballistic shields during high energy impacts, it was essential to develop a measurement device that could be used that would appropriately obtain these data. This chapter highlighted the development of the first highly instrumented upper extremity ATD that could be used to characterize BABT type impacts for ballistic shields. Experimental testing jigs for both DRDC and McMaster University were designed and manufactured that supported the ATD during impact.

The only previous work that aimed to evaluate loading behind ballistic shields used a single rigidly mounted force sensor [2]. While this provided force evaluation it was limited by the overly stiff boundary conditions, resulting in forces being measured that were not representative of real-world impact scenarios. This work aimed to improve the boundary conditions used when characterizing the behind shield impact event. Less rigid boundary conditions allowed the upper extremity to translate post-impact, which better simulated kinematics of actual behind shield impacts. While the addition of translation is an improvement to previous research, it is not possible to validate the specific boundary conditions used in this work. To validate the boundary conditions, it would be necessary to evaluate how a real human would respond to a ballistic shield impact, which is not possible to do safely or ethically. Therefore, while non-rigid boundary conditions are likely more representative of behind armor kinematics since a human arm is not rigid, the lack of validation must be noted.

Uniaxial force sensors were added at the elbow, wrist, and hand location to measure the force of impact, resulting in the most highly instrumented upper limb ATD to date. One limitation of this design is that the PCB force sensors are discrete and if an impact were applied at a location other than exactly where the sensors are placed, the loading would not be measured. However, the discrete location of measurement is a typical limitation of all ATDs, and with the expected control during all testing (both at McMaster University and DRDC), the influence from this error was minimized.

While this jig design provided a highly versatile set-up that interfaced both with the McMaster University and DRDC facilities there was one primary drawback, the number of components and fasteners that were required for this jig to properly function. With over 100 fasteners in the final design, having to do adjustments became a tedious endeavor. Having many components move relative to each other resulted in the aluminum extrusion components occasionally binding and not providing easy translation. Future iterations to this jig design will identify the critical degrees of freedom and only include those, as well as reduce the total number of fasteners needed to rigidly secure the assembly.

Finally, the influence of the impact location as well as the repeatability were quantified for the ATD. Firstly, for both the low and high-velocity impacts, the hand location measured the highest peak force, followed by the elbow, then the wrist. This order corresponds to decreasing rigidity of the boundary conditions, where the hand was the most rigid and the wrist was the least rigid. This observation indicated that the boundary conditions had a large effect on the resultant forces due to their rigidity. The boundary conditions were selected to best represent the boundary conditions that the arm is exposed

to during behind shield impacts, as such, the observation that the impact force was dependent on the impact location/ boundary condition strongly suggested that certain areas on the upper extremity are at higher risk of experiencing an injury. Considering this finding, a particular focus must be given to providing extra protection to the high-risk locations as any contact force can be greatly exaggerated by the rigidity of the associated boundary conditions.

The repeatability was evaluated at each of the impact velocities for each location. After the high velocity impacts at the hand, the Infinisil rubber material was observed to have experienced severe damage, where in some cases the material at the direct point of impact was punched out. This likely led to varying degrees of energy absorption through the damage of the rubber for different shots, resulting in the much higher coefficient of variation in the high velocity hand impact scenario. Since all coefficients of variation were below 10%, the newly designed ATD was considered to behave 'marginal (acceptable)' repeatability [52].

2.6 Conclusion

This work presents the most highly instrumented upper extremity ATD that can be used for the characterization of shield BABT loading profiles. The modified ATD was based off the WorldSID 50th percentile ATD arm with instrumentation added to collect uniaxial force data at the elbow, wrist, and hand. The final device had an acceptable level of repeatability over the range of forces expected in this project. Additionally, the location of impact was identified to have a substantial effect on the measured impact force. Custom testing jigs were designed that allowed the ATD to be mounted and tested both in the DRDC

and McMaster University testing apparatuses. This device will act as the starting point for the development of an evaluation tool for the safety of shield BABT scenarios.

Chapter 3 – Characterization of Ballistic Shield Loading Profile and Back-face Shield Response

3.1 Motivation

Ballistic shields, typically strapped to the forearm, are designed to stop high energy projectiles/ bullets. When impacted, they undergo material deformation in order to dissipate the incoming kinetic energy. Even if penetration of the projectile does not occur, there is still a risk of injury to the upper extremity due to possible contact between the back-face deformation and the arm. No known studies have been conducted to evaluate the loading limits to the upper extremity in this scenario; however, one previous study investigated ballistic shield Behind Armor Blunt Trauma (BABT) [2]. This study developed a base understanding of the loading profiles behind ballistic shields due to transient back-face shield deformation by characterizing the loading using a single rigidly mounted load cell. Unfortunately, the boundary conditions associated with a rigid load cell are not representative of true upper extremity BABT type loading. Additionally, this study evaluated only a single shield model, only minimal shots were conducted, and it had a high variability among impacts at the same conditions.

In Chapter 2 an instrumented surrogate was developed to measure loading during ballistic shield impacts while using boundary conditions that were more representative of upper extremity impacts in this context. Upon completion of the design and manufacturing of the modified Anthropomorphic Test Device (ATD), the next step was to carry out impact testing on ballistic shields. The primary objectives when conducting the ballistic testing were to characterize the loading profile from the back-face deflection using more realistic

boundary conditions, collect a greater quantity of data, and collect data that can feed into future Post Mortem Human Specimen (PMHS) testing for the evaluation of upper extremity injury criteria. While quantifying the loading profile, three additional relationships were investigated: how impact location (boundary conditions), stand-off distance, and shield type affected loading profiles measured during impact.

3.2 Methodology

Two types of composite ballistic shields (a flat Armor Express (AE, 20 in x 30 in) and a curved TYR Tactical (TYRT, 24 in x 36 in)), both rated level III in NIJ 0108.01 [1], were acquired and tested during this work (Figure 3.1). Since they were rated to Level III an IVI C21 ball projectile (9.6 g) fired at 850 m/s was used for all trials, as this is the standard testing protocol for this shield rating [1]. With this impact condition, the ballistic shields were designed to stop the projectile without experiencing perforation and would result in a ‘worst case’ back-face deformation impact, which was desired for evaluation. The projectile (bullet) was fired from a universal receiver test barrel, Wiseman 09-2016(08) (Bill Wiseman and Co. Inc, College Station, TX), with a length of 22" and right-hand twist rate of 1:12-inches (Figure 3.2). A laser sight was used to align the universal receiver with the desired location of impact.

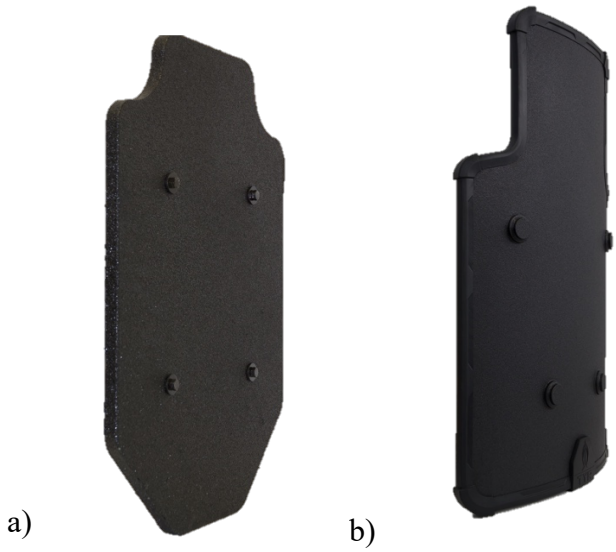

Figure 3.1: Ballistic shields used during testing

This image shows the two shields that were used during the ballistic testing, the a) flat Armor Express (AE) and b) the TYR Tactical (TYRT). Both shields were rated to Level III and were rated to stop a 9.6 g projectile traveling at approximately 850 m/s. Note: photos are not to scale.

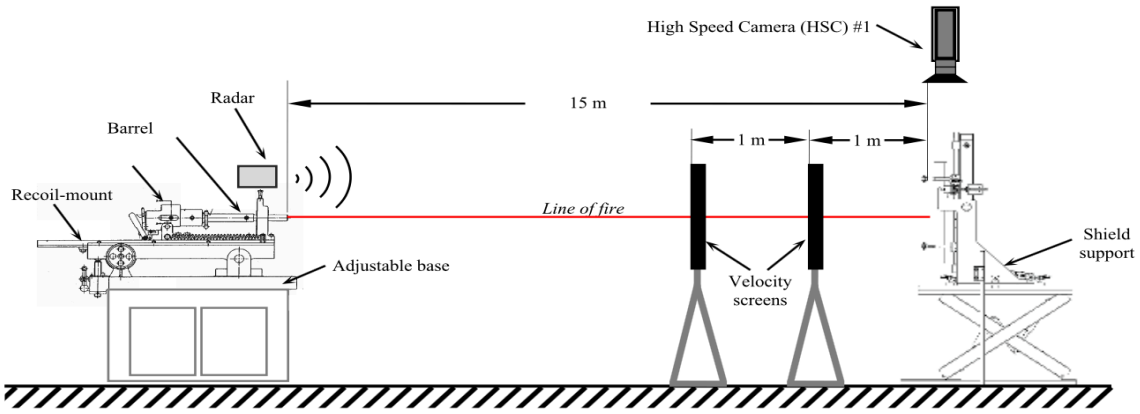

Figure 3.2: Schematic of the ballistic test range

The universal receiver barrel was set 15 m from the front face of the ballistic shield. Two velocity screens recorded the projectile velocity before impact and an overhead camera captured footage of back-face deformation for analysis [53].

The first step when setting up each trial was aligning the universal receiver with the desired impact location on the ATD using the laser sight. This alignment was completed before the shield was put in place (Figure 3.3). The ATD was positioned so the PCB force sensor was centered on the laser sight. This was done by adjusting the vertical and horizontal position of the ATD with the testing jigs (Chapter 2). The flesh surrogate was removed from the ATD (discussed in Section 3.2.2) and two 2 cm x 2 cm x 0.16 cm sections of Infinisil silicon rubber with a durometer of 50 shore A (Warco Biltrite, Orange, CA, USA) were placed over the top of the sensors. Images within this document occasionally show the ATD with the flesh surrogate as these images were taken prior to the removal of the flesh.

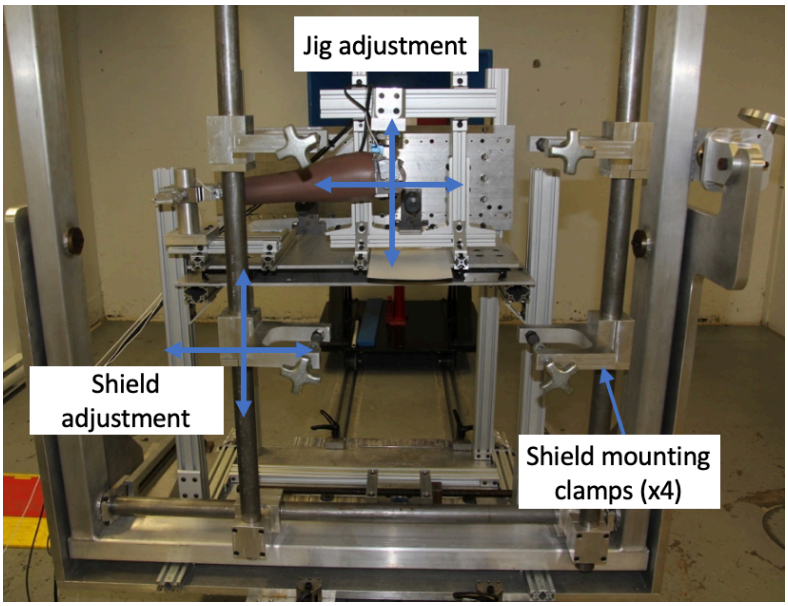

Figure 3.3: Front view of the set-up before the shield was put in place

Arrows in this image show the directions of adjustability of both the jigs as well as the shield positioning. The jig adjustment allowed the PCB force sensor to be aligned with the laser sight, while the shield adjustment allowed the shield to be positioned. Note: The ATD flesh is shown but was not used during impact testing.

Next, the shield was secured in place using four mounting clamps built into the frame of the support structure and positioned so the selected impact location aligned with the laser sight. After each trial, the shield was re-positioned to align a new location that had no previous damage. The final adjustment was to control the stand-off distance. A physical spacer (ranging from 10 mm to 40 mm depending on the trial) was placed between the back-face of the shield and the impacted sensor and the jig was moved towards the back-face of the shield (via the bearings) until contact was made to control the stand-off distance. Finally, the shock absorbers were positioned 40 mm from the rear impact plate to provide consistent travel distance for the jigs in each trial (also using a physical spacer).

After the shield and ATD were secured in place, the projectile was loaded into the universal receiver, then fired. The projectile traveled down the 15 m test range where its velocity was measured by two photoelectric screens (Model 53131A, Oehler Research Inc., Austin, TX) that were spaced 1 m apart. Upon impact with the shield, deformation was captured by an overhead high-speed camera (Fastcam SA-X type 324K-M2, Photron USA Inc., San Diego, CA, USA) that sampled at 30000 fps. The velocity screens, camera, and firing mechanism were integrated into the ballistic test range and data collection was triggered by a microphone at the end of the universal receiver.

Two separate data acquisition systems (DAQs) were used. The first, an NI PXIe-1082 (National Instruments, Austin, TX, USA) with an NI TB-4330 terminal block, collected data from the forearm and elbow load cells at 100 kHz. The second was a Genesis 5i (HBM Inc., Marlborough, MA, USA) with an HBM BAS1M_512 acquisition card, supplied by Defense Research and Development Canada (DRDC), which collected data

from the PCB force sensors at 1 MHz. The PCB force sensors required an Integrated Electronics Piezo-Electric (IEPE) current, as well as needed to be sampled at 10 times their 90 kHz bandwidth [51]. This required a separate DAQ since the available NI TB-4330 terminal block was not capable of sampling at the required 1 MHz. The Genesis 5i only had input channels capable of running the PCB force sensors, therefore both DAQs needed to be used in conjunction. The DAQs were positioned beside the test area and protected by a metal screen.

3.2.1 Testing Setup

As discussed in Chapter 2, the ATD was designed to be mounted in the shield jigs in a horizontal position. When mounting the ATD in this orientation behind the curved TYRT shield there was interference between the arm and the curved edge of the shield, not allowing the ATD forearm to be moved close enough to the back-face of the shield. For this reason, it was not feasible to do full arm testing on the TYRT shield. Therefore, two sets of tests were conducted: full arm tests using the flat AE shield, and single force sensor tests using the TYRT curved shield.

For the flat AE shield, the ATD was mounted in the jigs in the same orientation as was designed and discussed in Chapter 2 (Figure 3.4), allowing the ATD to be positioned behind the shield in the horizontal orientation. The flat AE shield was secured to the mounting frame, then the ATD was positioned behind the shield at the desired stand-off distance.

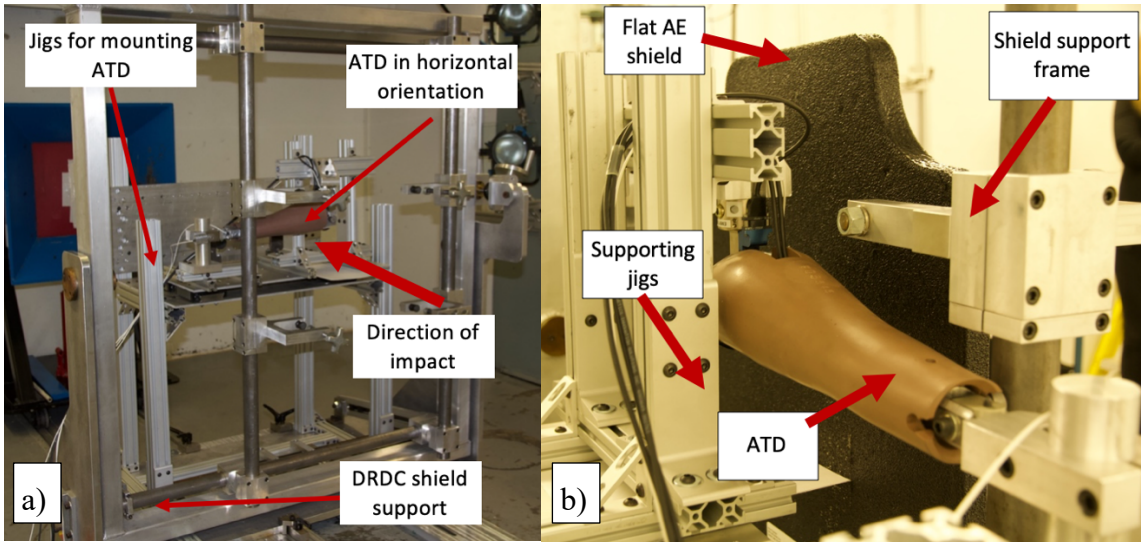

Figure 3.4: Horizontal orientation of ATD for AE shield testing

The ATD arm was secured in the DRDC testing jigs for conducting testing on the flat AE shield where it is shown in the a) front view (shield not shown) and the b) rearview. Note: The flesh shown in the image was not used during testing.

For the curved TYRT shield, a modified assembly was required. To maintain consistent post impact kinematics in all collected data, the modified assembly was secured to the same linear bearings. The wrist to elbow portion of the ATD limb was removed and only the hand was tested, which eliminated the interference between the shield and ATD. The rigid boundary conditions that were created in the modified assembly were the same as those that would be present if the full arm was attached to the hand, since the handle's response was not influenced by the presence of the ATD arm. As such, the modified assembly allowed the desired hand testing to be accomplished (Figure 3.5).

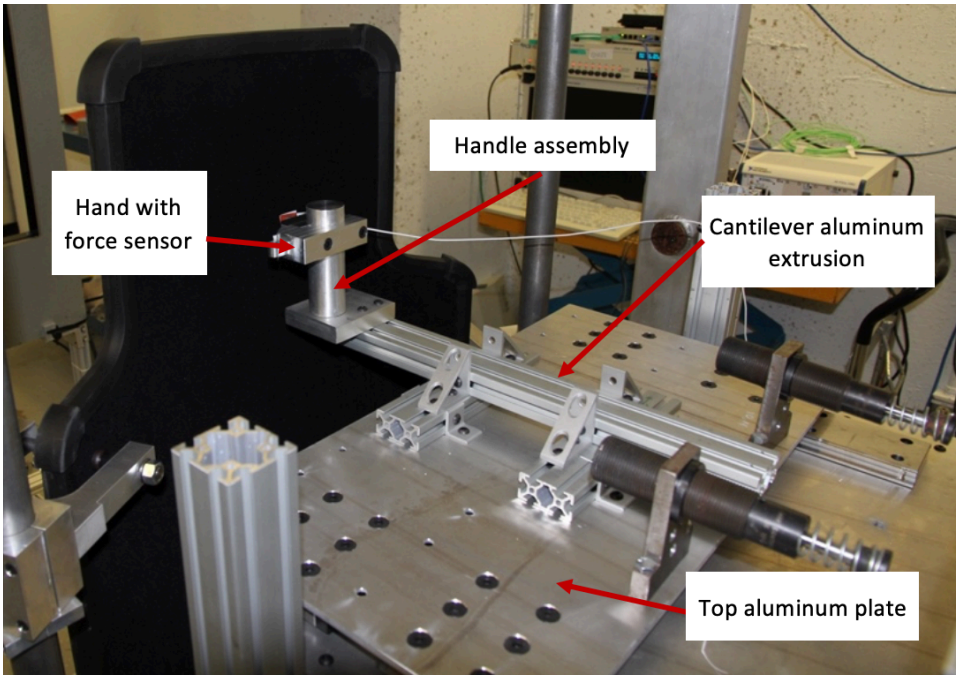

Figure 3.5: The modified jig for positioning the force sensor behind the TYRT shield
The hand and handle were mounted to a piece of cantilevered aluminum extrusion to allow the force sensor to come close enough to the back-face of the shield to meet the stand-off distance requirements.

To assemble the new force sensor mount, the handle assembly and modified hand were fastened to the end of a piece of cantilevered aluminum extrusion. This structure was secured to the top aluminum plate, which allowed the force sensor to be translated close to the shield (via linear bearings) without the edges of the shield coming into contact with the ATD.

3.2.2 Test Shot Plan

As ballistic shields are expensive, only five shields were available for testing: three flat AE shields and two curved TYRT shields. Each shield was used for multiple shots, where new shots were spaced at least 120 mm from both previous shots and the edge of the

shield [2]. After each impact, the location was examined, and if delamination exceeded 60 mm the next shot was placed at least 60 mm from the edge of the delamination. To minimize any adjacent effects due to delamination, shot order was randomized and thus shots were presumed to be independent.

The number of shields and required shot spacing limited the number of impacts to 32 on all the shields combined. The first 12 shots were used to identify specific stand-off distances that would contact the ATD (as the shields had different responses than those used in previous work [2]), as well as deal with data acquisition issues (summary of shots highlighted in Appendix D). Three issues were identified during these initial impacts that led to changes in the test plan (summarized in Table 3.1). First, the delamination that occurred during each impact was greater than initially anticipated. The delamination was the greatest close to the edge of the shields where delamination was once observed to blow out the side (shot 4). This resulted in fewer shots being possible, as the spacing between impacts tended to be greater than 120 mm (requiring shots to be spaced so their delamination did not overlap). Secondly, during the initial 12 shots, only the NI PXIe-1082 DAQ was used, which did not sample the PCB force sensors at a high enough frequency. As such, the two DAQ setup was used for the remaining 20 shots. Thirdly, the damping of the ATD PVC flesh was unknown and positioning the load cell was very difficult while underneath the flesh. It was also more valuable to specify the stand-off distance from the solid underlying ‘bone’ structure than the pliable skin surface. Therefore, for the final 20 shots, the ATD flesh was removed and replaced by the Infinisil silicon rubber.

Table 3.1: Overview of the ballistic testing

Shot Number	Shield Model	Location	Note
1-12	AE	Elbow	Evaluating appropriate stand-off distance and validating sample frequency
13-14	AE	Forearm	Focal loading damaged the forearm load cell
15-22	AE	Elbow	Data used for analysis
23-32	TYRT	Hand	Data used for analysis

After the initial 12 shots, two shots were conducted on the AE shield at the forearm impact location to characterize its response. During these impacts, the back-face deformation was found to be highly focal, causing permanent deformation on the side of the forearm load cell, resulting in both the failure of the forearm load cell (Figure 3.6) and having to discard these two shots. This left only 18 shots for data collection: eight on the AE shields and 10 on the TYRT shields. Due to the limited shots, repeatability was prioritized over the evaluation of multiple impact locations. Since the elbow was now the most highly instrumented location (providing both moments and impact force) it was used. The hand was prioritized over the wrist as it could more easily be used in the TYRT shield set-up.

A revised test protocol was thus developed that focused on two impact locations (hand and elbow), each of which was fit to the respective shield design. Two stand-off distances were tested at each impact location, where different distances were selected for each shield given their differing back-face response. At least four shots were carried out at each location to replicate the protocol followed by Bolduc, and characterize the variability in the results [2].

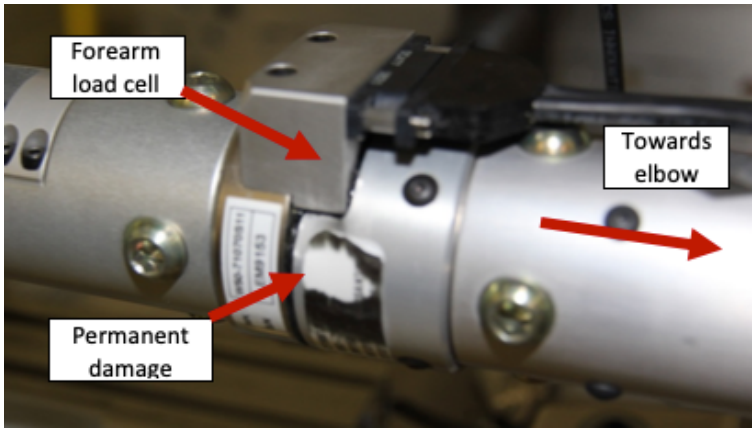

Figure 3.6: Damaged forearm load cell

The figure shows the permanent damage experienced by the forearm load cell due to the direct forearm impact.

For the flat AE shield, the expected behind shield response was based on the work by Bolduc et al. [2], as such stand-off distances of 30 mm and 40 mm were planned. However, during the initial impact trials, the flat AE shield deformed much less than the shields tested by Bolduc et al., in the range of 20 mm. As such, with only eight shots available, four shots were completed at each of the 10 mm and 20 mm stand-off distances (Table 3.2). As the TYRT shield was a different design than the AE shield, the back-face deflections had to first be assessed to create the test plan for this shield. The expected shield response from Bolduc et al. [2] was up to 40 mm, so the first test shot was conducted at 40 mm to evaluate the deformation. At the 40 mm stand-off distance the shield made contact with the force sensor, so five impacts at each of 30 mm and 40 mm were completed for testing the TYRT shield (Table 3.2).

Table 3.2: Summary of final shot plan

Location	Shield	Stand-off distance (mm)	Repetitions
Elbow	AE Flat	10	4
Elbow	AE Flat	20	4
Hand	TYRT Curved	30	5
Hand	TYRT Curved	40	5

3.2.3 Data Analysis

The high-speed video footage was analyzed in Photron FASTCAM Viewer Software (Photron USA Inc., San Diego, CA, USA) to characterize and compare the responses of the different ballistic shields. The apex of the deformation profile was used as the landmark and was tracked in each frame to determine the total shield displacement and shield velocities. Three impacts were analyzed for each shield for the portion of the video in which there was no contact between shield and ATD (~10 frames), so the back-face motion was not obstructed. Fortunately, three of the initial impacts conducted on the AE shield did not experience any contact with the ATD. These were analyzed allowing the full velocity profile to be characterized uninterrupted. However, there were no shots conducted on the TYRT shield that did not experience contact with the ATD. Therefore, to minimize the interference between the ATD and the TYRT shield, three shots at the 40 mm stand-off distance (furthest stand-off distance used with the TYRT shield) were analyzed.

The ATD load cell data were filtered in Matlab (MathWorks, Natick, MA, USA) with a 2-pole 2nd order Butterworth filter with a cut-off frequency of 1,250 Hz [54], while the DRDC technical team filtered the PCB data with a 50 kHz two-pole low-pass Bessel filter. The peak forces and moments, the duration of impacts, and the impulse were identified

using Matlab. To determine the impact durations an algorithm searched either side of the peak force until the point that was 5% of the peak force was found. These points were identified to be the 'start' and 'end' of the impact and the time difference was the impact duration. While the peak force was easily identified, the start and end point locations were complicated due to noise in the system (likely from vibrations). A Gaussian smoothing filter was applied to the data to remove extreme peaks that would interfere with the calculation of the start and end points (Figure 3.7). This filter was selected as it was a moving average filter that was particularly good at removing high frequency noise.

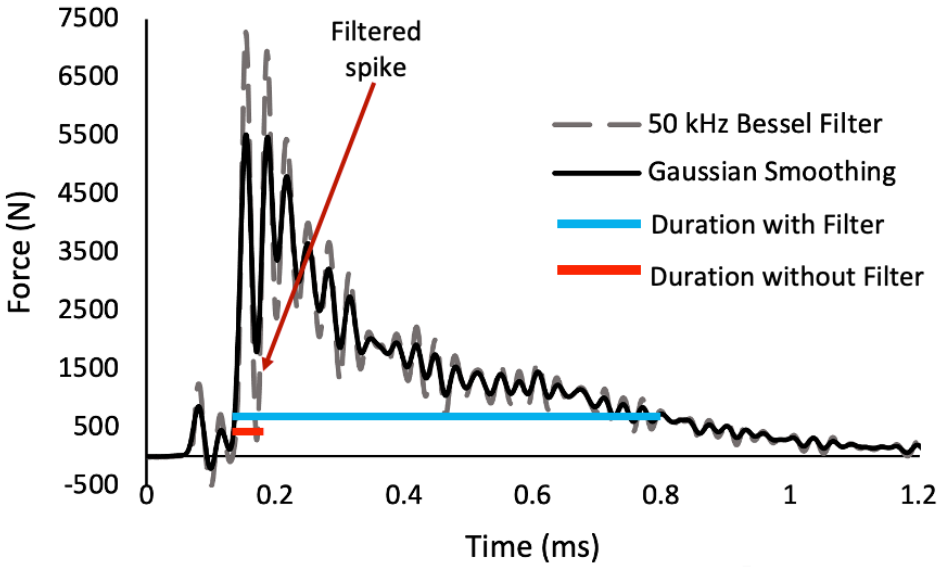

Figure 3.7: Comparison of the filtered PCB impact data and smoothed data

The impact data is plotted with both the 50 kHz Bessel filter and the Gaussian smoothing function, where large data spikes were removed. Removing these large spikes allowed the impact duration to be evaluated more consistently, as the initial step response was maintained, and large data spikes were smoothed.

A noise spike is defined as being made of a discrete number of points [51]. With a sample frequency of 1 MHz and a cut-off frequency of 50 kHz, the noise spikes were calculated to be made up of 10 data points. A window size of 30 points was used for the Gaussian filter to ensure that any spike would have 10 points on either side of it, ensuring that all the spikes would be averaged with points outside the spike width.

During the smoothing process, extreme points were removed to allow the search function to identify the start and end points; however, this also reduced the max force. While this may appear problematic it is important to note that the maximum force and time of peak force (where the search function would start) were identified before the smoothing was applied to the data. As such, the smoothing was only used to determine the duration of impact and did not have any effect on the magnitude of the peak force. Finally, the impulse was calculated in Matlab by doing rectangular integration over the force time curve on the original filtered data but using the time points found from the smoothed data. This ensured that the impulse corresponded to the peak forces that were experienced, but also contained the full duration that was present in the force curve.

Finally, the impact data were analyzed and the peak forces and moments, impact durations, and impulses were characterized at each impact condition. The mean, standard deviation, and coefficient of variation were calculated for each of these variables, which were then compared using a two tailed student t-test (α=0.05).

3.3 Results

3.3.1 Comparison of Shield Back-face Velocity

Throughout all trials, the IVI C21 projectile had a mean velocity of 841.9 ± 16.9 m/s. The back-face shield velocity from the video footage was related to the shield deformation. For the three videos analyzed for each shield, both the AE and TYRT shield had a roughly parabolic velocity profile, where the peak velocity for the AE and TYRT shields occurred at 58% and 38% of the maximum deformation, respectively (Figure 3.8). The peak velocity for the AE shield was 181 ± 35.5 m/s with a max deflection of 1.77 ± 0.3 cm, whereas the peak velocity for the TYRT shield was 275 ± 13.9 m/s with a mean max deflection of 3.96 ± 0.1 cm. The AE and TYRT shields had their maximum velocity occur when the shields had deformed by 1.02 ± 0.2 cm and 1.50 ± 0.34 cm, respectively. The AE shield had a significantly lower maximum back-face velocity compared to the TYRT shield (34% lower, p=0.026) (Table 3.3). Further, the AE shield had a maximum distance traveled that was 55% lower than the TYRT shield, which was also statistically different (p<0.001).

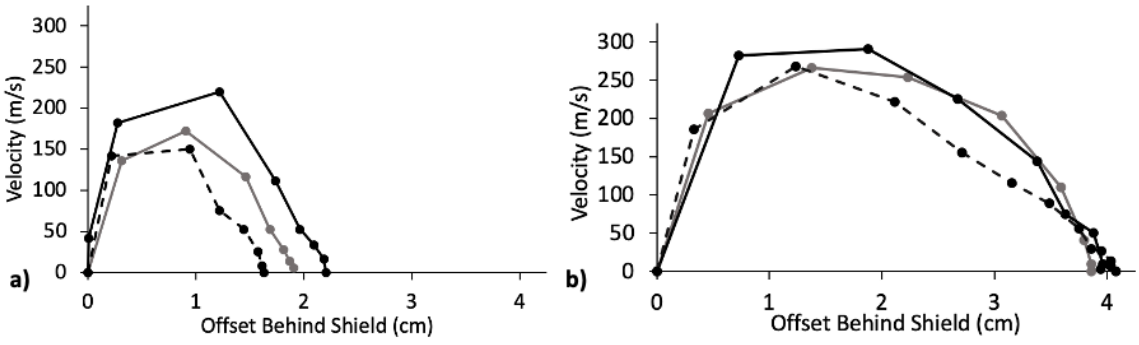

Figure 3.8: The back-face shield velocity related to the offset from the shield

Comparison of the back-face shield velocity related to the distance behind the shield for the a) AE and b) TYRT shields. Note: The TYRT shield experienced contact between the shield and ATD while the AE shield did not.

Table 3.3: Comparison of the back-face shield velocity, deformation, and location of peak velocity for the AE and TYRT shields

Shield	Peak Velocity (m/s)	Deformation (cm)	Deformation at point of Peak Velocity (cm)
Flat AE Shield	181 ± 35.5	1.77 ± 0.3	1.02 ± 0.2
Curved TYRT Shield	275 ± 13.9	3.96 ± 0.1	1.49 ± 0.3

Due to the lighting and video resolution, it was difficult to identify the shield borders, which introduced some error. Samples frames from the analyzed footage are shown in Figure 3.9. To quantify this error, the max velocity for the first shot on the AE shield was analyzed six times by the same person. This resulted in a mean peak velocity of 201.3 ± 16 m/s, with a coefficient of variation of 8%.

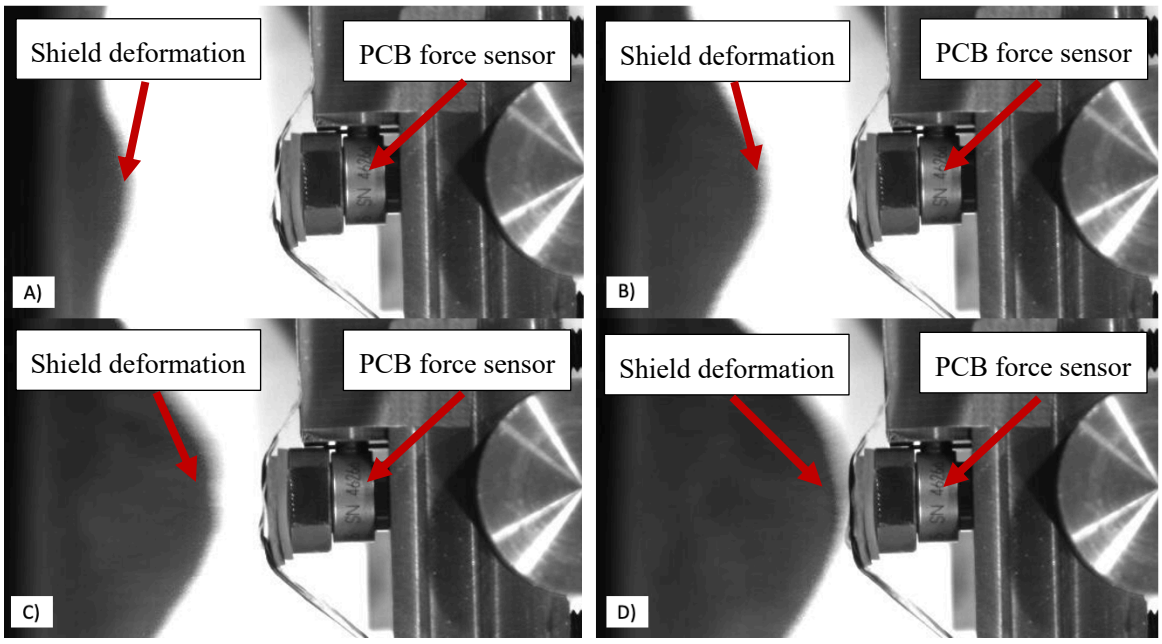

Figure 3.9: Sample video frames from the video footage

The behind shield deformation that was captured with an overhead highspeed camera is shown, where the deformation progresses from A) the least deformation to D) the greatest deformation. The deformation profile is shown to be slightly blurred at the border due to lighting challenges and extremely high-speed motion.

The velocity at each stand-off distance (*i.e.* 10 mm and 20 mm for the AE shield) was approximated. To do so, the velocity data for each shield was plotted in a scatter plot (separate graphs for AE and TYRT shields) to provide an average shield response. A fourth order polynomial with a y-intercept of zero was fit to the velocity data for each shield as it provided the best R^2 value of the available trendlines on Microsoft Excel (Figure 3.10). The R^2 values for the AE and TYRT shield data were 0.72 and 0.96, respectively. For the AE shield stand-offs of 10 mm and 20 mm were used, which corresponded to approximate back-face velocities of 160.0 m/s and 20.4 m/s. The TYRT shields were struck at 30 mm and 40 mm, which corresponded to approximate back-face velocities of 163.6 m/s and 6.5 m/s, respectively.

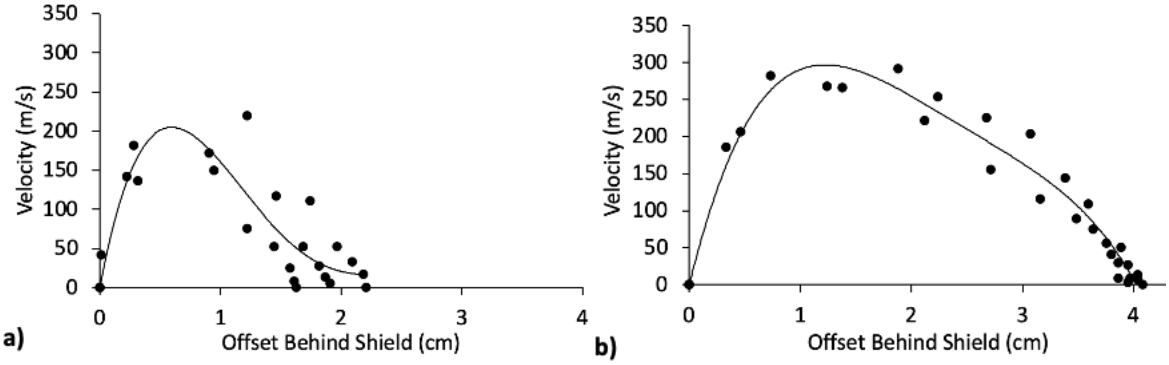

Figure 3.10: Trendlines fitted to back-face velocity data for approximating shield velocity at specific deformations

A fourth order polynomial trendline was fit to a) the flat AE (R^2=0.72) and b) the curved TYRT (R^2=0.96) shield back-face velocity data. This trendline allowed the velocity at stand-off distances for each shield to be approximated.

3.3.2 Flat AE Shield

The peak force and load duration were measured for the PCB force sensor and peak moment was measured in the ATD elbow load cell (Table 3.4). When moving from 20 mm to 10 mm stand-off, impact force increased by 40% (p=0.21) and elbow moment increased by 128% (p=0.046). While both the force and moments showed a trend of decreasing as the stand-off distance was increased, only the moments were found to be statistically different. The loading duration also changed when moving from 20 mm to 10 mm stand-off distances, with the force duration dropping by 66% (p<0.001), which was statistically significant. Finally, the impulse (measured by the PCB impact load cell) decreased by 39% (p=0.11) when the stand-off distance was moved from 20 mm to 10 mm. Force curves in Figure 3.11a) and c) illustrate each shot, while the mean force curve and standard deviation are shown in Figure 3.11b) and d).

Table 3.4: Results from elbow shots (N=4 for each test condition). Data from PCB impact force sensor and ATD elbow moment load cell

Measure	Stand-off (mm)	Mean ± SD	Coefficient of Variation (%)
PCB Impact Force (N)	10	5083 ± 1647	32.4
	20	3624 ± 720	19.9
PCB Elbow Impact Force Duration (ms)	10	0.39 ± 0.06	14.6
	20	1.16 ± 0.16	14.1
Impulse of PCB Impact Force (Ns)	10	0.70 ± 0.24	34.4
	20	1.15 ± 0.33	29.0
Elbow Moment (Nm)	10	37.4 ± 20.9	55.9
	20	16.4 ± 3.3	19.9

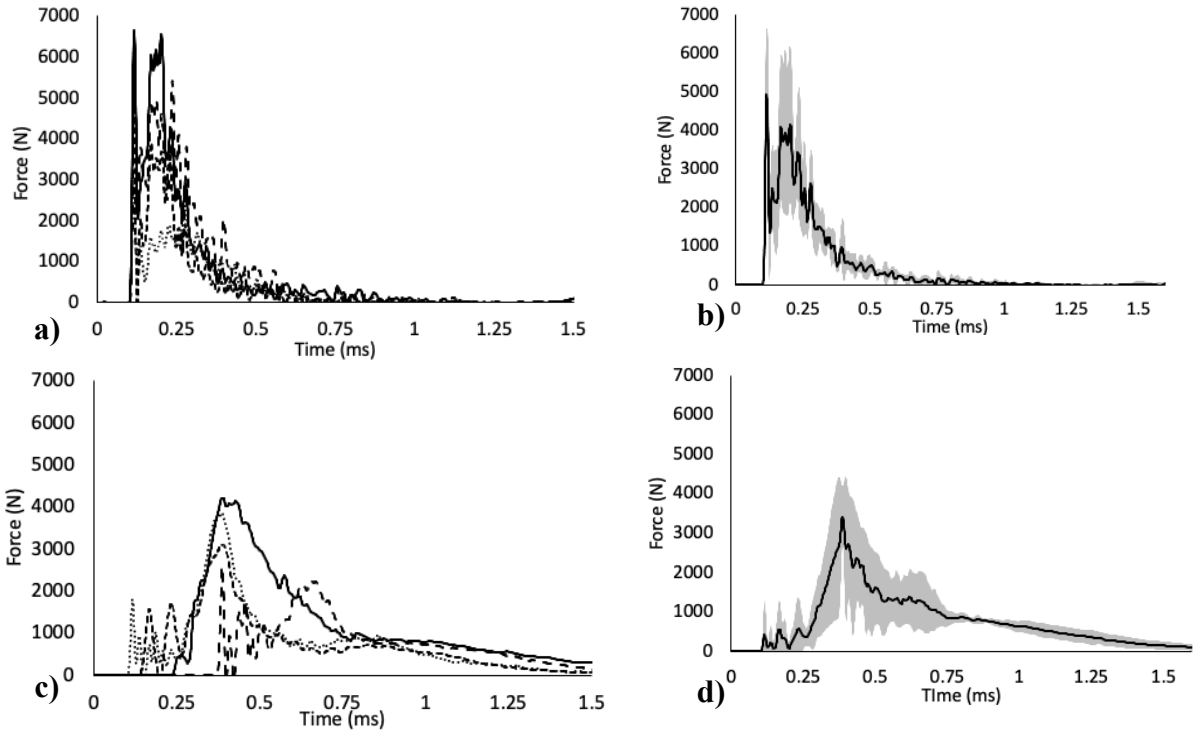

Figure 3.11: Loading profiles collected for flat AE shield

The force curves are shown for a) the 10 mm stand-off elbow force traces, b) the mean (± SD) 10 mm stand-off elbow impact force, c) the 20 mm stand-off elbow force traces, and d) the mean (± SD) 20 mm stand-off elbow impact force.

3.3.3 Curved TYRT Shield

The peak forces, impact durations, and impulses were calculated from the PCB force sensor on the hand. When reducing the stand-off distance from 40 mm to 30 mm, the peak force and impulse both increased significantly by 129% ($p=0.016$) and 79% ($p<0.01$), respectively, while the impact durations remained approximately the same ($p=0.72$). As with the elbow shots, the standard deviations remained quite large, resulting in substantial coefficients of variation ranging from 7% to 36% (Table 3.5). Sample force curves for the TYRT shield impact are found in Figure 3.12. Note: during all impacts, there was very little

post impact motion (<2 cm) as such the shock absorbers mounted to the jigs never contacted the rear plate.

Table 3.5: Results from hand shots (N=5 for each test condition). Data from PCB impact force sensor

Measure	Stand-off (mm)	Mean ± SD	Coefficient of Variation (%)
Hand Impact Force (N)	30	5321 ± 1157	21.7
	40	2323 ± 833	35.9
Hand Impact Force Duration (ms)	30	0.85 ± 0.16	18.2
	40	0.86 ± 0.06	7.3
Hand Impact Impulse (Ns)	30	1.13 ± 0.13	11.8
	40	0.63 ± 0.23	36.0

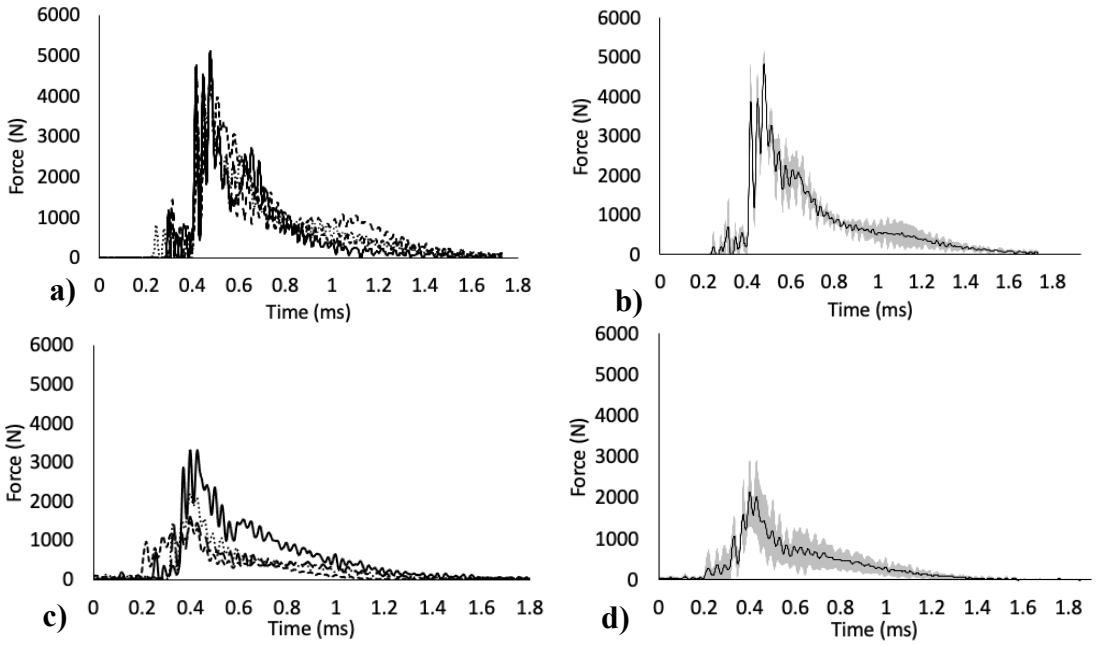

Figure 3.12: Loading curves from the curved TYRT shield

The force curves are shown for a) the 30 mm stand-off hand force traces, b) the mean (± SD) 30 mm stand-off hand impact force c) the 40 mm stand-off hand impact force traces, and d) the mean (± SD) for 40 mm stand-off hand impact force.

3.4 Discussion

This study subjected a customized upper extremity ATD to behind shield blunt trauma testing to develop a thorough characterization of the loading profiles experienced during shield BABT. This study represents the most complete assessment of behind shield loading that has been performed to date. As this work directly aimed to continue the work conducted by Bolduc et al. [2] the tests conducted were designed to avoid the limitations in the previous study. Boundary conditions were selected to better represent the post kinematic motions by allowing translation of the ATD after impact. This work also tested both a rigid hand (crushing hand against handle) and a cantilevered elbow, which represent realistic loading conditions. Therefore, the data presented in this work were measured with more realistic boundary conditions than any previous studies. The back-face shield motion was characterized to allow the velocity at any stand-off distance behind the shield to be estimated. In addition, this study compared the response of two different ballistic shield models, which both had the same ballistic rating, to investigate the differences in response for equally rated shields.

3.4.1 Comparison of AE and TYRT Shields

All video footage analyzed for the TYRT shield had contact with the ATD, while the footage for the AE shields did not have contact. While it is true that the entire velocity profile could not be characterized when there was contact with the ATD, conclusions about the shield response can still be made. The contact with the ATD did not affect the peak velocity and only influenced the maximum shield deformation since the ATD stopped the deformation early. However, due to the larger stand-off distances used during TYRT shield

tests, comparisons between the shield responses could still be made, even if the true maximum deflection was not characterized. While it was valuable to observe the differences between the two shield designs, the critical data collected from this analysis was the predicted velocity at the point of impact. Both the velocity profiles for the AE shield and TYRT shield were very different and followed a roughly parabolic shape with velocity starting at zero. This emphasizes that the NIJ 0108.01 ballistic ratings are not indicative of the back-face deflections that each shield has. Additionally, velocity curves allowed shield velocities to be approximated at specific stand-off distances, which will be targeted during future PMHS testing.

The objectives outlined in Chapter 1 aimed to compare the impact profiles generated from the two shield types when the stand-off distances were the same. Unfortunately, directly comparing the two shields impact profiles was not possible, since the shields were both impacted at different stand-off distances and had different sensor configurations. However, it was still possible to conclude valuable information about the differences in the shield responses and speculate about the relationship to the impact profile. Since the maximum velocities and deflections between shields were different, if both shields were tested at the same stand-off distance the shields would exhibit vastly different impact profiles. This highlights a need to characterize the maximum deflection as well as a maximum force when specifying shield designs.

Each of the shields were designed as Level III ballistic shields under NIJ 0108.01 [1] but performed very differently under the same Level III testing protocol. This can be misleading to those purchasing and using these shields as the TYRT shield provides a lower

level of protection through force attenuation but is not clearly communicated or tested during the shield evaluation. Even when shields are specified as being able to withstand the same ballistic rating, there are still significant differences in their response. Therefore, a standard is needed against which shield designs can be evaluated so that they not only consider risk due to projectile penetration but also consider the back-face deformation.

3.4.2 Shield Impact Profiles

For both shields, it was noted that as the stand-off distance was increased, the mean peak impact force decreased. This observation is consistent with what was found by Bolduc et al. where they observed the same trend [2] (Figure 3.13). While the shield model used during the work by Bolduc et al. was not known, the trends they observed aligned well with the magnitudes of back-face deflection for the TYRT shield. The data collected during the present work was highly variable, which was unsurprising given that the previous study also had high variability. However, the data collected during this work was less variable than that of the previous work. This was likely due to the use of the Infinisil silicon rubber flesh and linear bearings, both of which provided mechanical damping to the system. This resulted in more consistent force measurement as extreme data points were filtered out. Additionally, the magnitudes of forces varied from the previous study, which can be attributed to differences in test setup and the shield used.

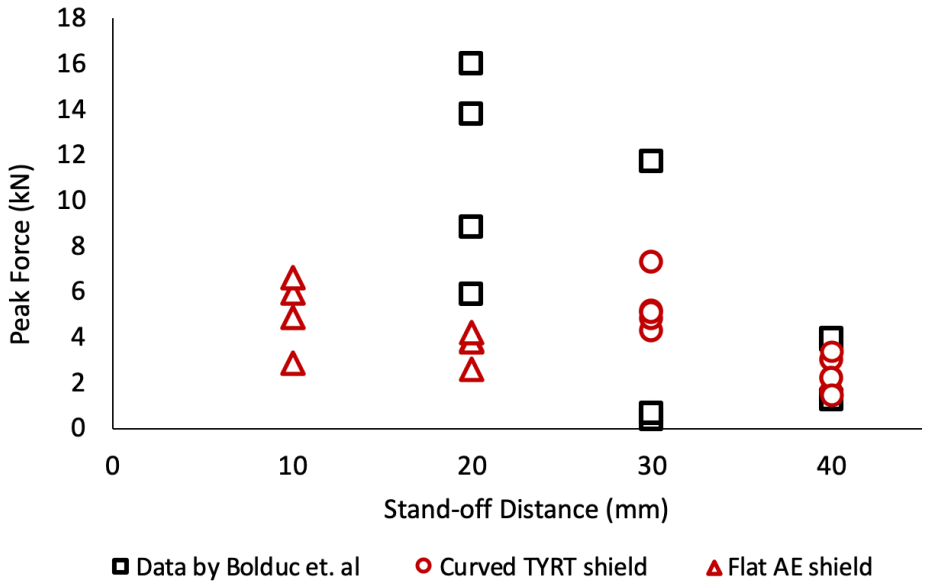

Figure 3.13: Comparison of impact data from this work and Bolduc et al.

This plot illustrates the peak impact forces measured during behind shield BABT impacts during this work and in the work by Bolduc et al. [2]. The data collected during this work was less variable than the data collected by Bolduc et al.

As the back-face shield velocity decreased with shield stand-off distance so too did the transferred force. This trend was observed both for the AE and TYRT shields and was due to more energy being absorbed by the shield deformation as the stand-off distance was increased. Interestingly, during the AE shield impact, with the same increase in stand-off distance, the peak elbow moment decreased by a much higher percentage than the peak force. Based on the definition of moment, if the moment arm is held constant than the force should be proportional to the moment. Since these impacts were applied to the same locations, the force and moment should have increased or decreased proportionally. However, based on video analysis, the peak deflection was found to not always be perfectly aligned with the sensor's central axis, therefore, this discrepancy is likely due to impacts

being applied off-axis (Figure 3.14). The PCB force sensors were only capable of measuring uniaxial forces and had no indication of the force that was applied directly along the central axis. This observation highlights the difficulty in aligning the apex of the back-face deflection with the load cell as a slight off-set of the bullet could lead to off-set of the deformation. Additionally, this provides insight for the selection of the force sensor dimensions in future iterations of an ATD, as they must have a large enough impact cap to capture for off-axis loading while being able to resist bending moment. Finally, this highlights the importance of proper contact between the back-face deformation and the force sensor so that the force is properly characterized.

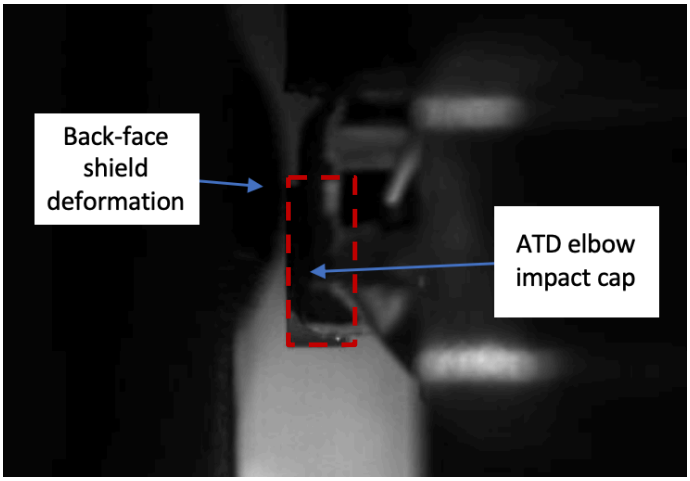

Figure 3.14: Off-axis back-face shield deformation

The back-face shield deformation impacting off the central axis of the ATD impact cap, where the border of the impact cap is outlined in red. The footage was inspected after each impact to ensure the apex of the shield deformation contacted the impact cap.

The trends observed with the duration of impact were counterintuitive. For the AE shield, the impact duration increased when the stand-off distance was increased, while the TYRT shield did not change when the stand-off distance was changed. The difference in these two trends is likely due to the change in inertia of the impacted jigs between the two tests, where the ATD structure (except the hand) and some of the associated frame were removed during the TYRT shield testing. This reduction in inertia allowed the testing jigs to move out of the way more readily during the TYRT testing which likely resulted in a more consistent impact duration.

Since the impulse is dependent on both the force and duration it can be observed that the AE shields impulse was most influenced by the significant increase in the duration of impact when the stand-off distance was increased, where the TYRT shield was more influenced by the significant force increase (since its duration of impact remained constant between the two events). Previous studies have identified that there is an inversely proportional relationship between impulse and injury risk [55], [56]. This would imply that if only the impulse was used for injury prediction, for the injury risk behind an AE shield would increase with increased stand-off distance, while the injury risk for the TYRT shield would decrease with increased stand-off distance. These relationships indicate that reducing the peak force experienced during behind shield impacts may not be the only way to control the reduction of injury risk, as controlling the duration of impact with trauma attenuating backings (TABs) may be equally useful at mitigating injury risk. It would be valuable to further investigate the effect of impact duration on injury criteria during future PMHS work.

Since the force was reduced by increased stand-off distance, the transferred force to stand-off distance relationship should be used as an evaluation metric to assess the safety of a shield. Additionally, the duration of impact must be considered during shield design as it is related to injury risk and is not necessarily consistently correlated to stand-off distance. These metrics would provide shield designers with more information for selecting both custom stand-off distances and TABs for each shield, resulting in safer products for end users.

3.4.3 Limitations

While a number of interesting outcomes came from this work, the primary limitation was the number of possible shots available. This led to only two locations being investigated (instead of four), only four impact trials for repeatability, and required shots to be placed in close proximity. The close shot placement may have led to effects from adjacent shot damage. Steps were taken to reduce this effect, but it was not possible to verify that residual damage had no effect as internal imaging was not available for use in this work.

A secondary limitation was that it was not possible to do a direct force comparison between the AE shield tests and the TYRT shield tests. This is because the TYRT set up used the handle and hand PCB to measure the loading at the hand, while the AE shield used the full arm to measure loading at the elbow. The boundary conditions that each of the locations experienced would be different and thus a direct comparison cannot be made. This does not directly affect any of the results discussed herein, however, it is crucial to

understand the difference in boundary conditions as it limits the ability to directly compare the measured forces between the AE and TYRT shields.

The final limitation was the limited number of shots that were possible during the testing. As there were only five ballistic shields that could be tested (three AE and two TYRT) it was not possible to collect a lot of data for each impact condition. For this reason, the AE impact scenarios only had four shots and the TYRT shields had five shots for each condition. With the limited number of data points, data would be sensitive to sensor misalignment (as observed in video footage), which likely led to large standard deviations. Despite this error, the variability found during this work was lower than that of Bolduc et al. and will guide future test plans in selecting a larger number of shots for each impact scenario.

3.4.4 Next Steps

As this testing was the first set of ballistic trials that is to be conducted at DRDC there were three things identified that must be done before the second round of testing, is possible. These include a re-design of the ATD, a re-design of the testing jigs, and obtaining a greater quantity of ballistic shields.

Firstly, due to the damage that was experienced by the ATD arm during the ballistic testing, a revision of the design must be completed. The re-designed ATD arm needs to include instrumentation to collect loading at the elbow, forearm, wrist, and hand, and be as similar as possible to the original design to provide an easier comparison between the first trials discussed herein, and future testing. A primary goal of the re-design will be having

the ATD load cells more durable than the ones in the original design. While the load cells included with the WorldSID 50th percentile were designed to withstand automotive collisions (blunt impacts), the impacts experienced during ballistic testing were much higher magnitude of loading at more localized points, which led to the failure. For this reason, either protecting and securing the previous load cell model or incorporating a more durable load cell into the design is required.

Secondly, the jigs that were used to evaluate the shield must be re-designed. The geometry of the curved shields was not compatible with the jigs as the shield design that was to be tested had not been determined when the initial jigs were designed. Future iterations of the jigs must be capable of bringing the ATD arm into contact with the shield without any interference with the jigs. This change would allow the same set of jigs to be used for all testing completed regardless of shield curvature, allowing a direct comparison between the shields.

The final step will be obtaining a greater number of ballistic shields for the next round of testing. As there were only five shields in total, the number of shots was lower than expected, greatly limiting the number of possible trials and resulting in very few data points for each test. This error will be avoided on the second set of trials by obtaining at least 10 ballistic shields to double the amount of data that will be collected.

3.5 Conclusions

This chapter highlighted the first study that quantified ballistic shield BABT type force curves using a custom ATD. The mean forces and moments, durations of impact, and

impulses were measured for two different shield designs and their relationship to stand-off distance was investigated. A strong trend was observed where the maximum impact force and elbow bending moment increased as the stand-off distance was reduced. This information is particularly valuable as it indicates that the applied force from behind shield impact can be greatly reduced if the upper extremity is moved further from the back-face of the shield.

The back-face response was highly dependent on the shield model being tested, even when they had the same ballistic rating. The AE shield was capable of reducing the back-face velocity and the deformation when compared to the TYRT shield. This indicates the need to have a secondary metric for evaluation of shield safety. A standard or evaluation tool is needed to allow designers to safety position the arm behind the shield, and ensure users are informed about the level of protection each shield provides.

The impact durations and force ranges were measured, and the back-face shield velocity was approximated for the associated stand-off distances. All of the parameters gathered from this work provide ranges of impact conditions to target when re-creating the impacts for the future development of injury criteria. Finally, many of the injury criteria that were discussed in Chapter 1 were in the range of 4 kN, which is within the ranges of forces that were identified during this work. As such, there is potential to reduce injury risk by increasing stand-off distances in shield design.

Chapter 4 – Development of Modified Pneumatic Impacting Apparatus

4.1 Motivation

Due to the rapid back-face deformation of ballistic shields during impact, the upper extremity is at risk of being injured as high forces can be transferred if this deformation contacts the arm. No known previous studies have evaluated the injury tolerance of the upper extremity in this context, as such no metric exists to limit the transferred force in this Behind Armor Blunt Trauma (BABT) scenario. To determine a limit to the allowable transferred force, a study is needed to develop the injury criteria for the upper extremity for high energy, short duration impacts.

To develop these injury criteria, force-time profiles similar to those found during ballistic shield testing must be delivered to Post-Mortem Human Specimens (PMHS) to identify fracture limits, as well as locations where injuries occur. Due to the practicalities surrounding the testing of biological tissues, testing with PMHS is not generally conducted in a ballistic test range. A system was therefore needed that could deliver the representative impact profiles in a laboratory where PMHS could be tested. The final objective of this thesis was to adapt an impacting apparatus to be used in the future to develop injury criteria for the upper extremity in BABT type injury scenarios.

The McMaster Injury Biomechanics laboratory had an existing pneumatic impacting apparatus that could deliver impacts to PMHS and provide both a high degree of control and repeatability in the impact profiles created [43]. This apparatus has been used in the context of developing injury criteria for a range of scenarios [56]–[59]; however, it has never been used to assess the risk of upper extremity injuries nor has it created loading

profiles like those found behind shields. This chapter will highlight the re-design and modification of the previous pneumatic impactor, focused on both increasing the maximum obtainable velocity and modifying the configuration to test upper extremities to allow impacts collected during DRDC ballistic trials (Chapter 3) to be replicated in the lab.

4.2 Methodology

4.2.1 Previous Pneumatic Impactor Design

The original impactor design was made up of four main sub-assemblies: the pneumatics, the acceleration tube, the projectile, and the impact chamber. The function of each of these will be discussed herein.

4.2.1.1 Pneumatic System

Compressed air was inlet from the building (max pressure 80 psi) through an air regulator (NBC-400, Royal Fluid Power, Burlington, ON, Canada), allowing the inlet air pressure to be adjusted as desired. A hose ran from the regulator to a pressure tank (A10040-MOD, Samuel Pressure Vessel Group, Marinette, WI, USA), which was bolted to the floor and monitored by a digital pressure gauge (DG25, Ashcroft, Stratford, CT, USA) (Figure 4.1).

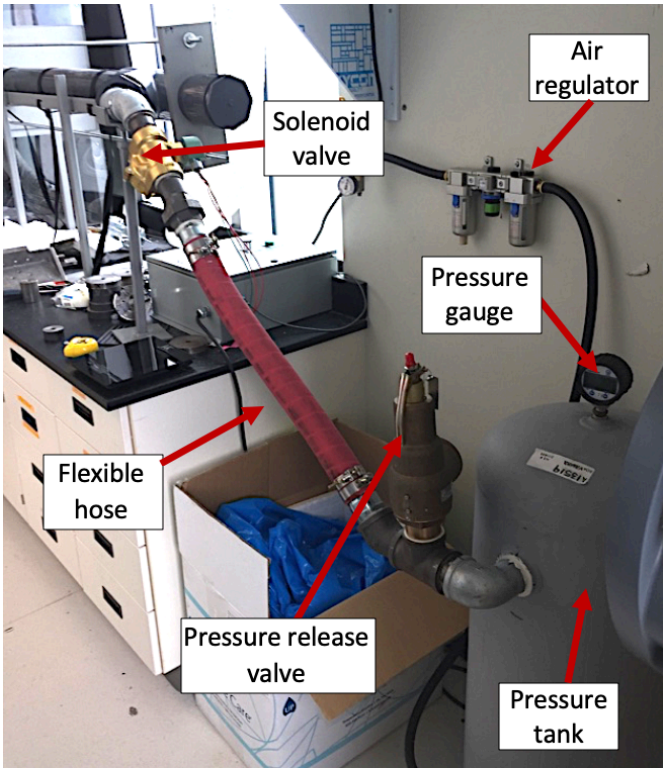

Figure 4.1: Pressure tank assembly

The pressure tank was mounted on the floor and was connected to the acceleration tube with a flexible hose. The air was inlet to the pressure tank through an air regulator and released to the acceleration tube by a solenoid valve.

Between the pressure tank and the acceleration tube was a 2” diameter flexible hose that countered vibrations or slight translation of the system during impacts. A solenoid valve released the air (821010324, ASCO, Florham Park, NJ, USA), which was controlled by a relay (Zelio Logic 2, Schneider Electric, Rueil-Malmaison, France). This relay opened the solenoid for a set time, thus controlling the duration over which pressure was applied to the projectile during firing.

4.2.1.2 Acceleration Tube

The acceleration tube (into which the projectile was placed) was made from a four-inch diameter PVC pipe (four feet in length). The acceleration tube was rigidly fastened to the impact chamber through the use of two tie rods (Figure 4.2A). There were two separate entrances to the acceleration tube, split with a PVC wye joint (Figure 4.2). The first leg of the wye joint was connected to the solenoid valve and pressure tank that injected the pressurized air. The second was an opening that allowed the projectile to be loaded. When loaded, the projectile was pushed past the inlet of the air, so once the pressurized air entered, it drove the projectile forward.

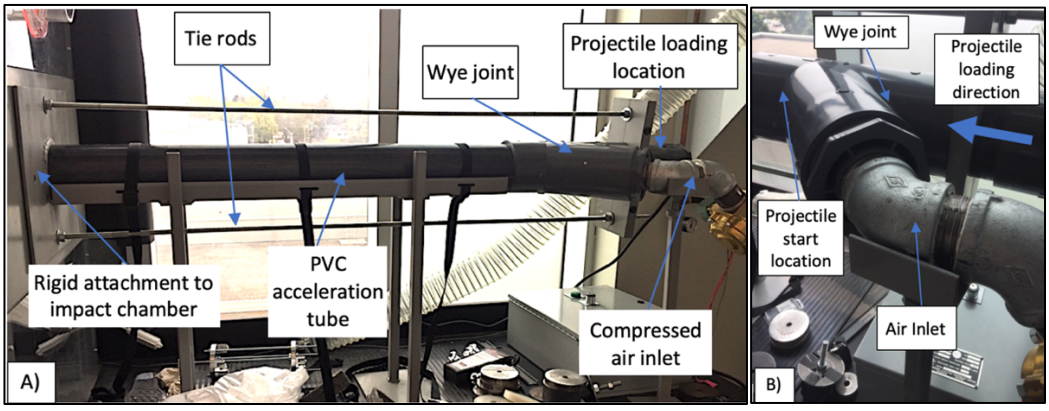

Figure 4.2: PVC acceleration tube

A) The PVC acceleration tube was rigidly mounted to the impact chamber with tie rods. B) The PVC wye joint is shown, where the direction of projectile loading and the location where the projectile was set before being fired are labeled.

4.2.1.3 Projectile

The original projectile was designed to have a variable mass and provided a simple design. Circular disks (each approximately 1 kg), with clearance holes in the center, were

placed on a threaded rod. These disks were stacked to achieve the required mass, and a nut on either end was tightened to secure them. A steel cylinder was threaded onto the front of the projectile (impact punch), which passed through the retaining cap at the end of the acceleration tube to contact the test specimen. On the rear end of the projectile, a plastic seal of similar diameter to the inside of the tube was secured to reduce air leakage.

4.2.1.4 Impact Chamber

The impact chamber (Figure 4.3) is where a specimen (PMHS or Anthropomorphic Test Device (ATD)) was mounted during impact trials. The frame of the chamber was manufactured of 2-inch steel square tubing welded together and sat on a rubber mat on the countertop. Polycarbonate shielding was fastened to the outside of the chamber's frame to stop anything from exiting the chamber after the impact. Additional square tubing was welded at the exit of the acceleration tube to support a linear rail. Linear bearings mounted to this rail, provided locations for jigs to be secured. The acceleration tube was permanently fixed at the center of the chamber, locating all impacts over the linear bearings.

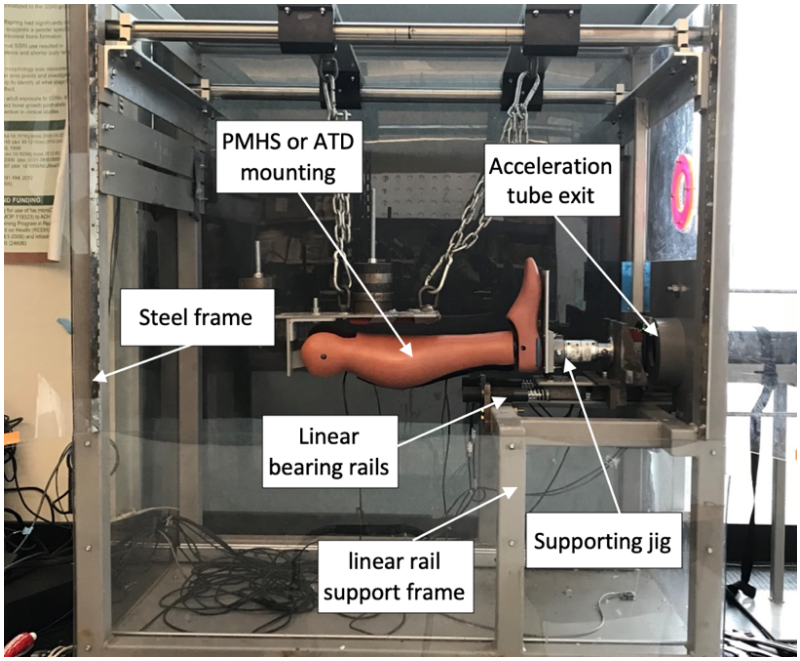

Figure 4.3: Original impact chamber

The entrance of the acceleration tube was rigidly mounted at the center of the impact chamber so that impacts were aligned with the linear bearings.

4.2.1.5 Capabilities

This apparatus's projectile mass ranged from 2.5 kg to 31.6 kg and had a velocity ranging from 2.0 m/s to 17.3 m/s. It could achieve impact durations between 7 ms and 25 ms depending on the attenuating surface used. Finally, the velocity could be repeatably controlled with a coefficient of variation of 4.56% (Appendix E). During prior calibrations of the apparatus, four trends were identified: projectile mass had a proportional relationship with duration of impact, velocity had an inversely proportional relationship to impact duration, the mass has an inversely proportional relationship to velocity, and velocity had a proportional relationship to tank pressure.

4.2.2 Requirements for Replicating BABT Impacts

During ballistic shield testing the anticipated impact velocity was estimated to be between 20 m/s and 160 m/s (Chapter 3), with a duration of impact ranging from 0.4 ms to 1.2 ms. Additionally, the peak impact forces ranged from 2 kN to 7 kN, where the targeted average impact profiles are illustrated in Figure 4.4. Using impact parameters with similar values as those found during ballistic shield testing would make it easier to recreate the desired impact profiles. While the highest velocities would not be safe to conduct in the lab, the velocities at the larger stand-off distance are close to the range of the impactor's capabilities, as such can likely be re-created.

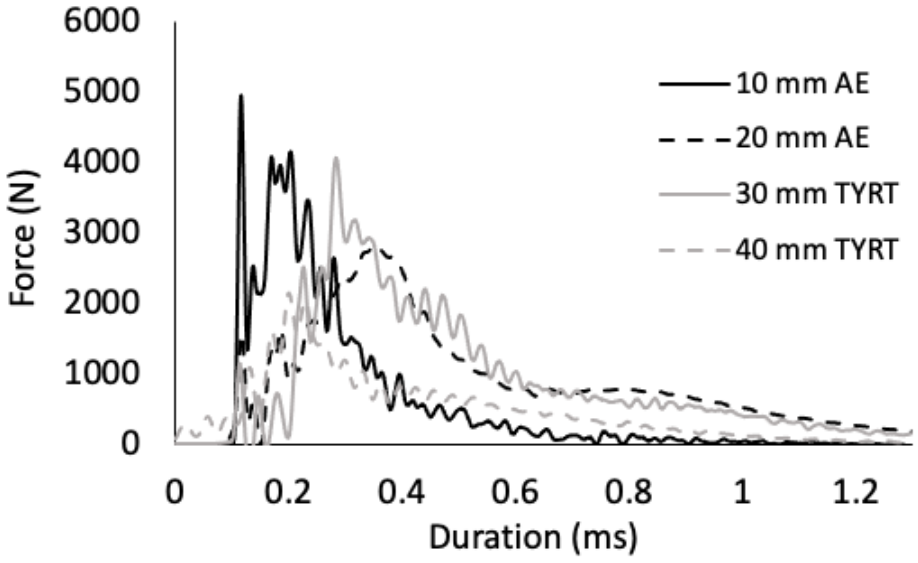

Figure 4.4: Target average impact profiles for behind shield impacts

The average impact profiles for both the AE and TYRT shields at their two associated stand-off distances are shown. These are the target impact profiles that are to be re-created in the McMaster Injury Biomechanics lab.

The original impactor produced both lower impact velocities and longer durations than those found during the ballistic testing. Therefore, a new system was required that could better produce the behind shield impact profiles. Finally, as the upper extremity ATD and future PMHS needed to be impacted at the hand, wrist, forearm, and elbow, there would need to be enough room to translate the arm within the impact chamber to align the desired locations with the projectile's exit from the acceleration tube. The largest PMHS that would be used is a 95th percentile male that has a center of elbow to center of grip dimension of 39 cm [49].

4.2.3 Design Requirements

In addition to modifying the pneumatic impactor for use in this work, three additional design constraints were considered. At the time of the redesign the Injury Biomechanics Laboratory was moving to a new lab, so the impactor was modified to fit within the new space. There was limited room on the floor, requiring the impactor to be mounted on the countertop. As these counters were to be used for other experimental work, the impactor had to minimize its countertop usage and had to be mounted without causing damage. Secondly, to save money as many components as possible were reused from the previous impactor. The final design constraint was that it must still be able to accommodate a heavy projectile since experimental work simulating other scenarios still needed to be conducted with the new apparatus.

An analysis of each of the previous impactor's subassemblies was done to provide insight into the limitations of its design and highlight the required changes. Firstly, the pneumatics were assessed. As designed, there were no limitations identified with the

pneumatics, which were the components between the air inlet and the solenoid valve. As such, all components used in the original pneumatics design were recycled and used in the modified design in a similar orientation.

A few issues were noted with the acceleration tube design, specifically with the wye joint. This wye joint presented two primary issues: poor ergonomics for loading heavy projectiles and it had a large volume of air behind the projectile in its starting location (approximately 3.5 L). Since the projectile must be placed in front of the air entrance, when the solenoid valve was opened the entire wye joint had to be pressurized, leading to significant losses. As a result, the projectile would begin accelerating at a lower pressure than desired. Therefore, reducing the amount of volume between the back of the projectile and the outlet of the solenoid would transfer more energy to the projectile, providing higher velocity impacts with the same impact conditions.

A second issue with the acceleration tube design was the use of PVC material. This material can degrade due to ultraviolet light, reducing its impact strength. As this acceleration tube experienced rapid loading due to the pressurized air, the reduction of impact strength could become a safety concern over time. Furthermore, the use of PVC likely made the internal tube dimension unstable. As the projectile was steel and dragged along inside of the tube, there was likely wear that accumulated over time, changing the inner diameter by small amounts. This inconsistent inner dimension could affect the pressure velocity relationship (due to leaking around the projectile) and ultimately lead to inconsistent forces.

Two primary issues were identified with the projectile design: the friction and the mass. When firing, this projectile would drag along the inner face of the acceleration tube before impacting the specimen in the impact chamber. As such, there was a large amount of friction due to the contact between the projectile and the acceleration tube, leading to wear of the acceleration tube (as discussed) and possible inconsistency of the impactor. Additionally, the large amount of friction reduced the maximum possible output velocity of the original projectile. The second issue was that the minimum mass of the projectile was approximately 2.5 kg (due to the mass of the rod, supporting disks, and punch). As such, design changes were needed to reduce the friction, to increase the maximum velocity, and to reduce the minimum mass of the projectile.

The final limitations were identified with the impact chamber. Over the course of numerous impacts, observable motion was noted where the impact chamber translated along the counter. While the specific amount of translation during individual impacts was never characterized, a trend of post impact translation was noted. As such, controlling this motion, both to ensure energy is safely distributed and for consistent force application during testing, was necessary. A secondary benefit of controlling the post impact kinematics was reducing the risk of damage to both the counters and impactor. Finally, the impact chamber had a width of approximately 76 cm, resulting in the impact being delivered 38 cm from the side of the impact chamber. As the elbow to center of grip dimension for a 95^{th} percentile male is 39 cm, impacts could not be applied at the hand and elbow locations of large specimens in the original configuration.

4.2.4 Modified Pneumatic Impactor

The limitations to the previous pneumatic impactor design informed the following six requirements for the modified design:

1. Remove the excessive losses due to the projectile friction and the large starting volume behind the projectile.
2. Manufacture the acceleration tube of a material with higher mechanical strength.
3. Allow impacts to be applied at any location along the impact chamber.
4. Control the post-impact energy dissipation to ensure no unwanted translation of the apparatus occurs, to create a more reliable set-up.
5. Design a projectile with a minimum mass of 1.5 kg (40% mass reduction when compared to original projectile mass) that can reach a velocity of at least 20 m/s.
6. Provide repeatable impact conditions with coefficients of variation less than 5% to be comparable to or better than the previous impactor.

4.3 New Pneumatic Impacting Apparatus Design

The four sub-assemblies (pneumatic system, acceleration tube, projectile, and impact chamber) were re-designed to account for the new requirements and assembled in the new lab space (Figure 4.5). All engineering drawings can be found in Appendix F. One of the features that affected all sub-assemblies was the method used to apply impacts at any location along the impact chamber. This could be accomplished by either keeping the acceleration tube rigidly fastened and translating the impact chamber or having the impact chamber rigidly mounted and translating the acceleration tube. Since the large mass and size of the chamber would make moving it very difficult, the smaller and lighter acceleration tube was designed to translate along the horizontal direction (Section 4.3.1.2).

This required modification to the other sub-assemblies to account for this change, which will be individually discussed.

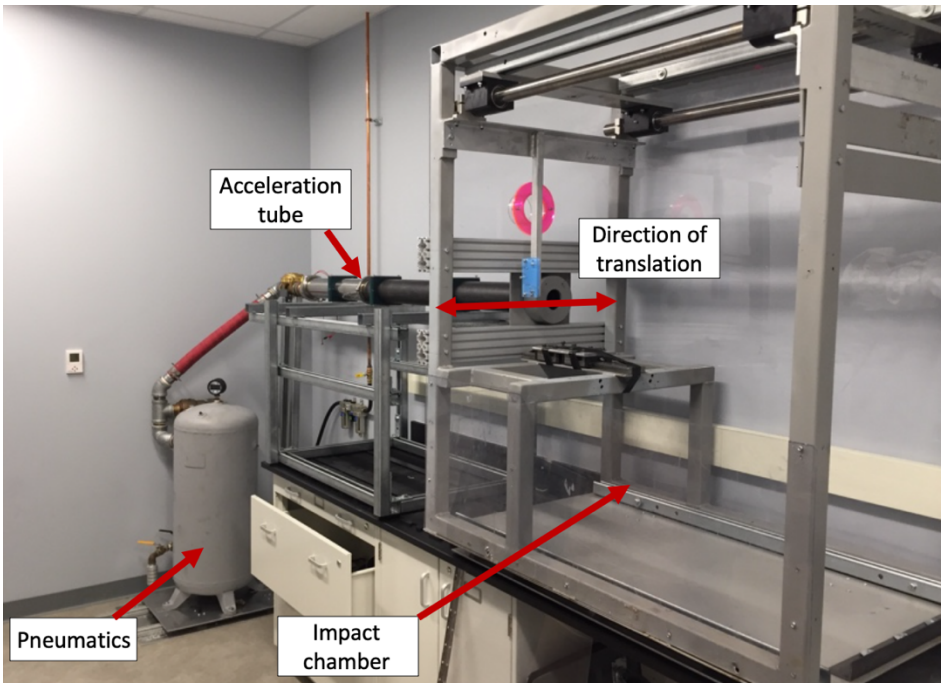

Figure 4.5: Final modified pneumatic impactor design

The modified pneumatic impactor illustrating three of the sub-assemblies (pneumatics, acceleration tube, and impact chamber). It is shown to be set up with the acceleration tube delivering impact to the center of the impact chamber.

4.3.1 Sub-assembly Design

4.3.1.1 Pneumatic System

The modified pneumatic system aimed to re-use as many components as possible from the original design to reduce costs; however, the orientation was slightly adjusted for the space constraints of the new lab space (Figure 4.6). The piping was reconfigured to decrease the large amount of air loss in the system by aligning the solenoid valve directly

behind the projectile's starting position, resulting in the unnecessary volume behind the projectile being reduced by over 95%. This was accomplished by using a custom welded metal reducer assembly. This assembly (Figure 4.7) consisted of a 2" low-pressure stainless steel threaded female to butt weld pipe fitting (4464k478, McMaster-Carr, Santa Fe Springs, CA) (#1), a butt-weld straight reducer (45605K122, McMaster-Carr, Santa Fe Springs, CA) (#2), and a welded tri-clamp flange (4" Outer Diameter with 4" Tri Clamp Furrule, Triclamp.co) (#3) welded in series. This allowed the volume behind the projectile to become fully pressurized more quickly, providing more rapid force application to the projectile.

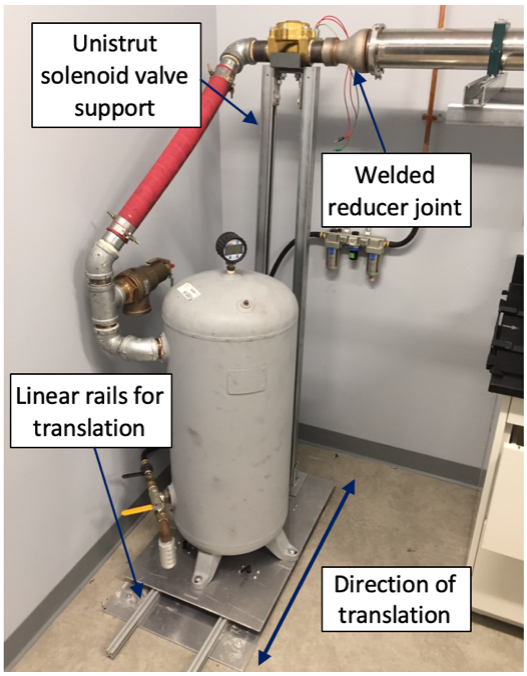

Figure 4.6: Pressure tank assembly

The pneumatic system reused all critical components from the original design. The modified pneumatics were mounted on aluminum extrusion rails to allow translation. The solenoid valve, supported by a Unistrut frame, was connected to the acceleration tube via the welded reducer joint.

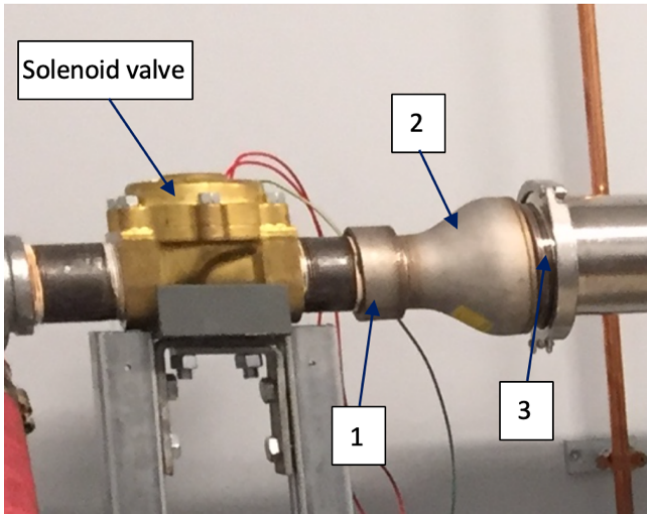

Figure 4.7: Solenoid valve placement directly behind the acceleration tube

The solenoid valve was positioned directly before the entrance of the acceleration tube. A custom reducer joined the solenoid and the acceleration tube and was made up of 1) a threaded female to butt weld pipe fitting, 2) a butt-weld straight reducer, and 3) a welded tri-clamp flange.

The second change that was made to the pneumatic assembly was the mounting of the pressure tank. As the acceleration tube was required to translate, all of the piping also had to translate. This was accomplished by manufacturing two aluminum plates. The first was secured to the floor and had two sections of aluminum extrusion (25-2525, 80/20 Inc., Colombia City, IN) mounted to it (Figure 4.8). The pressure tank was then mounted on the second plate, which was supported by four linear bearings (25-6425, 80/20 Inc., Colombia City, IN). These linear bearings interfaced with the aluminum extrusion and provided linear translation in the same direction as the acceleration tube. The linear bearings had a UHMW bearing surface to reduce the friction. One of the linear bearings on each aluminum extrusion had a brake (25-6850, 80/20 Inc., Colombia City, IN) that could be tightened to secure the linear bearings in place once aligned in the desired location.

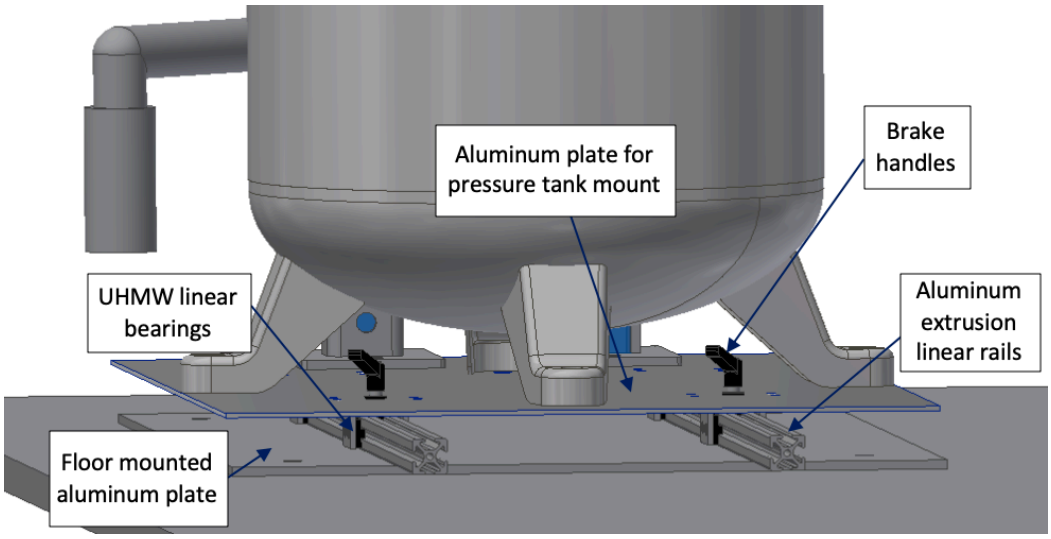

Figure 4.8: Linear pressure tank translation system

An aluminum plate was mounted to the floor with two aluminum extrusions fastened to it. A second aluminum plate was mounted to the pressure tank and four linear bearings, two of which had brakes. The bearings mated with the aluminum extrusion to allow translation of the entire pressure tank assembly.

The top aluminum plate that secured the pressure tank also provided mounting for a Unistrut structure that supported the solenoid valve, regardless of the tank position. The flexible tubing was used to account for any translation or vibration within the system as well as facilitated easier alignment as of the solenoid valve. All the pneumatics were installed by a certified Technical Standards and Safety Authority (TSSA) plumber.

4.3.1.2 Acceleration Tube

The new design was not rigidly mounted to the impact chamber, enabling the acceleration tube to be translated. De-coupling these components allowed all impact energy to be transferred into the impact chamber, and no impact forces would be experienced by

the acceleration tube or its supports. This reduced the need for intensive mounting and support systems. As discussed in Section 4.3.1.1, the solenoid valve was located immediately behind the entrance to the acceleration tube. Without the wye fitting, there needed to be a new way to load the projectile. As such, the projectile was loaded in a 4-inch diameter, 24-inch length sanitary spool with tri-clover flanges (BHO Extractor Column, Triclamp.co) that acted as a removable tube section (Figure 4.9). This section was removed from the acceleration tube, the projectile was placed inside, then it was secured in line with the solenoid valve. It was attached with a stainless-steel tri-clamp (4" tri-clamp, triclamp.co) on tri-clover flanges on both the reducer and sanitary spool.

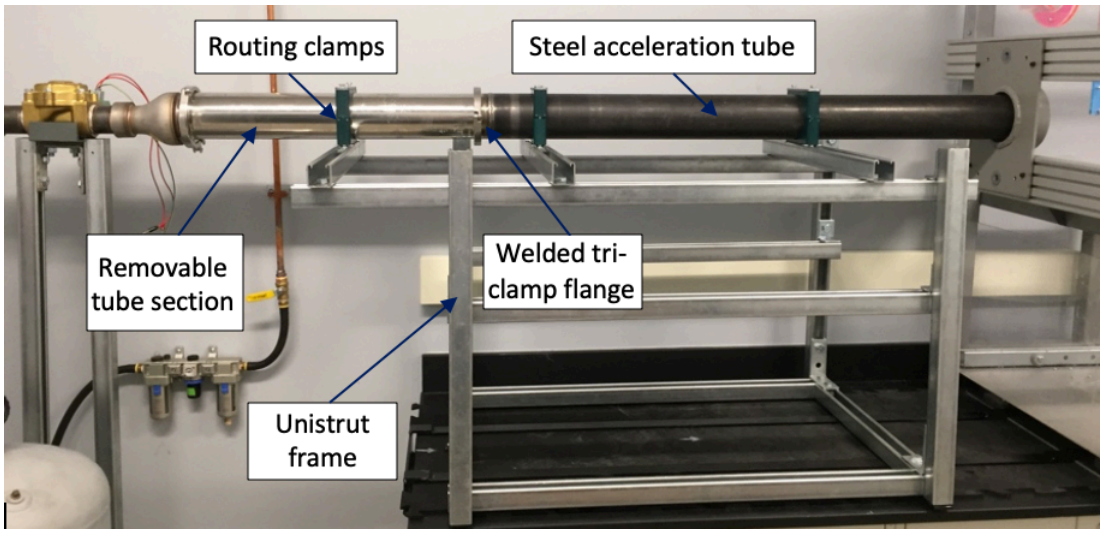

Figure 4.9: Modified acceleration tube assembly

The final assembly of the acceleration tube is shown with the removable tube section secured to both the reducer joint and the steel acceleration tube. The acceleration tube was secured by three anti-vibration routing clamps mounted to a Unistrut frame.

The next change was modifying the acceleration tube material from PVC to cold rolled steel. As the PVC was susceptible to degradation, the selection of steel provided a

much safer option as it would not become weak over time. The steel also provided better dimensional stability and would be less prone to wear on the internal surface, as was a problem with the original PVC tube. The dimensional accuracy enabled a custom projectile to fit the internal geometry of the tube more accurately. A tri-clover flange (4" Outer Diameter with 4" Tri Clamp Furrule, Triclamp.co) was welded to one end of the acceleration tube to allow it to mate with the end of the removable section. The steel acceleration tube was clamped in place using a stainless-steel tri-clamp (4" tri-clamp, triclamp.co) on the side that interfaced with the removable tube.

To achieve higher impact speeds, a longer acceleration tube was selected. The total length of the assembled acceleration tube was 6 feet long, with the steel section being 4 feet and the removable section being 2 feet. This provided an increase in travel distance by 50% compared to the previous impactor design.

To allow impacts to be applied at any location along the upper limb, the acceleration tube could translate along the horizontal axis. A Unistrut frame was designed that would hold the acceleration tube at the proper height (Figure 4.9). The acceleration tube was clamped in place using routing clamps (2804N36, McMaster-Carr, Santa Fe Springs, CA) that were fastened to horizontal Unistrut braces. Three clamps were used and could be loosened to allow the acceleration tube to translate so it could be positioned anywhere along the impact chamber.

4.3.1.3 Projectile

The new projectile (Figure 4.10) was designed to reduce the mass of the lightest option of the original projectile by 40% and have lower friction. Two aluminum disks were designed as supporting structure for the projectile. Aluminum was selected as it was a lighter material while providing relatively high strength, and the thickness was selected to resist damage when contact with the projectile exit guard retaining lip occurred. These disks were joined with four threaded rods, three towards the outer edges to provide structural rigidity, and one at the center of the disks to extend in front to support a newly designed impact punch. The diameter of the supporting rods was thinner than the original projectile to reduce mass. The punch had a diameter of 2.5 cm so that it's diameter was greater than the force sensor's impact cap. This allowed the force to be applied evenly to the entire impact cap and account for any misalignment of the projectile and impact location. Each of the aluminum disks had three running wheels (Shower Door Rollers, CY101, Amazon, Seattle, WA, USA) that would interface with the inside of the acceleration tube. These wheels reduced the friction when compared to the original design as there was no longer contact between the metal disks and the inside of the acceleration tube.

The bearing wheels were designed to be offset from the edge of the supports by 2.5 mm to allow them to interface with the inside of the acceleration tube while ensuring that the aluminum disks did not make contact with the inner surface. The small offset of the wheels also ensured a very small gap between the projectile and tube to limit the amount of air that could pass through that location. The air gap was designed to be less than 5% of the inner cross-sectional area. This projectile was designed to have a minimum mass of

1.36 kg with an approximate maximum mass of 14.5 kg when additional masses were added.

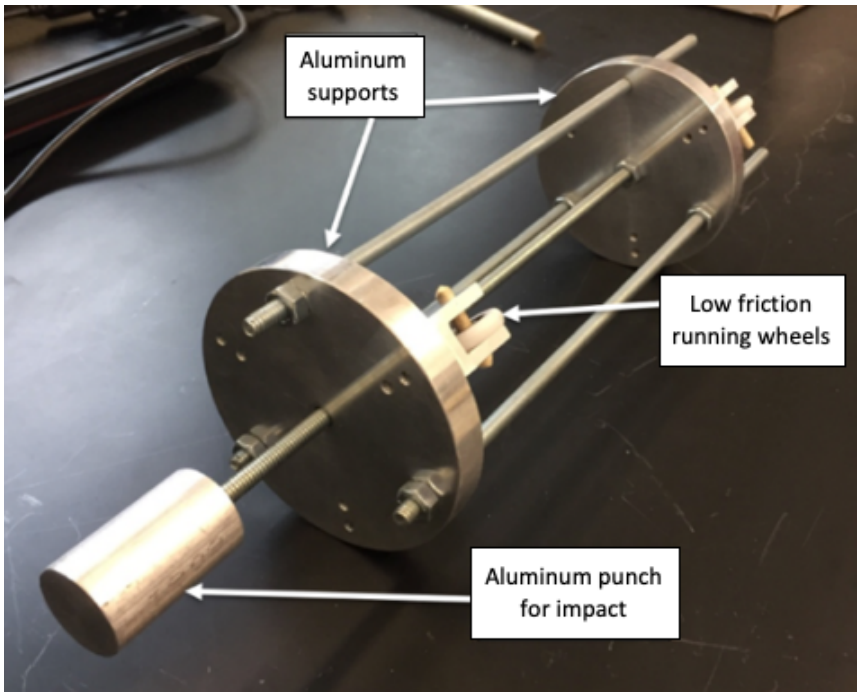

Figure 4.10: New projectile design
The revised projectile design is shown with the linear bearing wheels that reduced friction, the removable aluminum punch, and the lightweight aluminum end supports.

4.3.1.4 Impact Chamber

The interface between the outlet of the acceleration tube and the impact chamber was modified to account for the translating acceleration tube. Two aluminum extrusion cross beams (25-5050-CL, 80/20 Inc., Colombia City, IN) were bolted to the front of the impact chamber, which the existing projectile exit guard was bolted against (Figure 4.11). This guard had a smaller hole on the rear side that the punch could exit while the rest of the projectile was retained by a lip, preventing the projectile from leaving the acceleration tube.

The guard could be translated independently of the acceleration tube and would be adjusted prior to alignment.

Where the previous design used tie rods to maintain a rigid connection between the acceleration tube and the impact chamber, the revised chamber de-coupled the acceleration tube from the impact chamber. This design effectively removed any impact stress on the acceleration tube, since impacts were transferred solely to the impact chamber. However, two primary forces were experienced during the firing of the projectile, reaction forces from the acceleration of the projectile (acting on acceleration tube), and impact forces from the contact between the projectile and specimen (acting on impact chamber). These forces acted in opposite directions and would tend to separate the acceleration tube and impact chamber. However, the routing clamps on the Unistrut frame were designed to resist this reaction force and secure the acceleration tube post impact, while the impact chamber was permitted a limited amount of post impact motion.

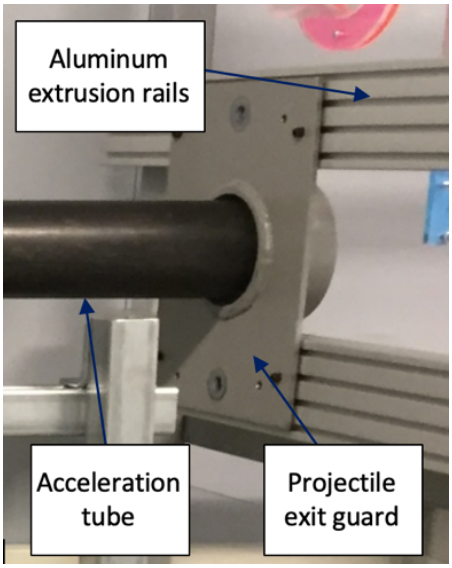

Figure 4.11: Projectile exit guard

The exit guard was mounted at the end of the acceleration tube to keep the projectile contained as a safety measure. The guard could translate along the aluminum extrusion channels and be secured in the required spot to impact anywhere along an upper limb.

Since the original impactor experienced uncontrolled translation of the entire system during impact, a method for restricting this motion was required. To accomplish this linear bearings (6674K160, McMaster-Carr, Santa Fe Springs, CA) were mounted to the bottom side of the impact chamber that interfaced with two one-inch cylindrical rails (6061K750, McMaster-Carr, Santa Fe Springs, CA) (Figure 4.12), which facilitated controlled linear motion. These rails were mounted to an aluminum base plate using easy access base mount shaft supports (1865K600, McMaster-Carr, Santa Fe Springs, CA). The holes in the base aluminum plate were cut using waterjet to ensure the accurate alignment of the linear rails.

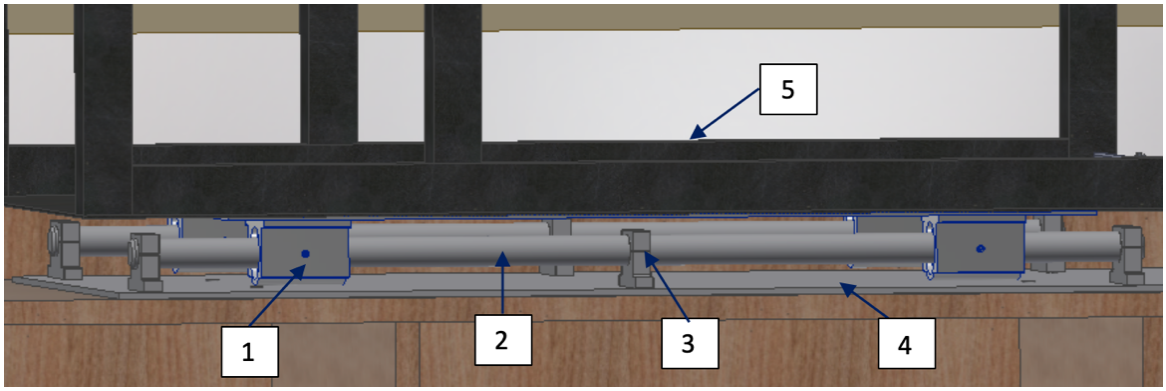

Figure 4.12: Linear railings under impact chamber

Linear motion was controlled on the impact chamber with bearings mounted on the underside of the chamber. This figure shows the 1) linear bearings, 2) linear cylindrical rails, 3) easy access base mounts, 4) aluminum base plate, and 5) impact chamber.

Armor Rubber "C-Lock" Interlocking Tiles (Rymar, Mississauga, ON, Canada) were positioned on the countertop, onto which the aluminum base plate was placed. This rubber provided a high co-efficient of friction between the countertop and aluminum plate that was calculated to resist the transferred impact force. A steel brace was manufactured that would bolt to the aluminum plate and hook over the edge of the countertop (Figure 4.13). This design was intended to remove the need to bolt into the counters when securing the impactor, leading to less damage to the counters. Further, it provided a mechanical stop for the aluminum base plate, because if the impact force ever exceeded the frictional forces, the entire pneumatic impactor would not be allowed to translate due to the contact between this brace and the countertop.

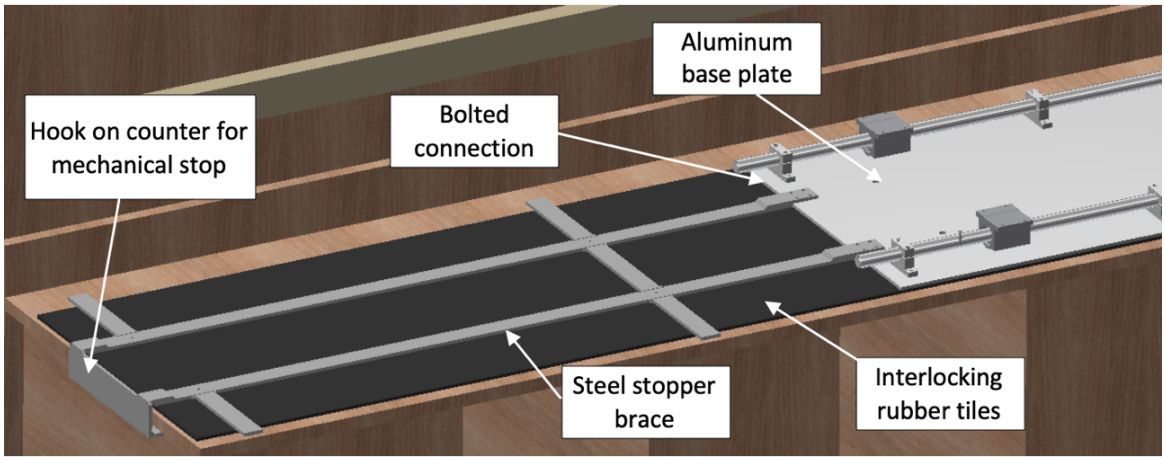

Figure 4.13: Steel brace for securing the aluminum base plate

The steel brace that bolted to the aluminum base plate under the impact chamber and created a mechanical stop against the countertop is shown. Both the steel stopper and the aluminum base plate were placed on top of interlocking rubber tiles.

Upon impact, the impact chamber translated along the linear bearings. For a worst-case scenario, it was assumed that the projectile would transfer 100% of its momentum to the impact chamber. Therefore, the worst-case momentum scenario occurred with the highest mass projectile (31.6 kg) with a maximum velocity of 5.9 m/s (since this was the greatest velocity used with the large mass). With an impact chamber mass of 270 kg, with perfect conservation of momentum, the resultant impact chamber velocity would be 0.6 m/s, with associated energy of 64.4 J. As a means to dissipate this kinetic energy, two shock absorbers (3740K18, McMaster-Carr, Santa Fe Springs, CA) were installed at the rear of the impact chamber. These shock absorbers were each able to dissipate 73 J of energy resulting in a safety factor for energy dissipation of over 2.28. Finally, these absorbers had a stroke length of 1 inch, as such would allow the impact chamber to move at most 1 inch. The acceleration tube was placed 6.5 cm into the projectile exit guard so that even if the

impact chamber moved its full distance the projectile would remain contained within the acceleration tube. The shock absorbers were supported in a custom-made steel frame that was mounted to the same aluminum base plate as the linear rails. They were placed in contact with a bolted L-bracket and upon impact compressed to absorb the impact energy (Figure 4.14). After each impact, the impact chamber was then pushed back into place, so the projectile impact guard was always in contact with the acceleration tube.

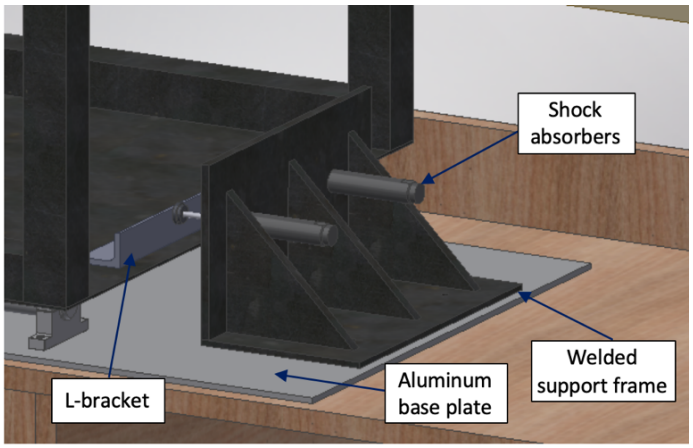

Figure 4.14: Impactor shock absorbers

Two shock absorbers were mounted behind the rear of the impact chamber to control translation during impact. A custom welded steel frame supported the two shock absorbers that were in contact with an L-bracket, which was bolted to the frame of the impact chamber. The welded steel frame was bolted to the same aluminum base plate as the impact chamber linear rails (Figure 4.12, #4).

4.4 Modified Pneumatic Impactor Evaluation

While the original pneumatic impactor provided the ability to create high energy impacts, the specific BABT impact profiles would have been difficult to recreate due to the relatively low impact velocity and high durations of previous impacts. Upon completing

the re-design of the impacting apparatus, the limits to velocity and the repeatability were assessed to characterize the range of possible impact parameters.

4.4.1 Maximum Impact Velocity

To evaluate the impactor's velocity capabilities, the projectile was fired with a tank pressure of 5 psi, then increased by 2 psi for each subsequent shot. A 5 cm x 5 cm x 15.25 cm piece of aluminum extrusion was bolted to the custom jig mounting plate (Figure 2.9). Since the impact force was not being evaluated, eight layers of foam were positioned at the point of impact to reduce the transferred forces to the impacted structure. The pressure was increased until either the tank pressure was maximized, the output velocity was 20 m/s or any damage to impacted aluminum extrusion was identified (Appendix E). During the evaluation of the impact velocity range, the lightest projectile mass was used (1.36 kg). Unfortunately, due to the high energy of impact, the central threaded rod on the projectile experienced slight buckling when the velocity was increased to 13 m/s. As such, a revised projectile design was created where the carriages that supported the bearing wheels were modified to accommodate a thicker central rod. Due to the modified geometry of the rear carriage, there was a substantial increase in air leakage around the projectile. Therefore, an acetal disk was fastened to the rear end of the projectile and interfaced close to the inner diameter of the pipe to reduce the air flow past the projectile. The modifications resulted in a minimum impact mass of 2.88 kg.

The tank pressure was increased to 23 psi with an associated velocity of 18 m/s, at which point damage to the testing jigs was identified. The slotted T-nuts that were holding together the aluminum frame began to deform the aluminum material they were in contact

with. This resulted in the aluminum supports not maintaining right angled connections and the shape of the structure became distorted. As such, the velocity response was only characterized up to 18 m/s so not to further damage the testing structure. Therefore, as currently tested, the impactor could produce impacts ranging from 4 m/s to 18 m/s with the 2.88 kg projectile (Figure 4.15). Additionally, the two impact conditions that were evaluated with the 1.36 kg mass were plotted and a linear trendline was fitted to the points. Assuming that with the lighter mass there would still be a linear relationship between pressure and velocity it is possible to extrapolate the relationship to determine the approximate pressure that would produce a 20 m/s impact velocity, which was 12.5 psi. This highlights that using a lighter projectile will allow much higher velocities to be achieved with the same impact parameters.

The pressure-velocity relationship for the 2.88 kg mass was linear with an R^2 of 0.99. The objective of the re-design was to achieve a velocity of 20 m/s with the newly designed projectile. Unfortunately, due to the limitations of the jig structure the impact testing was stopped when a velocity of only 18 m/s was achieved. While this shows that the impactor was capable of achieving velocities higher than were achieved with the previous impactor (18 m/s vs. 17.3 m/s), it did not truly identify the range over which the projectile could be fired. With the maximum working velocity of 80 psi, the heavier (2.88 kg) projectile could be fired up to 60 m/s, while the light (1.36 kg) projectile could be fired up to 130 m/s. While these ranges are theoretical, they will never be tested for both safety and durability of the impactor.

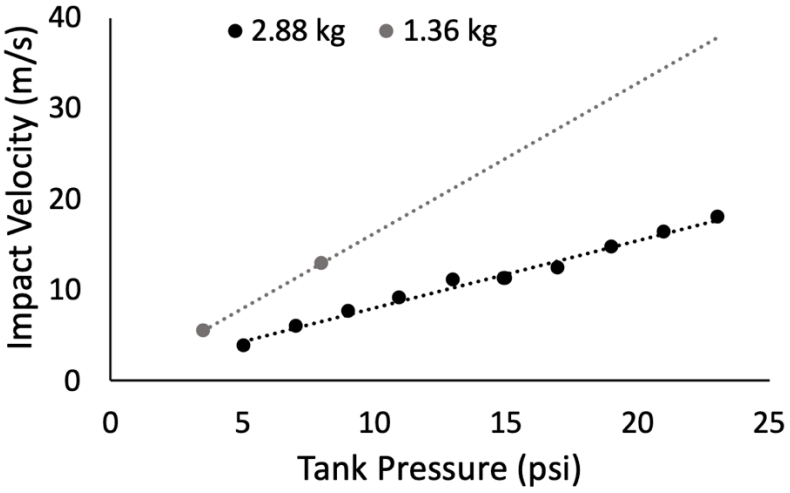

Figure 4.15: The modified pneumatic impactor pressure to velocity relationship

A linear relationship is shown between the pressure and impact velocity for the modified pneumatic impacting apparatus. The graph shows the calibration curve for impacts conducted with a 2.88 kg mass and 1.36 kg mass.

In reality, this testing identified the limits of the jigs, not the impactor. Based on the pressure-velocity relationship, to achieve a velocity of 20 m/s the pressure would need to be set to ~26 psi, well within the limits of the pressure tank assembly. Further, the true limitation in not achieving the 20 m/s velocity was the use of the heavier projectile. Since the mass of the projectile was increased to 2.88 kg instead of 1.36 kg the impact force that was present at the 20 m/s velocity was likely much higher, leading to the damage of the jigs. As such, the lighter projectile would likely have been able to achieve the 20 m/s impact condition at pressures around 12.5 psi without producing such high impact forces.

4.4.2 Repeatability

To evaluate the repeatability of the pneumatic impactor, 15 impacts were conducted. Three impact conditions (Table 4.1) were tested with two impact masses (1.36

kg and 2.88 kg) and three impact velocities, where five trials were done at each condition (Appendix E). To quantify the repeatability, the pressure tank was set to a consistent pressure and allowed to stabilize for seven minutes before the projectile was fired and its velocity was measured. The coefficient of variation of the impact velocity was calculated and is indicative of the system's repeatability. The coefficients of variations ranged from 1.48% to 5.26%, where the impactor behaved the most consistently when using a light impact mass with a low pressure compared to higher mass and velocity impacts.

Table 4.1: Summary of repeatability testing for modified impactor (N=5 for each test condition)

Mass (kg)	Tank Pressure (psi)	Velocity (m/s)	Coefficient of Variation (%)
1.36	3.5	5.53 ± 0.08	1.48
2.88	5.0	3.96 ± 0.09	2.36
2.88	13.0	10.65 ± 0.56	5.26

The original pneumatic impactor was able to deliver impacts with a coefficient of variation of 4.56%. This was evaluated from previous calibration data where 24 trials were conducted with a mass of 2.5 kg, tank pressure of 4.56 ± 0.05 psi, and had a resultant velocity of 5.9 ± 0.27 m/s. The modified impactor, with a comparable impact scenario (mass of 2.88 kg with a pressure of 5 psi), was able to achieve a coefficient of variations of 2.36%, which improved the impactor's repeatability by 37%.

From these data, the primary trend that was observed was that the repeatability of the pneumatic impactor was proportional to the tank pressure and velocity. The higher

coefficients of variations at higher tank pressures are likely due to the pressure tank not stabilizing as well at higher pressures. At low pressures, the digital pressure gauge would quickly stabilize to the desired pressure, whereas at the higher pressures it would continue to have fluctuations until the point of being released. While each impact was conducted when the pressure reading was exactly as listed (providing no variation in the pressure), the fact that there were fluctuations in the readings up until firing implies unstable internal pressures. For this reason, the stabilization period should be adjusted for the tank pressure so that at higher pressures the tank has sufficient time to stabilize.

Additionally, it is worth noting that the variables were selected for the repeatability testing to compare to the original impactor's repeatability (mass = 2.5 kg vs. 2.8 kg, pressure = 4.5 psi vs 5.0 psi). Surprisingly, with comparable testing parameters, the newly designed impactor produced a lower final velocity when compared to the original impactor (4 vs 6 m/s), even though all changes made to the design were selected to reduce losses and increase the output velocity. This is likely due to the air gap between the projectile and the inner face of the acceleration tube. The old projectile was had an air gap that was ~2% of the internal tube area, while the modified projectile had an air gap that was ~9% of the internal tube area. The much larger air gap on the new projectile was likely the reason for the lower velocities that were produced since a large amount of air could pass by the projectile without applying any force. To generate higher velocity impacts, the air gap should be reduced by replacing the rear seal on the projectile with one that better fits the internal geometry of the acceleration tube, which can be designed with a close tolerance.

4.4.3 Creation of Behind Shield Impact Loading Profiles

A preliminary investigation of the pneumatic impactor's ability to reproduce the ballistic impact profiles was completed. A number of impacts had been conducted with the modified pneumatic impactor while assessing the repeatability of the ATD (Section 2.4). These impact profiles were compared to the desired ballistic shield force-time curves as a starting point for identifying whether or not it will be possible to re-create the required profiles.

Two impacts were compared to the TYRT 30 mm stand-off impact profile (Figure 4.16). These impacts, using a 2.88 kg impact mass, were conducted at 2.7 m/s and 6.3 m/s, and impacted the ATD at the hand location (as was used for the TYRT shield). From these impact curves, three observations were made regarding the impactor's ability to re-create the appropriate impact profiles. Firstly, the peak force that was achievable was well above the impact force that was measured during ballistic testing. As such, this impactor will easily be able to achieve the magnitudes of forces that were seen during the ballistic tests. Secondly, when moving from the 2.7 m/s impact to the 6.3 m/s impact the timing of force application was much more rapid and approached the slope of the TYRT shield impact profile. Therefore, increasing the impact velocity will better allow the rate of force application to be replicated. Finally, the duration of impact decreased as the impact velocity increased, where the 2.7 m/s and 6.3 m/s impacts had durations of impact of 5.6 ms and 1.6 ms, respectively. This showed that as the impact velocity is increased the duration of impact will be decreased.

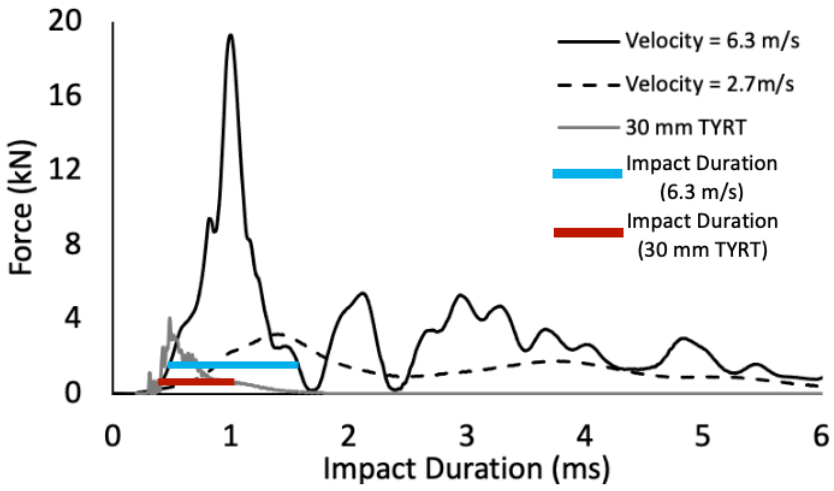

Figure 4.16: Impact profiles generated using the modified pneumatic impactor

Two impact profiles that were created in the pneumatic impactor compared to the targeted 30 mm TYRT impact profile. Both impacts were conducted with a mass of 2.88 kg at the ATD hand location and used two layers of Infinisil rubber for damping.

While the tests conducted did not adequately re-create the impact profiles that were measured during the ballistic testing, the comparison of the impact profiles provided insight into the possibility of re-creating these profiles. In order to successfully accomplish this, the impact velocity will have to be further increased to both reduce the impact duration and better match the initial rise to peak force. However, as the impact force increases so too will the magnitude of impact force. As such, the current projectile mass is likely still too heavy and further reductions to its mass will allow the appropriate impact curves to be produced. The duration of impact and impact force could further be reduced by lightening the jigs so that they accelerate along the linear rails more rapidly post-impact. With further calibration, it is likely that the desired impact profiles will be able to be re-created using the newly designed apparatus.

4.5 Discussion

This chapter presented the successful re-design of a modified pneumatic impacting apparatus designed to test both the custom ATD and future upper extremity PMHS. It was designed to reduce many of the losses identified in the previous impactor to provide more consistent high energy impacts. All the design criteria outlined in Section 4.2.4 were satisfied, with the exception of successfully generating an impact with a velocity of 20 m/s, since the lightest projectile was damaged during testing. Furthermore, while accounting for all design requirements for this project, the impactor was also designed to be able to be used for high mass projectile testing and be incorporated into the new laboratory space.

4.5.1 Limitations

In order to have the highest level of consistency between ballistic tests (at DRDC) and simulated impacts (at McMaster University), the conditions applied to the upper extremity have to be as similar as possible. It will not be possible to achieve identical impact speeds for the close tests, since the pneumatic impactor will not be able to safely create the same speeds as those found behind shields (>150 m/s). However, the impact velocity for the larger stand-off was approximately 20 m/s, which is likely achievable for the new impactor if the light mass is used. Additionally, it will be possible to control other impact parameters, such as impact energy, impact duration, and transferred force through the selection of projectile mass, damping material, and impact velocity. This adjustability will provide flexibility in creating the desired impact profiles. However, with the currently available impact mass, the impact profiles will be difficult to fully re-create as the required velocity will generate forces that are too high. As such, the projectile mass should be further

reduced to allow higher velocity impacts to be conducted while having a lower transferred force.

There were some design flaws that were identified with the newly designed pneumatic impactor. Firstly, when loading the projectile, the sanitary spool where the projectile is loaded must rest on a single Unistrut support. This results in the spool needing to be balanced as it is tightened in place, since if the projectile shifted within the tube its starting location would be changed, leading to inconsistent travel distance and variability. Providing a secondary support would assist in securing the projectile, make loading the projectile easier and more ergonomic when heavier projectiles are used in future work.

A second issue that was identified is the flexibility of the top aluminum plate in the pressure tank assembly. The structure that supports the solenoid valve is mounted to this aluminum plate but is cantilevered over the linear bearings. This results in slight vibration of the solenoid valve as there is very little material resisting this bending. Future iterations would either add an additional structure to provide rigidity at this location or move the linear bearings to avoid the cantilever type loading.

4.5.2 Next Steps

There are two specific steps that are required to further improve the pneumatic impactor. Firstly, the stabilization period of the pressure tank with respect to the internal pressure must be characterized. Having a more thorough understanding of the time required to reach stabilization will allow the pressure to be more consistent and allow for more repeatable impacts to be conducted at higher pressures. Secondly, the lighter projectile

needs to be re-manufactured with additional support on the central rod to resist buckling. This could be accomplished by using a stronger material for the center rod, increasing the diameter of the central rod, and positioning the punch closer to the front support to reduce the effective length of the punch. This would increase the force required to generate buckling. Additionally, it is suggested that the projectile be re-designed to consider further reducing the minimum mass even lower than 1.4 kg. This is due to the observed trend of very high force magnitudes in the impact curve when the velocity was relatively low. This could be accomplished by selecting a light plastic material for the rear support as it experiences little impact force and is primarily used for supporting the bearing wheels. Upon creating these changes, the pneumatic impactor capabilities will be fully characterized, and the 20 m/s impact velocity will ideally be achieved, which is in the range of the larger stand-off distances.

The continuation of this work will consist of replicating the ballistic impacts from DRDC in the custom pneumatic impactor at McMaster University. The ATD will be set-up in the pneumatic impactor and impacts will be carried out at the same elbow and hand locations that were conducted in the ballistic tests. The specific settings of the pneumatic impactor (projectile mass and velocity, impact geometry, and padding material) will be varied to determine the conditions that must be used for replicating the impacts.

Parameters will be identified to replicate the force-time profile at each location for each stand-off distance resulting in four sets of parameters (two stand-off distances at each of the two locations). The specific selected parameters will best replicate the impact profiles measured during ballistic testing but will not necessarily use identical projectile velocities

or masses as used during the ballistic testing. Upon tuning the parameters to represent the impact profiles found during the DRDC testing, injury criteria evaluation may begin.

4.6 Conclusion

The re-design of the pneumatic impactor successfully allowed the apparatus to be moved to a new lab space, improved the repeatability by ~37%, and made the apparatus more durable. With the adjustments to projectile and impactor parameters (mass, velocity, and damping material), the force-time profiles measured during ballistic shield testing will be able to be generated using the newly designed system, which can then be used to facilitate the development of future upper extremity injury criteria. Finally, the impactor was successful in achieving velocities of 18 m/s with a 2.88 kg projectile, implying a 20 m/s impact condition will be achievable with the 1.36 kg projectile. This re-design has resulted in a more versatile and repeatable pneumatic impactor that will be capable of providing a wide range of possible impact scenarios, not limited to the ballistic impacts in this work.

Chapter 5 – General Discussions and Conclusions

5.1 Summary

Ballistic shields are designed to protect the user from threats that can include explosions and gunfire. They are strapped to the forearm of the soldier with the upper extremity in close proximity to the back-face of the shield. Projectiles can carry a large amount of kinetic energy, and upon impact with a shield, the incoming kinetic energy is dispersed through material deformation. Behind Armor Blunt Trauma (BABT) is the injury that occurs when the back-face of the deforming armor contacts the body. This injury can occur even when the projectile does not exit through the back-face of the shield (projectile penetration). BABT type injuries are common in worn body armor but also can occur in other ballistic impact scenarios, in this case, shields.

The close distance between the back-face of the shield and the arm makes it likely for contact between them to occur due to the deformation. To fully understand the level of protection that a ballistic shield provides two things must be known: the force transferred to the upper extremity during a shield BABT impact and the limits of force that can be applied to the upper extremity. Unfortunately, no standard tool capable of measuring the loading from back-face shield deformation had been created, and no injury criteria have been developed for the upper extremity at ballistic conditions. One previous study evaluated the peak forces seen behind ballistic shields [2]. However, this study used overly rigid boundary conditions, only evaluated loading from a single shield model, and had large variations in their measurements. As such, the total impact response during shield BABT

type loading needed to be further characterized by accounting for the limitations of the previous work.

The overarching purpose of this research was to develop a technique to evaluate the injury risk behind ballistic shields due to BABT. This work was broken up into two phases. The first phase, this thesis, characterized the loading events behind ballistic shields, while the second phase will deal with developing injury criteria for the upper extremity for BABT type injuries. This thesis had three primary objectives: develop a testing device that could be used to evaluate the loading profiles behind ballistic shields, characterize the behind shield loading curve, and develop a testing apparatus that could be used in the future to re-create the impact profiles for use during the second phase of this work.

A custom upper extremity Anthropomorphic Test Device (ATD) was developed that could measure the loading from behind shield impact events (Chapter 2). It was advantageous to base the design off a device with existing industry history, so the WorldSID 50th percentile (Humanetics Innovative Solutions, Farmington Hills, MI, USA) was selected as the base model. The final modified device contained a six-axis load cell at the forearm, a two-axis moment load cell at the elbow, and three uniaxial piezoelectric PCB 201B05 (PCB Piezotronics, MTS Systems Corporation, Depew, NY, USA) washer style force sensors located at the elbow, wrist, and hand. At each location that contained a PCB force sensor, the structure was modified to allow mounting of the force sensor and a cable protection channel. A new hand design was created that was consistent with 50th percentile male anthropometric dimensions and allowed the hand to ‘grip’ a handle. Data were collected from the ATD through two separate Data Acquisition Systems (DAQs), one to

sample the PCB sensors and one to sample the ATD load cells. Further, testing jigs were designed to allow the ATD to be tested both at the Defense Research and Development Canada (DRDC) and McMaster University testing facilities with the same boundary conditions. The final ATD was demonstrated to be highly repeatable and the loading response was shown to be dependent on the impacted location.

Ballistic impact testing, conducted at DRDC, used the modified ATD to characterize impact loading profiles found during high energy ballistic shield impacts (Chapter 3). Two level III ballistic shield models were compared through the analysis of high-speed video footage to evaluate their back-face response. Both shields were found to respond statistically differently to the same impact conditions, indicating that ballistic shields not only need to be evaluated based on whether projectile penetration occurs but also need to characterize both the amount of back-face deformation and transferred forces that are experienced. The back-face shield velocity at the time of impact was also estimated for each of the shields. A comparison of transferred force to stand-off distance was evaluated, which found that the maximum force was inversely proportional to the stand-off distance. This emphasizes that increasing the stand-off distance can potentially lead to a drastic reduction in the injury risk. No clear trend was identified relating the impulse or duration to the stand-off distance, illustrating the complex mechanics that occur during these impacts.

Upon characterizing the force curves found during behind ballistic shield impacts, an experimental apparatus was developed to re-create these impacts in the McMaster Injury Biomechanics lab (Chapter 4). The previous pneumatic impactor was redesigned where the

minimum projectile mass was reduced, the maximum attainable velocity was increased, and the repeatability was improved. The acceleration tube was allowed to translate along the impact chamber to deliver impacts at all locations along the upper extremity. The modifications to the pneumatic impactor allowed the ATD to be tested in the McMaster Injury Biomechanics lab and provided an apparatus that can be used for the second stage of this research, re-creating the ballistic impact profiles and developing upper extremity injury criteria.

5.2 Limitations and Strengths

While the strengths and weaknesses of each chapter were discussed individually, the general strengths and limitations pertaining to the entire work are discussed herein. There are inherent limitations in the use of ATDs as a means of evaluating injury risk. Where ATDs are used to simulate human response, they are limited by their lack of biofidelity (how close the ATD's response is to the biological tissue). Within this work, an ATD was used as it represented 50th percentile male anthropomorphic dimensions, allowed the loading at the various locations of impact to be characterized, and provided repeatable measurements during high energy ballistic testing. However, the modified ATD was not evaluated for biofidelity as this would require multiple Post-Mortem Human Specimen (PMHS) tests to be conducted for comparison, which was out of the scope of this work. The response of this ATD, even upon applying boundary conditions that were as realistic as possible, still responded differently than a human. As such, this difference must be considered when applying the obtained data to other bodies of work.

To evaluate the force transfer, the composite ballistic shields were tested without any trauma attenuating backings. Real-world ballistic shields are equipped with this backing material, which would reduce the observable forces behind the shield. Furthermore, most soldiers who carry ballistic shields would likely be wearing sleeves and gloves that would further dampen the transferred impact forces, which is not modeled during these tests. Finally, the ATD flesh was removed and replaced with a thinner rubber material, due to both the unknown damping and difficulty aligning impacts while it was used. While this work removed the 'extra' materials that wound attenuate the force transfer, it successfully evaluated ballistic shields in a 'worst-case' situation. It is more valuable to assess the worst-case scenario as it is then possible to compare this to the addition of trauma attenuating surfaces to evaluate their improvements. Future work could look at appropriate damping materials that are durable enough to resist the impacts that can be used to model the removed materials.

The ballistic testing did not account for the straps that secure the shield to the arm, as the arm had to be positioned in many locations behind the shield and could not be restricted to being positioned just at the center of the shield. These straps would have provided a secondary pathway for load transfer between the upper extremity and the shield. As such, they would likely lead to reducing the overall force that was experienced, as the load would begin transferring to the upper extremity sooner instead of being delayed until the back-face of the shield contacts the arm. Again, by removing the straps from the measurement, the study effectively tested a worst-case scenario as it measured an isolated force transfer through the BABT mechanic alone, likely resulting in slightly higher forces.

The pneumatic impactor was designed to deliver ballistic impact conditions to the ATD and PMHS. However, the interface between the projectile and the specimen (ATD or PMHS) is designed as a flat metallic impact punch. It was observed during ballistic testing that the interface at the point of impact was not flat but instead appeared to be slightly rounded in nature. It is not clear whether or not this distinction will change the force transfer, but to distribute the load in a similar manner to the behind shield impacts, modification to the impact geometry may prove valuable. Further, it was identified that for the close stand-off distances the impact velocity for behind shield impacts occurred when the back-face of the shield had a velocity of approximately 160 m/s. Meanwhile, the pneumatic impactor has a maximum velocity of 18 m/s. As such, replicating the very high velocity will not be possible, which could make perfectly re-creating the impact profiles in the McMaster Injury Biomechanics lab difficult. Finally, due to damage to the ATD, the limited number of shields, and the shield geometry, the ability to compare anatomical locations was limited. As such, a secondary set of ballistic impacts may be required to further collect impact parameters and characterize the ballistic impact conditions.

Despite the aforementioned limitations to this work, it also made many valuable contributions to the field. The methodology of this work considered the limitations from previously conducted BABT shield impacts and was designed to characterize the impact profiles using the most realistic boundary conditions to date. Additionally, it identified that behind shield loading profiles are dependent on the anatomical location, highlighting the need for location specific protection. This work has set the foundation for the development of both upper extremity injury criteria and a more thorough standard for shield evaluation

that should consider both back-face deformation and transferred force. This thesis has developed clear requirements for the development of an ATD and jigs, as well as a methodology that can be followed for carrying out the ballistic testing. Furthermore, it has provided a method of analyzing ballistic impact data.

5.3 Future Direction

The completion of this work has laid the groundwork for the second phase of this research to be carried out. The second phase will have two objectives, re-creating the impact curves in the McMaster Injury Biomechanics lab, and applying these representative impacts to PMHS to develop injury criteria specific to upper extremity ballistic shield BABT injuries. The development of the specific injury criteria will be a valuable asset to this field as it provides a quantifiable limit of force that can be transferred to the upper extremity in ballistic impact scenarios. Upon evaluating the fracture limits, equivalent impacts will be applied to the ATD to determine what force readings correspond to the injury tolerance of PMHS. It will be possible to use the modified ATD, developed in this thesis, as an injury prediction tool for newly designed shields. Furthermore, these findings will be incorporated in a future back-face shield deformation standard.

5.4 Significance

This research outlined the high forces and short durations of impact that are found behind ballistic shields due to the contact between the back-face of the shield and the arm. This was the first study that characterized behind shield impacts using realistic boundary conditions and a highly instrumented ATD upper limb. The trends in this work were

consistent with those identified by Bolduc et al. [2]; however, the magnitudes of force that were observed were much lower than those previously found. This work has further demonstrated the need for applying appropriate boundary conditions to the evaluation of ballistic shield impacts, as the boundary conditions can play a large role in the measurements obtained.

The development of the modified pneumatic impacting apparatus will make it possible to re-create the ballistic impact conditions in the McMaster Injury Biomechanics lab so that injury criteria can be developed during the second stage of this work. This work was the first of its kind to develop an ATD for the characterization of BABT shield impact loading profiles. Data collected during this work can be used for the evaluation of specific upper extremity injury criteria in the context of ballistic shield impacts. These injury criteria, once developed, will prove valuable to shield designers as in conjunction with this ATD will provide a usable metric to evaluate the safety of ballistic shields, as well as allow users to be fully informed about the safety that a shield provides.

Reference List

[1] National Institute of Justice, “Ballistic Resistant Protective Materials,” *NIJ Standard 0108.01*. p. 16, 1985.

[2] M. Bolduc, J. S. Binette, D. Fisher, and D. Hammond, “Tactical ballistic shields operational testing protocol definition,” in *Personal Armor Systems Symposium*, 2018, p. 10.

[3] S. M. Duma, B. M. Boggess, J. R. Crandall, and C. B. MacMahon, “Injury risk function for the small female wrist in axial loading,” *Accid. Anal. Prev.*, vol. 35, no. 6, pp. 869–875, 2003.

[4] J. M. Reeves, T. A. Burkhart, and C. E. Dunning, “The effect of static muscle forces on the fracture strength of the intact distal radius in vitro in response to simulated forward fall impacts,” *J. Biomech.*, vol. 47, no. 11, pp. 2672–2678, 2014.

[5] T. Barclay, “Bones of the Arm and Hand,” *Innerbody Research*, 2018. [Online]. Available: https://www.innerbody.com/image_skelfov/skel20_new.html. [Accessed: 30-Jul-2020].

[6] A. W. Carroll and C. A. Soderstrom, “A New Nonpenetrating Ballistic Injury,” *Ann. Surg.*, vol. 188, no. 6, p. 753, 1978.

[7] L. Cannon, “Behind armor blunt trauma--an emerging problem.,” *J. R. Army Med. Corps*, vol. 147, no. 1, pp. 87–96, 2001.

[8] C. J. Freitas, J. T. Mathis, N. Scott, R. P. Bigger, and J. MacKiewicz, "Dynamic response due to behind helmet blunt trauma measured with a human head surrogate," *Int. J. Med. Sci.*, vol. 11, no. 5, pp. 409–425, 2014.

[9] J. van Bree and N. van der Heiden, "Behind armor pressure profiles in tissue simulant," in *Personal Armor Systems Symposium*, 1996.

[10] National Institute of Justice, "NIJ Standard 0101.04 Ballistic Resistance of Personal Body Armor," *Law Enforcement and Corrections Standards and Testing Program*. p. 67, 2000.

[11] C&G Wholesale, "E.R.T (Emergency Response Team) Ballistic Shield." [Online]. Available: https://www.cgwholesale.com/-ERT-EMERGENCY-RESPONSE-TEAM-BALLISTIC-SHIELD_p_1671.html.

[12] A. E. Dyke, S. Haq, and C. J. Morley, "Protective material," US 9,464,872, 2016.

[13] G. Cooper and P. Gotts, *Ballistic Trauma*. London: Springer, London, 2005.

[14] R. Critchley, "The preparation and characterisation of auxetic foams for the application of trauma attenuating backings," University of Southampton, 2015.

[15] M. Stuivinga, E. P. Carton, H. J. Verbeek, and J. L. M. J. van Bree, "Energy transfer mitigation using foam at porojectile defeat by body armor," *Pass 2012*, no. September 2012, pp. 1–10, 2012.

[16] A. Sondén *et al.*, "Trauma attenuating backing improves protection against behind armor blunt trauma," *J. Trauma Acute Care Surg.*, vol. 67, no. 6, pp. 1191–1199, 2009.

[17] A. A. Amis and J. H. Miller, “The mechanisms of elbow fractures: an investigation using impact tests in vitro,” *Injury*, vol. 26, no. 3, pp. 163–168, 1995.

[18] S. M. Duma, P. H. Schreiber, J. D. McMaster, J. R. Crandall, C. R. Bass, and W. D. Pilkey, “Dynamic injury tolerances for long bones of the female upper extremity,” *J. Anat.*, vol. 194, no. 3, pp. 463–471, 1999.

[19] S. M. Duma, P. H. Schreiber, J. D. McMaster, J. R. Crandall, and C. R. Bass, “Fracture tolerance of the male forearm: The effect of pronation versus supination,” *Proc. Inst. Mech. Eng. Part D J. Automob. Eng.*, vol. 216, no. 8, pp. 649–654, 2002.

[20] S. M. Duma, B. M. Boggess, J. R. Crandall, S. R. Hurwitz, K. Seki, and T. Aoki, “Upper extremity interaction with a deploying side airbag: A characterization of elbow joint loading,” *Accid. Anal. Prev.*, vol. 35, no. 3, pp. 417–425, 2003.

[21] S. M. Duma *et al.*, “Upper extremity interaction with a helicopter side airbag: injury criteria for dynamic hyperextension of the female elbow joint,” *SAE Tech. Pap.*, vol. 48, no. 2004-22–0007, 2004.

[22] F. A. Pintar and N. Yoganandan, “Dynamic bending tolerance of the human forearm,” *Traffic Inj. Prev.*, vol. 3, no. 1, pp. 43–48, 2002.

[23] J. Chiu and S. N. Robinovitch, “Prediction of upper extremity impact forces during falls on the outstretched hand,” *J. Biomech.*, vol. 31, no. 12, pp. 1169–1176, 1998.

[24] M. E. Muller, A. E. Colin, E. W. Ae, and M. L. Bouxsein, “Predicting the failure load of the distal radius,” *Osteoporos. Int.*, vol. 14, no. 4, pp. 345–352, 2003.

[25] E. R. Myers *et al.*, "Correlations between photon absorption properties and failure load of the distal radiusin vitro," *Calcif. Tissue Int.*, vol. 49, no. 4, pp. 292–297, 1991.

[26] P. Augat, H. Reeb, and L. E. Claes, "Prediction of fracture load at different skeletal sites by geometric properties of the cortical shell," *Bone Miner. Res.*, vol. 11, no. 9, pp. 1356–1363, 1996.

[27] P. Augat, H. Iida, Y. Jiang, E. Diao, and H. K. Genant, "Distal radius fractures: mechanisms of injury and strength prediction by bone mineral assessment," *J. Orthop. Res.*, vol. 16, no. 5, pp. 629–635, 1998.

[28] E. R. Myers, A. T. Hecker, D. S. Rooks, J. A. Hipp, and W. C. Hayes, "Geometric variables from DXA of the radius predict forearm fracture load in vitro," *Calcif. Tissue Int.*, vol. 52, no. 3, pp. 199–204, 1993.

[29] J. A. Spadaro, F. W. Werner, R. A. Brenner, M. D. Fortino, L. A. Fay, and W. T. Edwards, "Cortical and trabecular bone contribute strength to the osteopenic distal radius," *J. Orthop. Res.*, vol. 12, no. 2, pp. 211–218, 1994.

[30] R. M. Greenwald, P. C. Janes, S. C. Swanson, and T. R. Mcdonald, "Dynamic impact response of human cadaveric forearms using a wrist brace," vol. 26, no. 6, pp. 825–830, 1998.

[31] C. Fransson-Hall and A. Kilbom, "Sensitivity of the hand to surface pressure," in *Applied Ergonomics*, 1993, vol. 24, no. 3, pp. 181–189.

[32] D. Mewes and F. Mauser, "Safeguarding crushing points by limitation of forces," *Int. J. Occup. Saf. Ergon.*, vol. 9, no. 2, pp. 177–191, 2003.

[33] B. Hohendorff *et al.*, “Entrapment of adult fingers between window glass and seal entry of a motor vehicle side door: An experimental study for investigation of the force at the subjective pain threshold,” *J. Biomech.*, vol. 44, no. 11, pp. 2158–2161, 2011.

[34] D. Carpanen, A. E. Kedgley, D. S. Shah, D. S. Edwards, D. J. Plant, and S. D. Masouros, “Injury risk of interphalangeal and metacarpophalangeal joints under impact loading,” *J. Mech. Behav. Biomed. Mater.*, vol. 97, no. April, pp. 306–311, 2019.

[35] H. J. Mertz, “Anthropomorphic Test Devices,” in *Accidental Injury*, New York, NY: Springer New York, 1993, pp. 66–84.

[36] A. Bull, J. Clasper, and P. F. Mahoney, *Blast Injury Science and Engineering: A Guide for Clinicians and Researchers*. Springer New York, 2016.

[37] J. W. Melvin, “The engineering design, development, testing, and evaluation of an advanced anthropomorphic test device, phase 1: concept definition. Executive suimmary. Final report.,” 1988.

[38] A. Kemper, J. Stitzel, S. Duma, F. Matsuoka, and M. Masuda, “Biofidelity of the SID-IIs and a modified SID-IIs upper extremity: biomechanical properties of the human humerus,” in *Proceedings of the 19th Enhanced Safety of Vehicles Conference*, 2005, pp. 5–123.

[39] A. R. Kemper, “Response corridors for the medial-lateral compressive stiffness of the human arm: Implications for side impact protection,” *Accid. Anal. Prev.*, vol. 50, pp. 204–222, 2013.

[40] European New Car Assessment Programme, “2020 Roadmap.” 2015.

[41] F. V Törnvall, K. Holmqvist, J. Davidsson, M. Y. Svensson, Y. Håland, and H. Öhrn, “A New THOR Shoulder Design: A Comparison with Volunteers, the Hybrid III, and THOR NT,” *Traffic Inj. Prev.*, vol. 8, no. 2, pp. 205–215, 2007.

[42] Humanetics Innovative Solutions Inc., “Drawing: W50-61150-H.” 2015.

[43] A. B. Chakravarty, “Effects of Off-Axis Loading on Fracture Risk in the Human Tibia,” McMaster University, 2016.

[44] C. Bir, D. Viano, and A. King, “Development of biomechanical response corridors of the thorax to blunt ballistic impacts,” *J. Biomech.*, vol. 37, no. 1, pp. 73–79, Jan. 2004.

[45] B. Kimes, “Molded Hand Assembly, Right Drawing, W50-61067-H.” 2014.

[46] PCB Piezotronics, “Piezoelectric Force Rings.” [Online]. Available: https://www.pcb.com/contentstore/mktgcontent/linkeddocuments/force-torque/tm-frc-dynamic-force_lowres.pdf.

[47] PCB Piezotronics, “Piezoelectric Force Rings.” [Online]. Available: https://www.pcb.com/contentstore/images/pcb_corporate/pcb/products/photo/120/201b_211b_series.jpg?t=637292174927010102. [Accessed: 01-Jul-2020].

[48] Canadian Center for Occupational Health and Safety, “Hand Tool Ergonomics - Tool Design.” [Online]. Available: https://www.ccohs.ca/oshanswers/ergonomics/handtools/tooldesign.html.

[49] C. C. Gordon *et al.*, "Anthropometric Survey of U.S Army Personnel: Summary Statistics Interim Report," Massachusetts, 1988.

[50] J. W. Garrett, "The adult human hand: some anthropometric and biomechanical considerations," *Hum. Factors*, vol. 13, no. 2, pp. 117–131, 1971.

[51] H. Himelblau, A. G. Piersol, J. H. Wise, and M. R. Grundvig, "Handbook for Dynamic Data Acquisition and Analysis: IES-RP-DTE012.1 ; recommended practice, 12," Mount Prospect, IL, 1994.

[52] D. Rhule, H. Rhule, and B. Donnelly, "The Process of Evalution and documentation of Crash Test Dummies for part 572 of the Code of Federal Regulations," in *19th International Technical Conference on the Enhanced Safety of Vehicles*, 2005.

[53] J.-S. Binette and D. Bourget, "Evaluation of Injury Behind a Shield - Test Plan of the Ballistic Testing," 2020.

[54] NATO, "Procedures for Evaluating the Protection Level of Logistic and Light Armored Vehicles," 2006.

[55] L. V. Griffin, R. M. Harris, R. A. Hayda, and M. S. Rountree, "Loading rate and torsional moments predict pilon fractures for antipersonnel blast mine loading," in *International IRCOBI Conference on the Biomechanics of Impacts*, 2001, pp. 115–131.

[56] A. B. Chakravarty, A. A. Martinez, and C. E. Quenneville, "The injury tolerance of the tibia under off-axis impact loading," *Ann. Biomed. Eng.*, vol. 45, no. 6, pp. 1534–1542, 2017.

[57] A. A. Martinez, “The effect of impact duration on the axial fracture tolerance of the isolated tibia during automotive and military impacts,” *J. Mech. Behav. Biomed. Mater.*, vol. 78, pp. 315–320, 2018.

[58] F. Jazinizadeh, H. Mohammadi, and C. E. Quenneville, “Comparing the fracture limits of the proximal femur under impact and quasi-static conditions in simulation of a sideways fall,” *J. Mech. Behav. Biomed. Mater.*, vol. 103, 2020.

[59] M. W. Cameron, E. H. Schemitsch, R. Zdero, and C. E. Quenneville, “Biomechanical impact testing of synthetic versus human cadaveric tibias for predicting injury risk during pedestrian-vehicle collisions,” *Traffic Inj. Prev.*, vol. 21, no. 2, pp. 163–168, 2020.

[60] A. Waugh and A. Grant, *Ross & Wilson Anatomy and physiology in Health and Illness*, 12th ed. Elsevier Health Sciences, 2014.

Appendix A – Anatomical Glossary

All anatomical definitions retrieved from textbook Anatomy and Physiology in Health and Wellness [60].

Anterior – Describes a body part nearer the front

Articulate/Articulation – A joint

Distal – Further from the origin of a body part or point of attachment of a limb

Lateral – Structure further from the midline or at the side of the body

Medial – Structure that is nearer to the midline

Posterior – Lying to the back of the body

Pronation – The turning of the palms to face backwards

Proximal – Nearer the origin of a body part or point of attachment of a limb

Supination – Turning the palms to face forwards

Appendix B – Modified ATD Technical Drawings

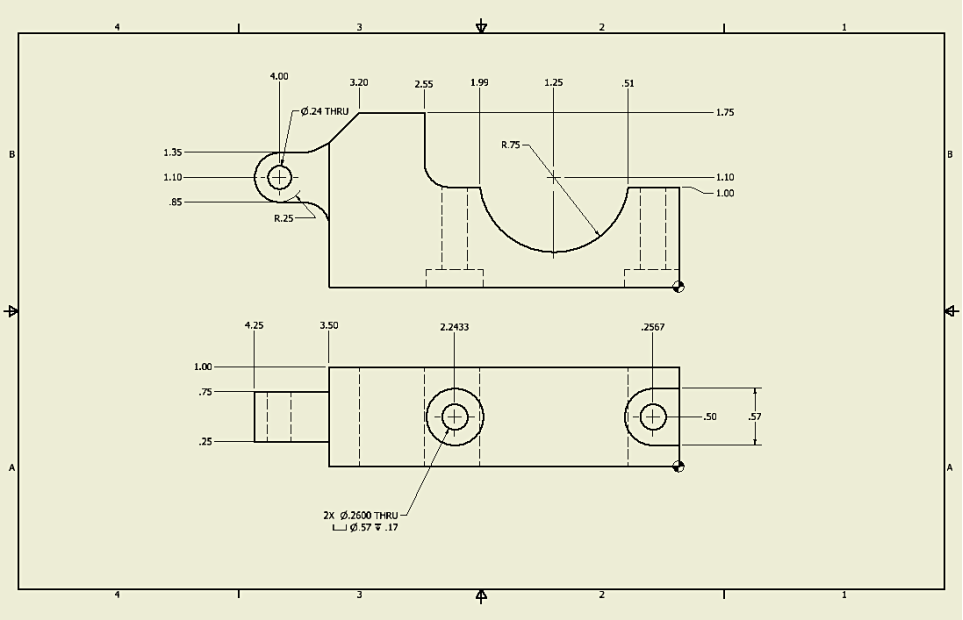

Figure B.1: Dimensional drawing of back of hand structure

All dimensions in inches, made of aluminum. Manufactured on CNC mill.

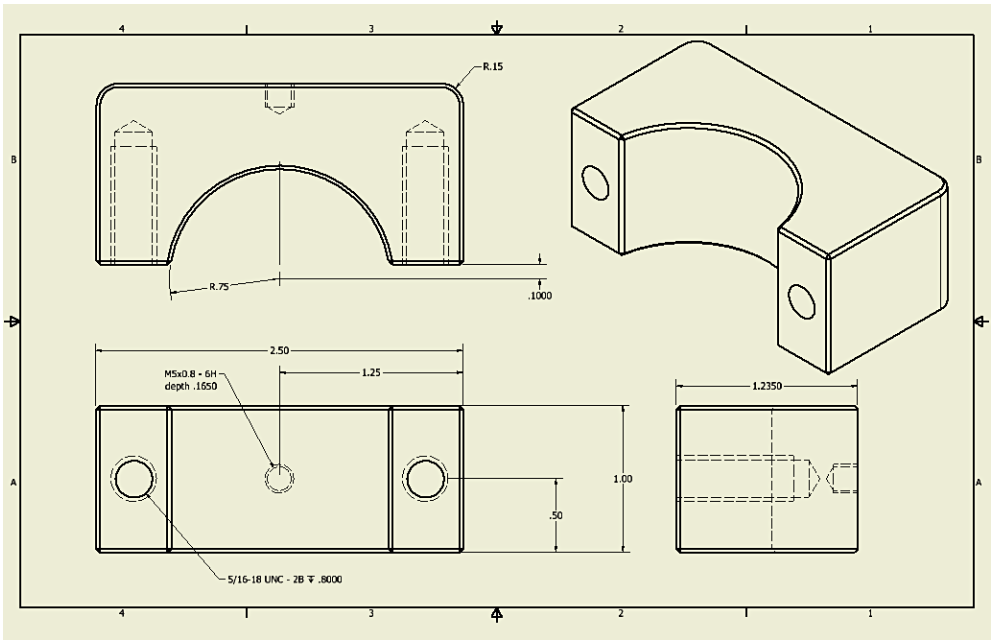

Figure B.2: Dimensional drawing of front of hand component

All dimensions in inches, made of steel. Manufactured on a CNC mill.

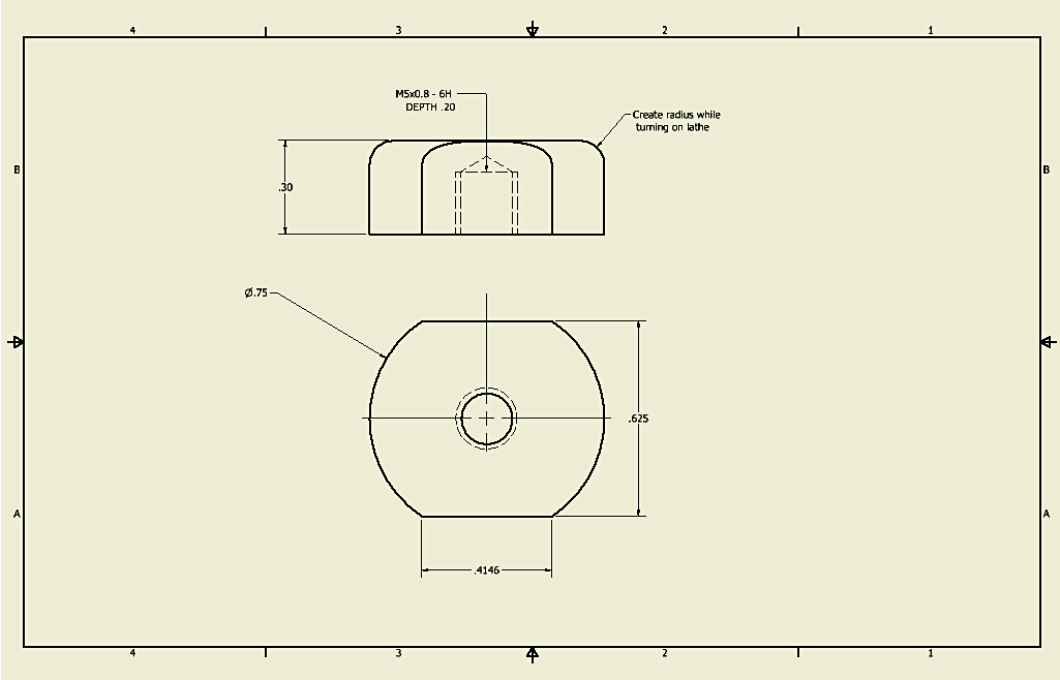

Figure B.3: Dimensional drawing of impact cap

All dimensions in inches, made of cold rolled steel.

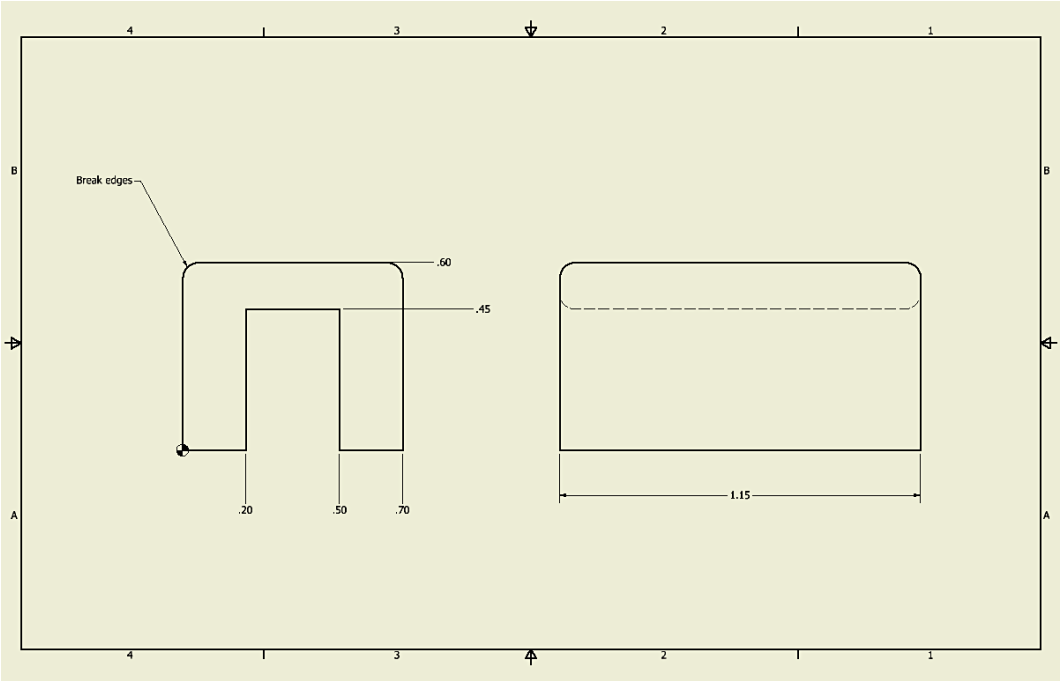

Figure B.4: Dimensional drawing of BNC cable protection channel

All dimensions in inches, made of cold rolled steel.

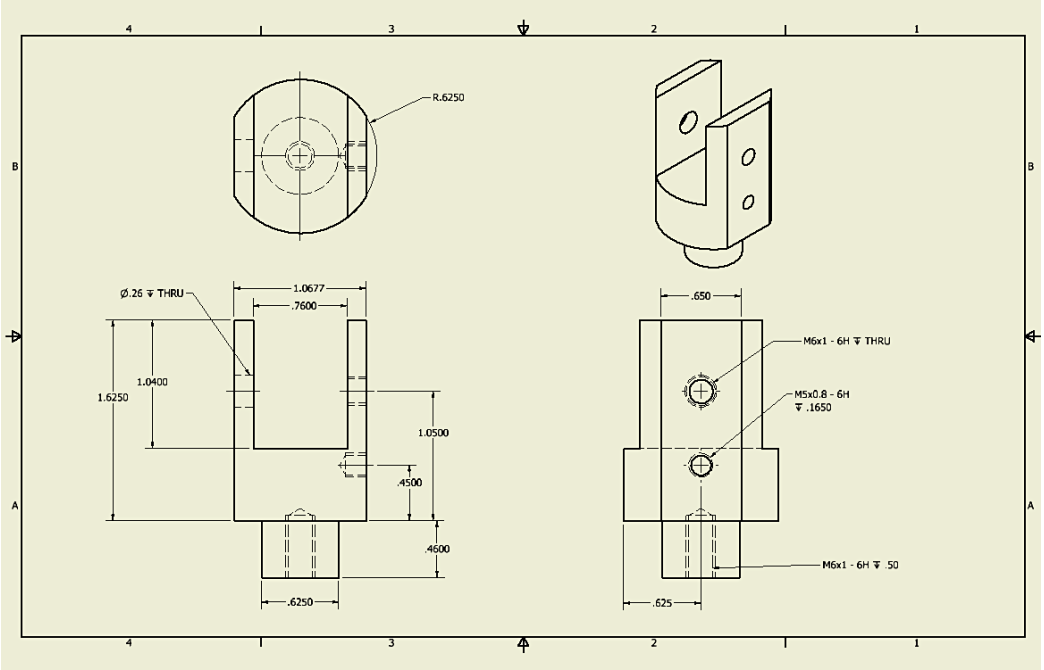

Figure B.5: Dimensional drawing of wrist component

All dimensions in inches, made of cold rolled steel.

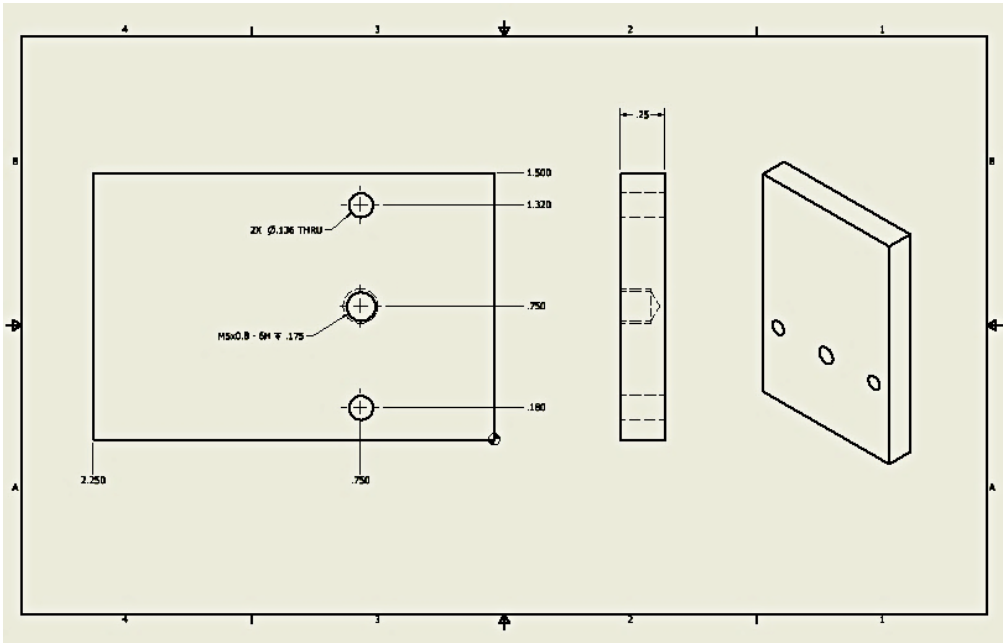

Figure B.6: Dimensional drawing of elbow load cell mounting plate

All dimensions in inches, made of cold rolled steel.

Appendix C – Experimental Jigs Technical Drawings

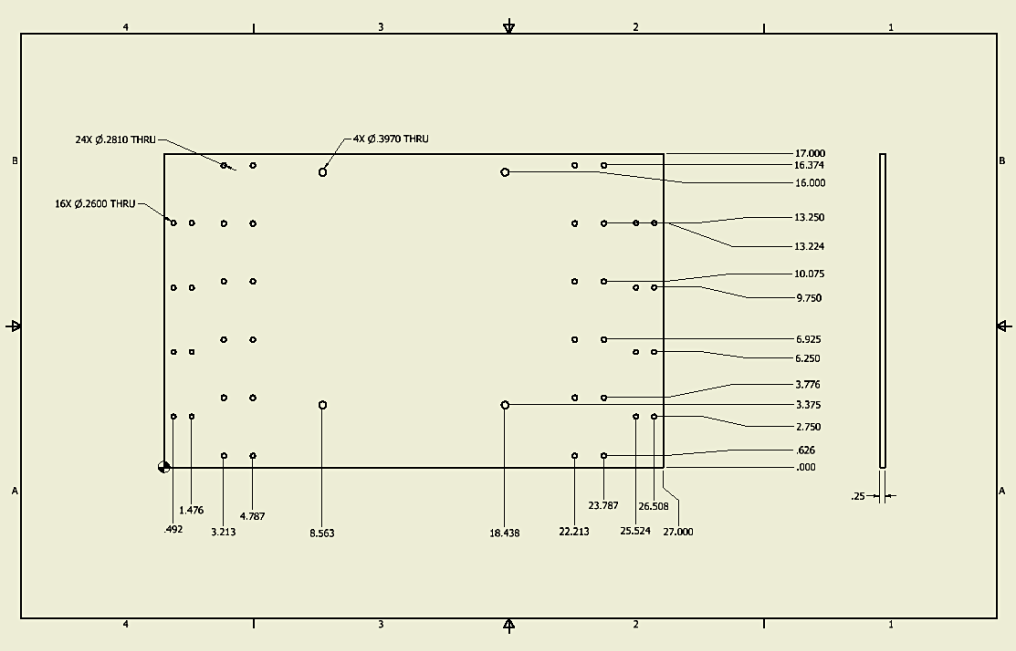

Figure C.1: Dimensional drawing of linear rail plate

All dimensions in inches, made of aluminum. Manufactured with waterjet.

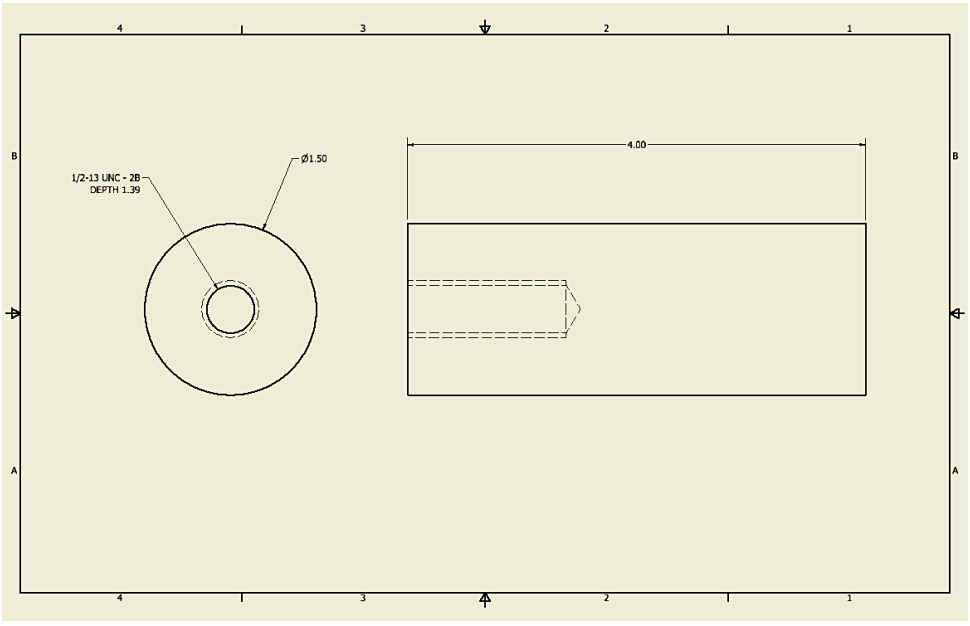

Figure C.2: Dimensional drawing of handle

All dimensions in inches, made of aluminum.

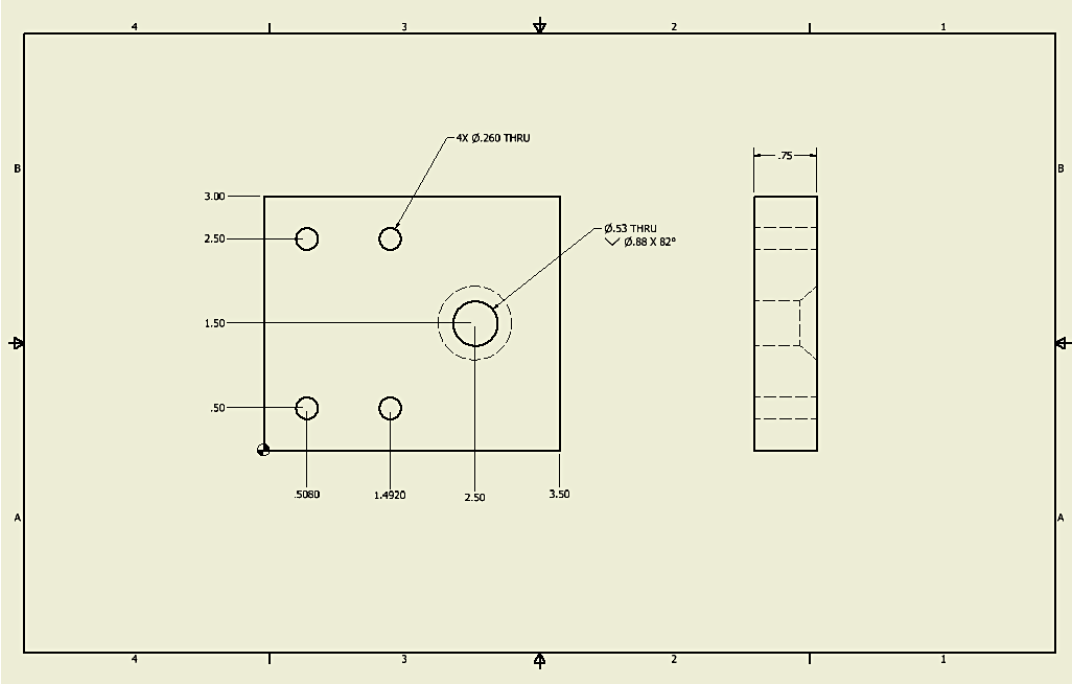

Figure C.3: Dimensional drawing of handle base

All dimensions in inches, made of aluminum.

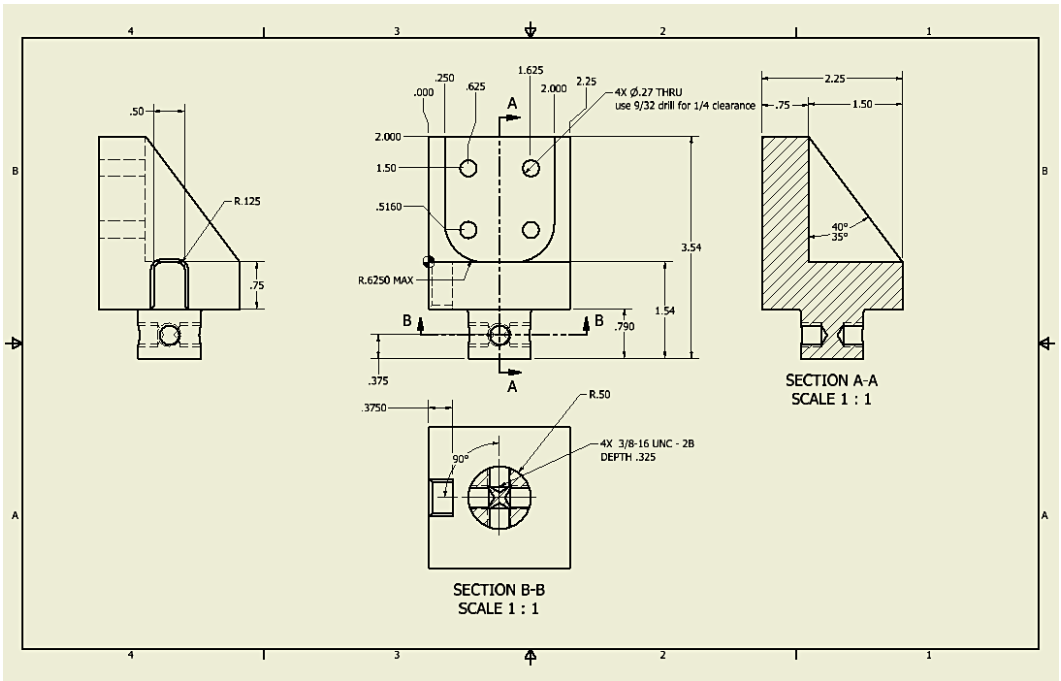

Figure C.4: Dimensional drawing of mid-humerus ATD support

All dimensions in inches, made of aluminum.

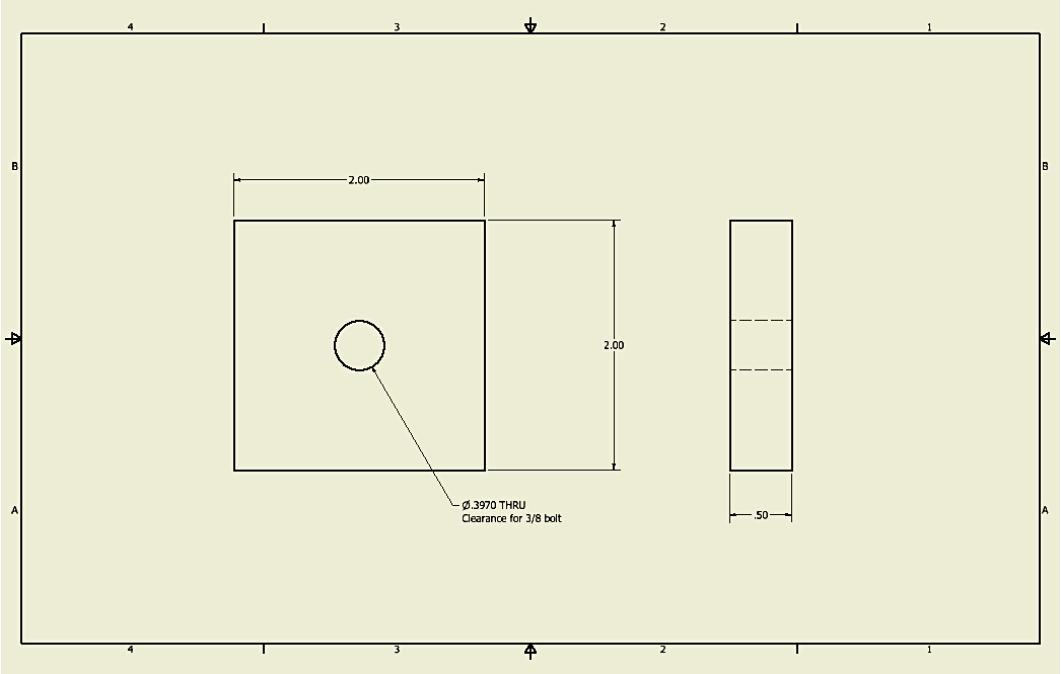

Figure C.5: Dimensional drawing for pneumatic impactor spacer

All dimensions in inches, made of aluminum.

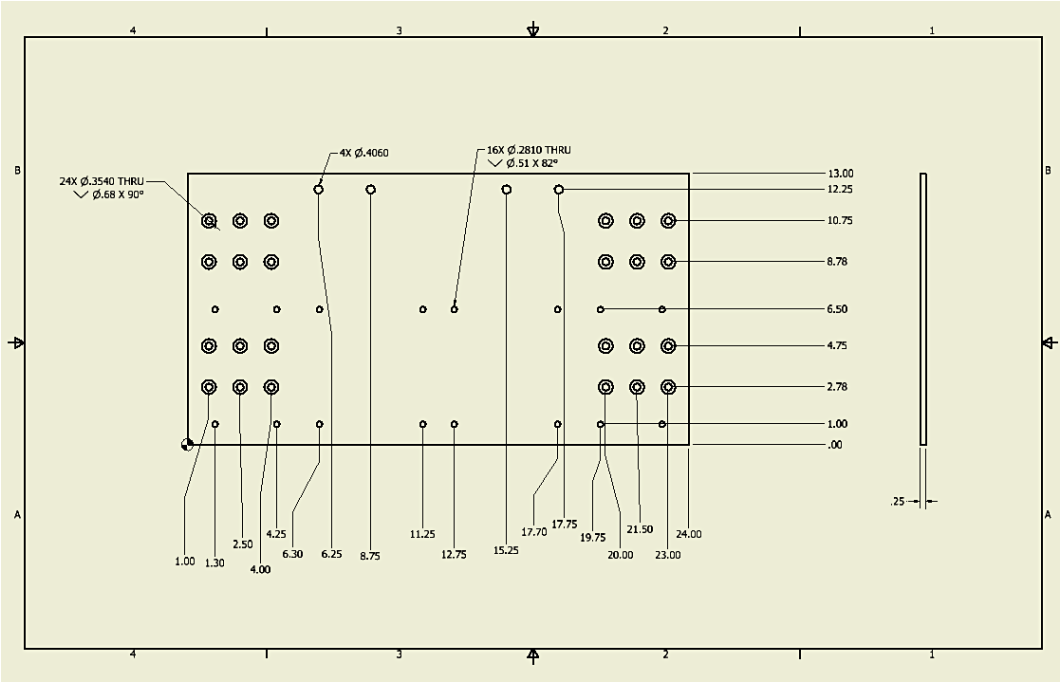

Figure C.6: Dimensional drawing of jig mounting plate

All dimensions in inches, manufactured using waterjet, made of aluminum.

Appendix D – Ballistic Impact Data

The data collected form ballistic impact testing, which was conducted at Defense Research and Development's ballistic test range, is presented here in. The 32 shots that were conducted are presented. Table D.1 illustrates the discarded shots, where shots 1-12 were discarded due to lack of contact and incorrect sample frequency, and shots 13 and 14 were discarded due to the highly focal deformation that damaged the forearm load cell.

Table D.1: The 14 shots not used for data analysis, all impacts conducted on AE shield

Shot ID	Force sensor	Stand-off Distance (mm)	Notes
1	Elbow	40	No contact
2	Elbow	40	No contact
3	Elbow	30	No contact
4	Elbow	20	Blow out on bottom edge of shield (discarded)
5	Elbow	20	Only NI PXIe-1082 used for all data collection. Identified to not have sufficient sampling capabilities
6	Elbow	20	
7	Elbow	20	
8	Elbow	15	
9	Elbow	15	
10	Elbow	10	
11	Elbow	10	~ 8 mm off set from center of sensor (discarded)
12	Forearm	10	Original PVC flesh evaluation
13	Forearm	20	No contact with arm
14	Forearm	10	Forearm load cell was damaged

Table D.2: Impact data from elbow impacts on the flat AE shields

Impact Force (N)	Impact Force Duration (ms)	Impulse (Ns)	Notes
10 mm stand-off			Added two layers of skin to PCB load cell Used Genesis 5i DAQ Stand-off distances were measured from surface of skin
5924.4	0.42	0.94	
4906.9	0.34	0.52	
2856.0	0.46	0.46	
6643.8	0.35	0.87	
20 mm stand-off			
2578.6	1.13	0.92	
3848.1	1.0	0.98	
3839.9	1.13	1.07	
4228.2	1.39	1.65	

Table D.3: Impact data from hand impacts on the curved TYRT shields

Impact Force (N)	Impact Force Duration (ms)	Impulse (Ns)
30 mm stand-off		
7288.3	0.78	1.29
5135.2	0.62	0.93
4245.4	0.92	1.09
4824.7	0.94	1.14
5109.0	1.01	1.19
40 mm stand-off		
1603.4	0.94	0.47
3031.3	0.84	0.81
1464.8	0.78	0.42
2192.0	0.84	0.52
3324.5	0.92	0.93

Appendix E – Pneumatic Impactor Evaluation Data

This data was collected to characterize the repeatability of the impacting apparatus. The repeatability for the original impactor and the new impactor, as well as the pressure velocity relationship are tabulated herein.

Table E.4: Original pneumatic impacting apparatus repeatability data

Mass (kg)	Pressure (psi)	Velocity (m/s)
2.5	4.6	5.12
2.5	4.6	5.63
2.5	4.6	5.90
2.5	4.6	5.90
2.5	4.6	5.86
2.5	4.7	6.20
2.5	4.7	6.49
2.5	4.6	6.20
2.5	4.5	6.16
2.5	4.5	6.16
2.5	4.5	5.90
2.5	4.5	5.90
2.5	4.5	5.90
2.5	4.6	5.94
2.5	4.5	5.86
2.5	4.5	5.63
2.5	4.5	5.63
2.5	4.5	5.90
2.5	4.5	5.90
2.5	4.5	5.63
2.5	4.5	5.99
2.5	4.5	5.90
2.5	4.5	5.90
2.5	4.5	6.20

Table E.5: Modified pneumatic impacting apparatus repeatability assessment

Mass (kg)	Pressure (psi)	Velocity (m/s)
1.364	3.5	5.56
1.364	3.5	5.41
1.364	3.5	5.63
1.364	3.5	5.56
1.364	3.5	5.48
2.876	5.0	3.90
2.876	5.0	4.09
2.876	5.0	3.95
2.876	5.0	3.88
2.876	5.0	3.92
2.876	13.0	11.04
2.876	13.0	10.00
2.876	13.0	10.37
2.876	13.0	11.18
2.876	13.0	10.63

Table E.6: Modified pneumatic impacting apparatus pressure velocity relationship

Mass (kg)	Pressure (psi)	Velocity (m/s)
2.876	5.0	3.92
2.876	7.0	5.94
2.876	9.0	7.73
2.876	10.9	9.14
2.876	13.0	11.04
2.876	14.9	11.33
2.876	15.0	11.33
2.876	17.0	12.50
2.876	19.0	14.66
2.876	21.0	16.35
2.876	23.0	18.09

Appendix F – Pneumatic Impactor Technical Drawings

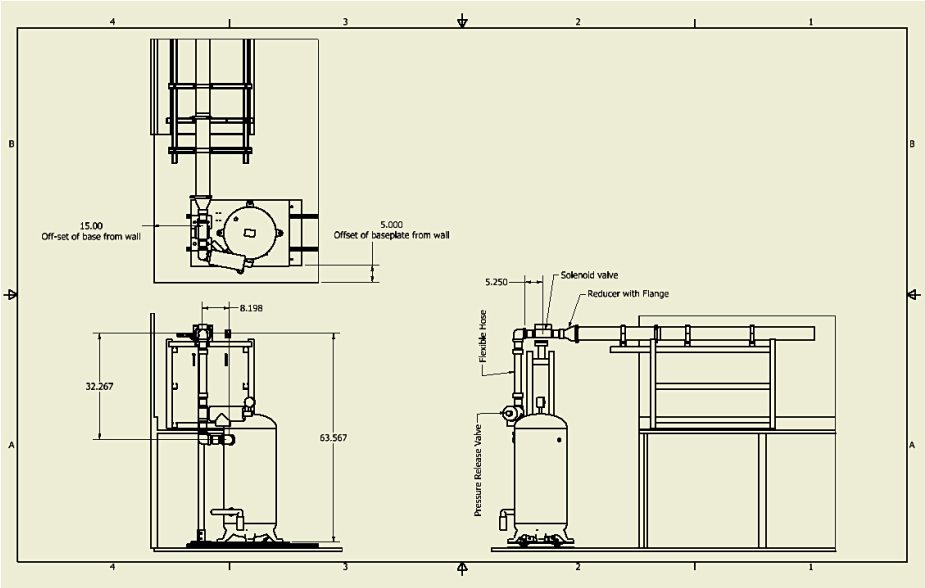

Figure F.1: Dimensional drawing of modified pneumatic impactor

All dimensions in inches, drawn for installation of pneumatics.

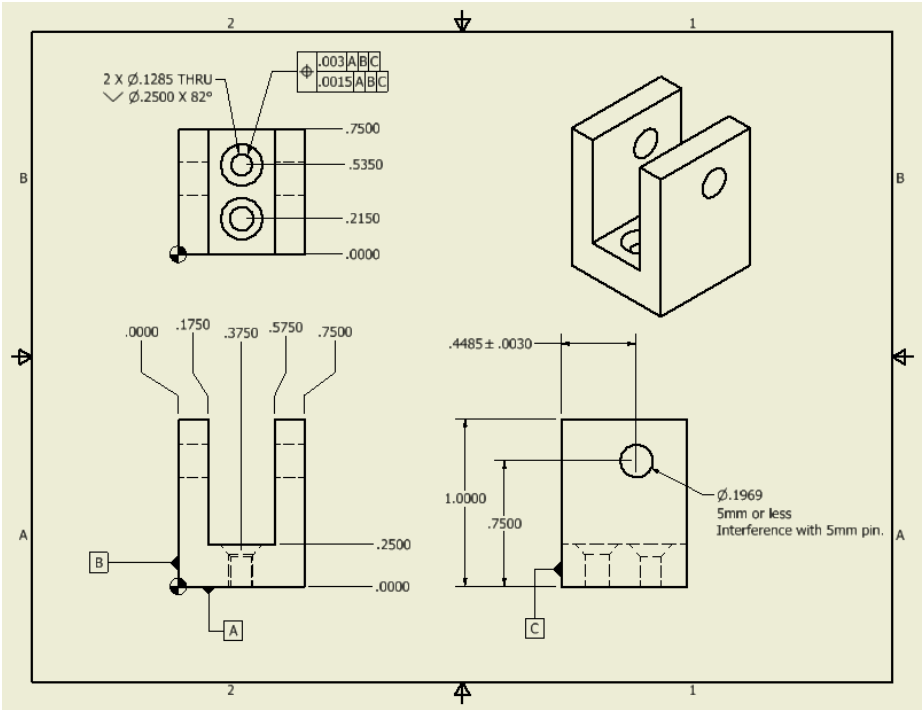

Figure F.2: Dimensional drawing of bearing wheel holder for projectile

All dimensions in inches, made of aluminum.

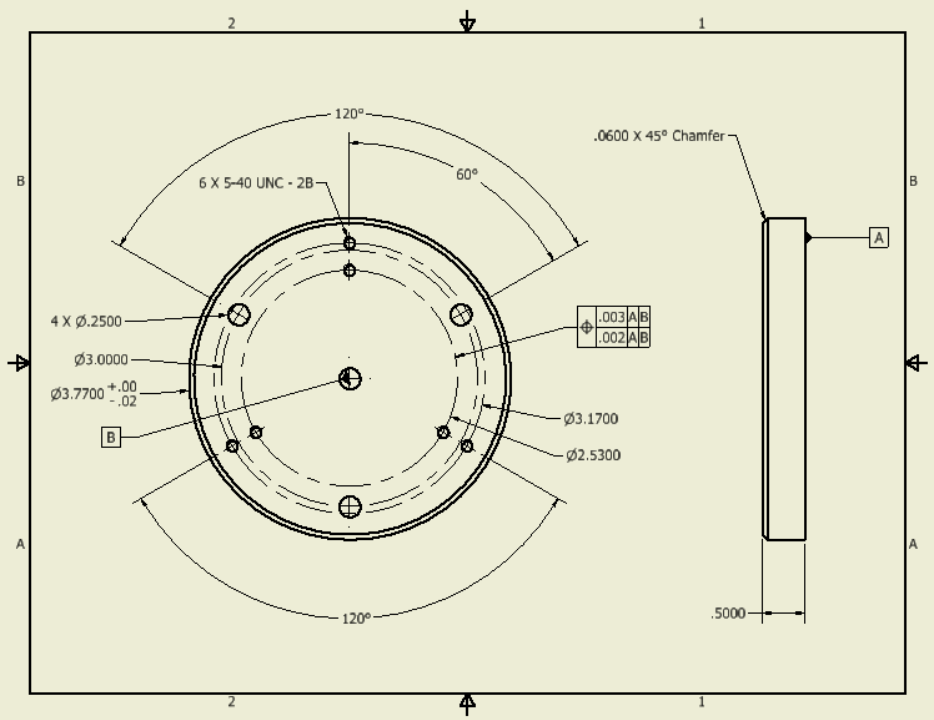

Figure F.3: Dimensional drawing of projectile end caps

All dimensions in inches, made of aluminum.

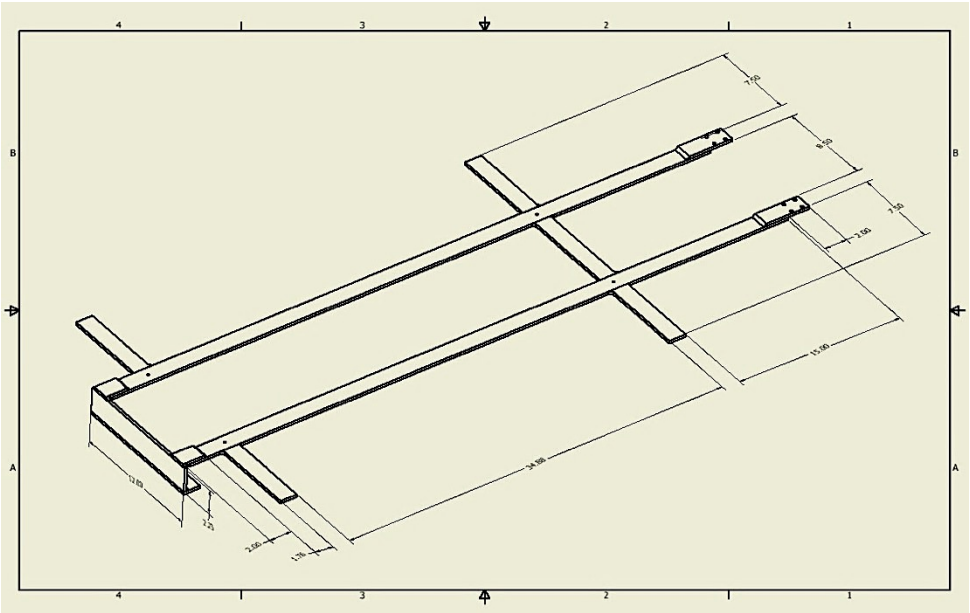

Figure F.4: Dimensional drawing of under impactor steel brace

All dimensions in inches, made of steel.

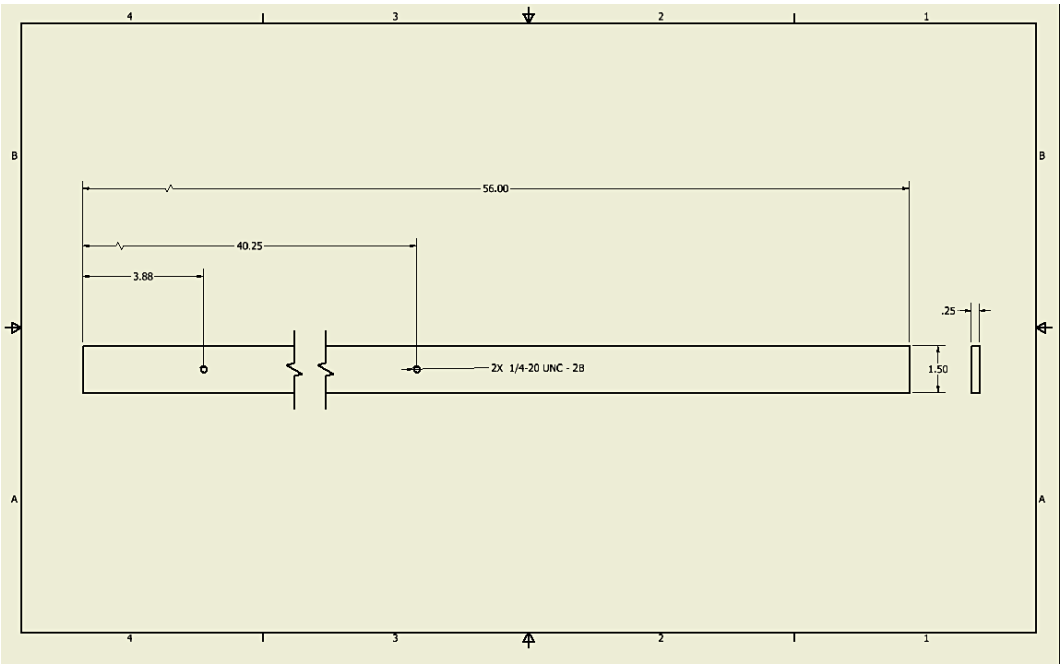

Figure F.5: Dimensional drawing of center material in steel brace

All dimensions in inches, made of steel.

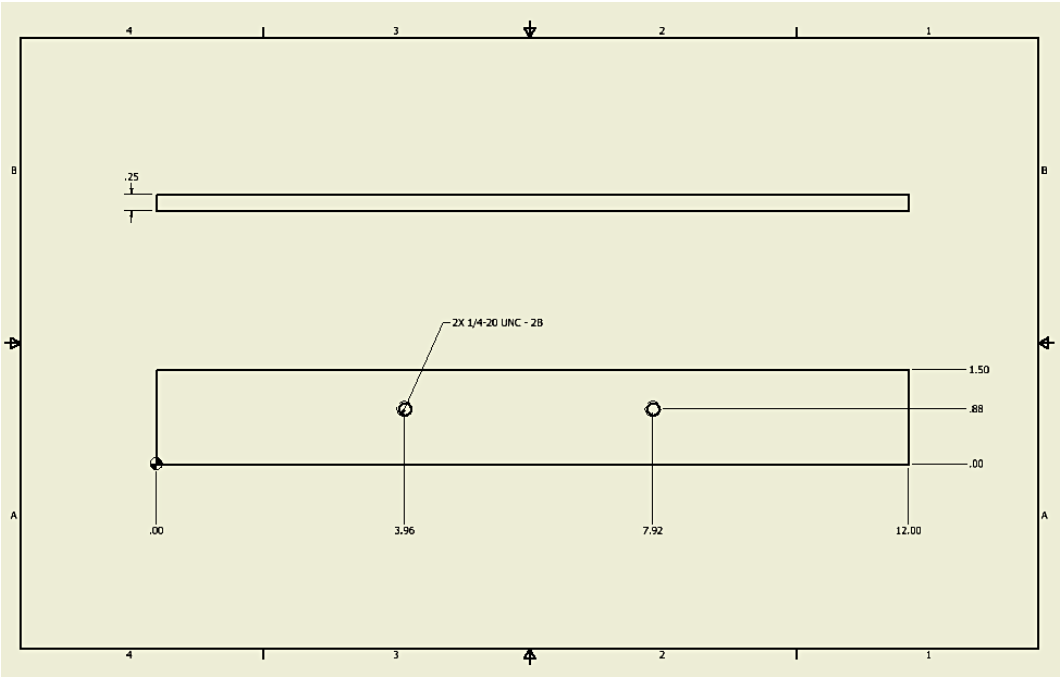

Figure F.6: Dimensional drawing for cross support of steel brace

All dimensions in inches, made of steel.

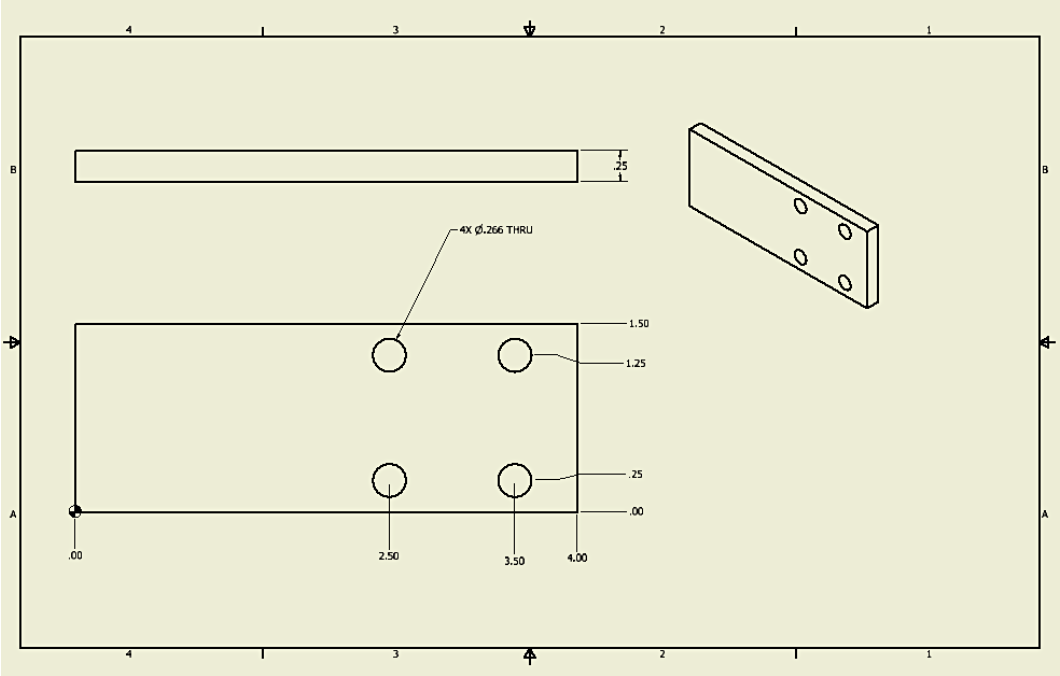

Figure F.7: Dimensional drawing of connector for steel brace and chamber

All dimensions in inches, made of steel.

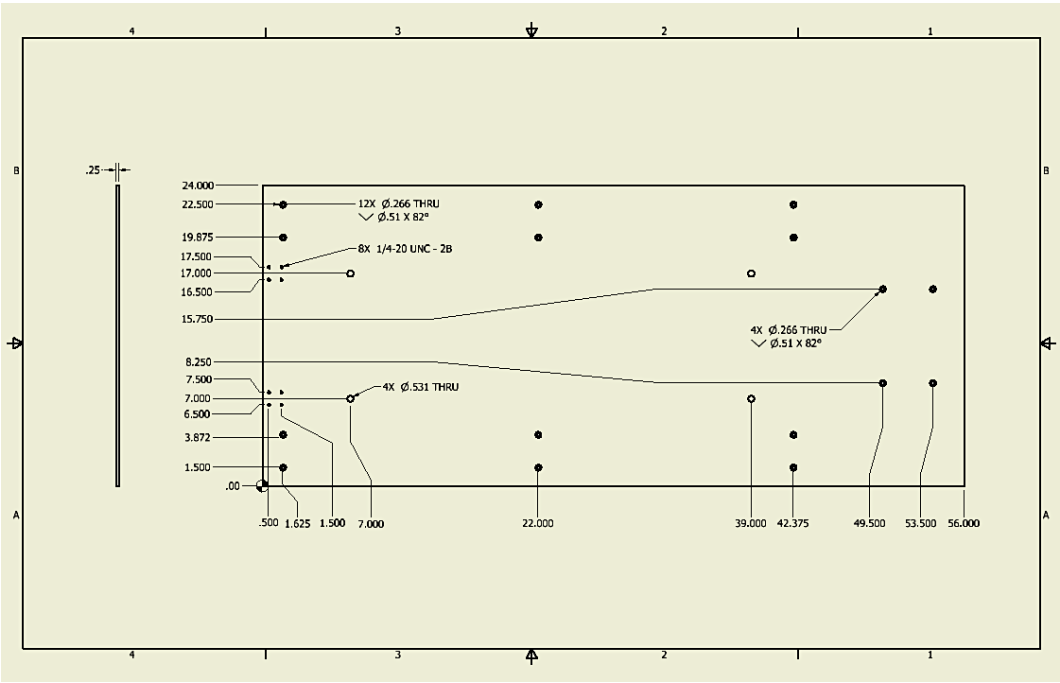

Figure F.8: Dimensional drawing for aluminum plate under impact chamber

All units in inches, made of aluminum, manufactured with waterjet.

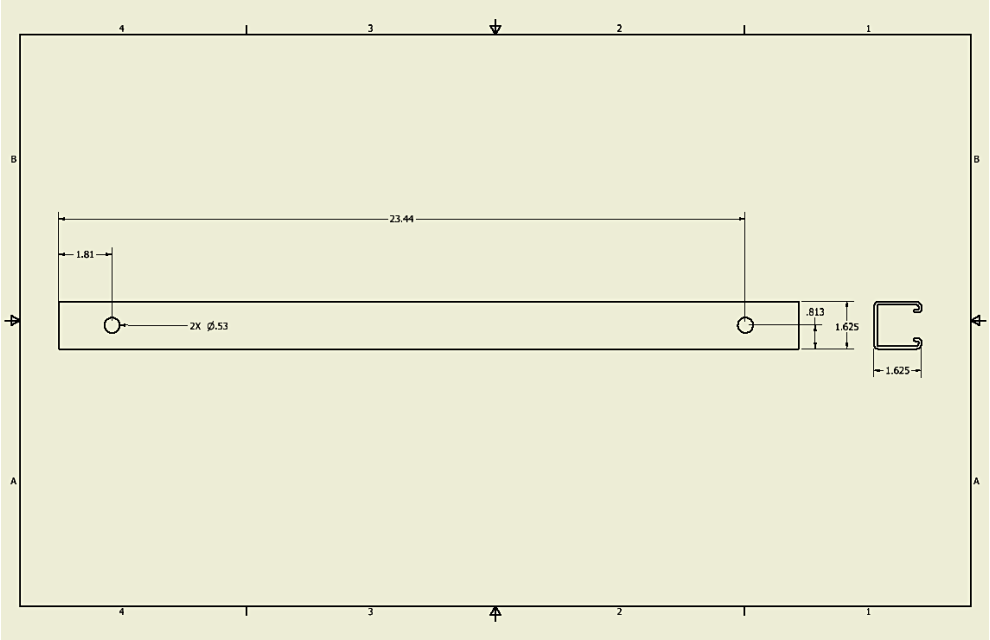

Figure F.9: Dimensional drawing for Unistrut cross support

All dimensions in inches, made of steel.

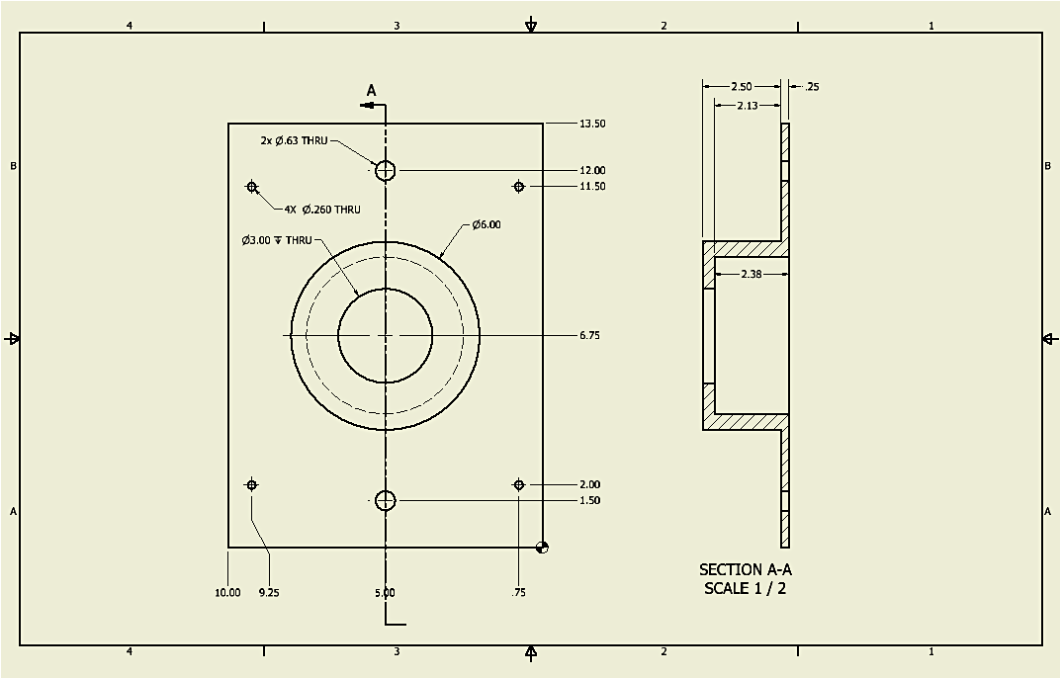

Figure F.10: Dimensional drawing for projectile exit guard

All dimensions in inches, made of steel.

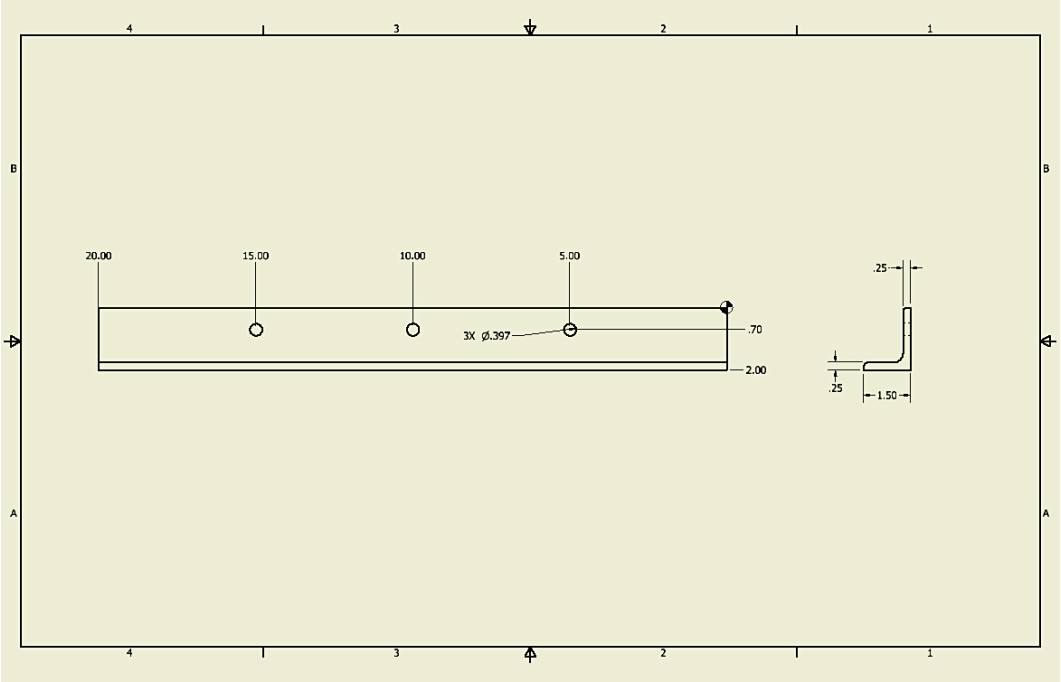

Figure F.11: Dimensional drawing for L-bracket for shock absorbers

All units in inches, made of steel L-channel.

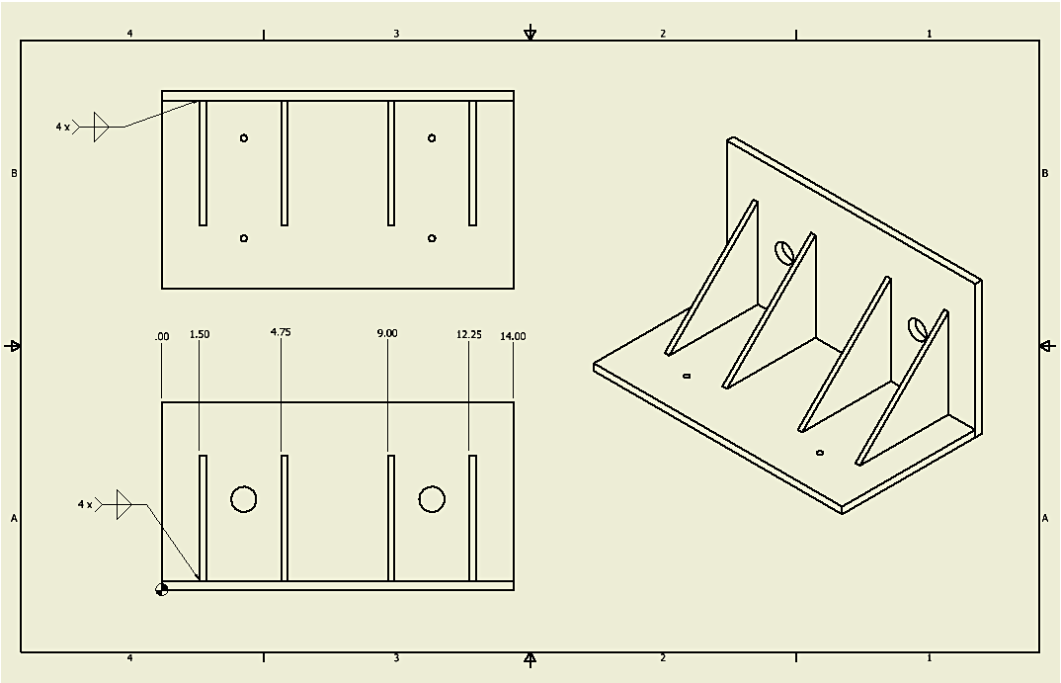

Figure F.12: Dimensional drawing of shock absorber frame

All dimensions in inches, made of welded steel components.

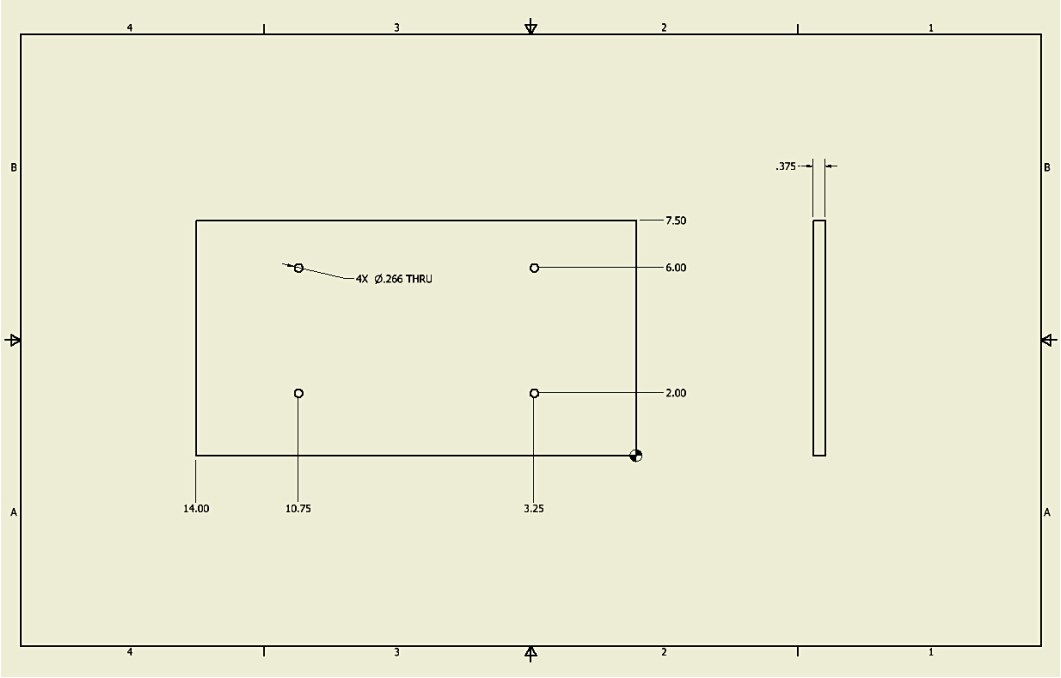

Figure F.13: Dimensional drawing of shock absorber base

All dimensions in inches, made of steel.

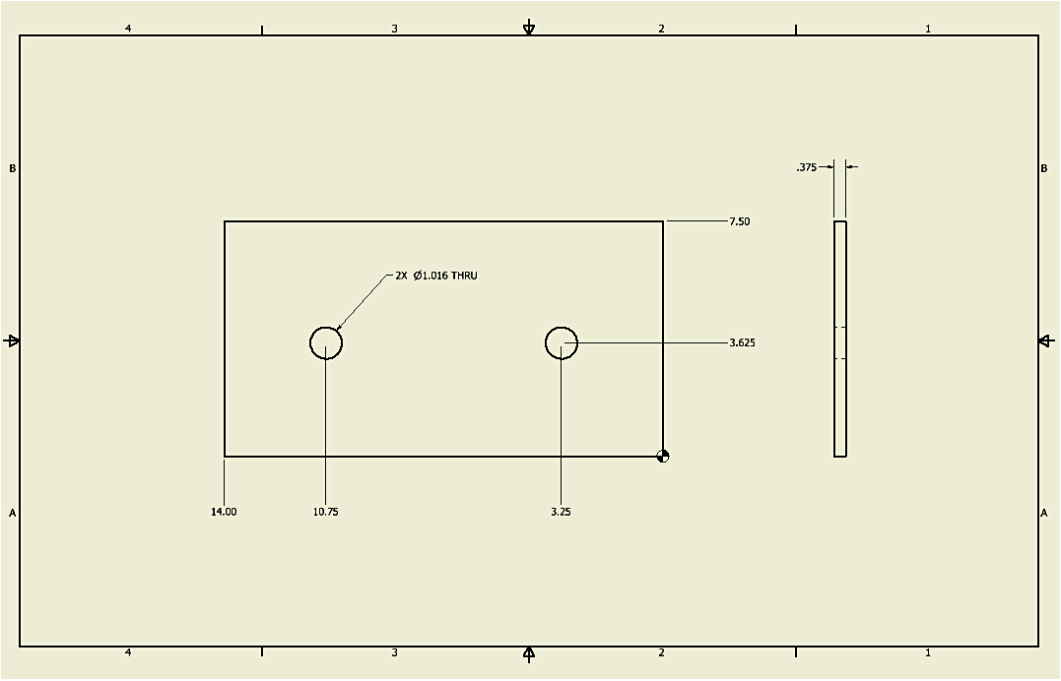

Figure F.14: Dimensional drawing for shock absorber mount plate

All dimensions in inches, made of steel.

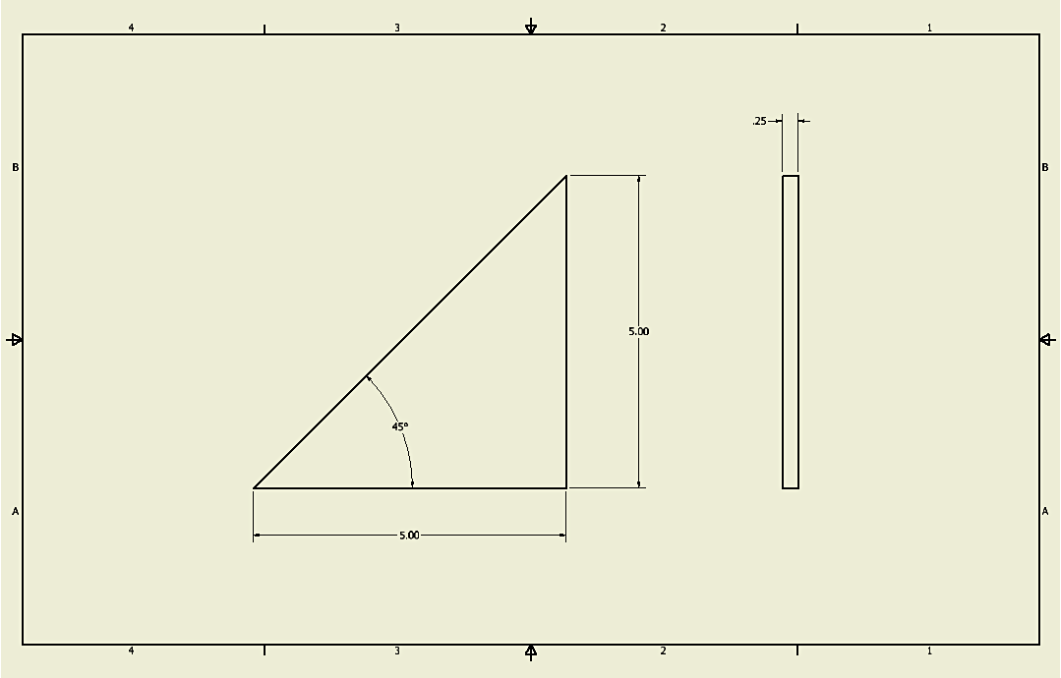

Figure F.15: Dimensional drawing of triangular shock absorber rib

All dimensions in inches, made of steel, manufactured with waterjet.

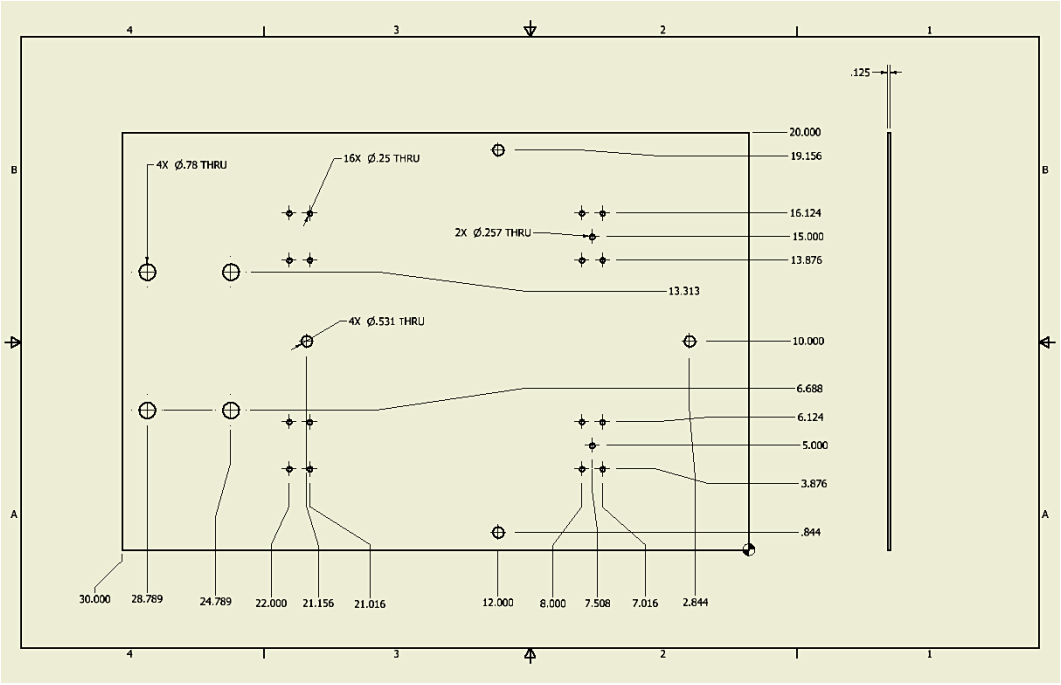

Figure F.16: Dimensional drawing of pressure tank mount plate

All dimensions in inches, made of aluminum, manufactured with waterjet.

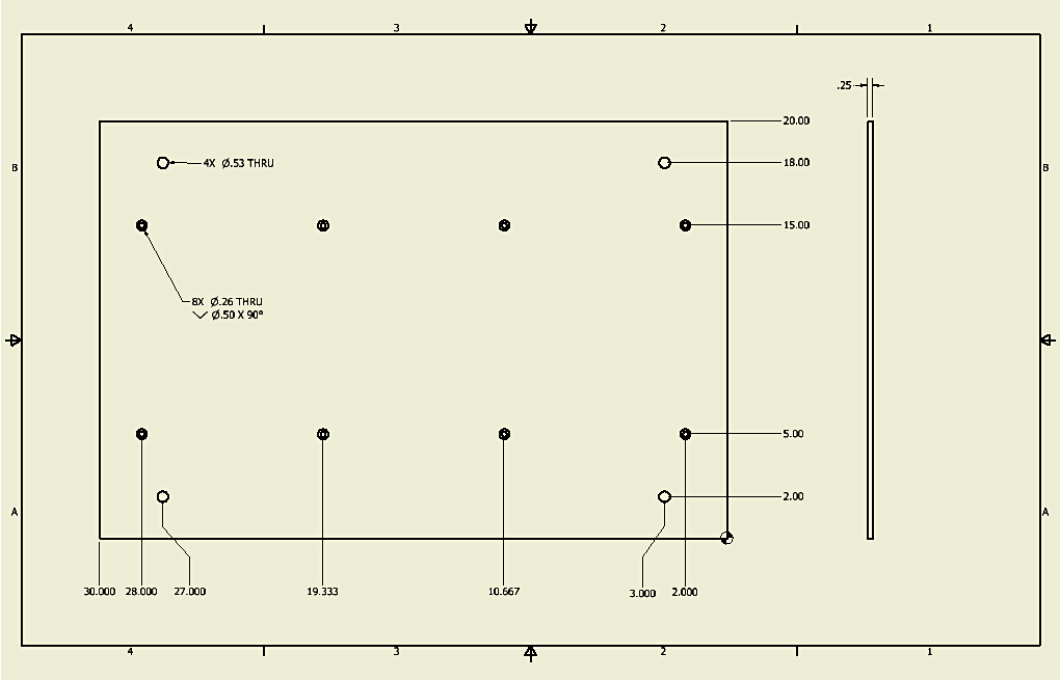

Figure F.17: Dimensional drawing of floor mounted pressure tank plate

All dimensions in inches, made of aluminum, manufactured with waterjet.